Structural Integrity of Steel Bridges: Environment-Assisted Cracking

by

Nirosha D. Adasooriya

Thesis submitted in fulfillment of
the requirements for the degree of
PHILOSOPHIAE DOCTOR
(PhD)

Faculty of Science and Technology
Department of Mechanical and Structural Engineering and Materials Science
2020

University of Stavanger
N-4036 Stavanger
NORWAY
www.uis.no

ISBN:
ISSN:
PhD: Thesis UiS No.

Preface

This thesis is submitted in partial fulfilment of the requirements for the degree of Doctor of Philosophy (PhD) at the University of Stavanger, Norway. The research work has been carried out at the Department of Mechanical and Structural Engineering and Materials Science, Faculty of Science and Technology, University of Stavanger. The research was fully funded by the Department of Mechanical and Structural Engineering and Materials Science. The required PhD courses have been completed at the University of Stavanger.

Acknowledgments

I would like to express my sincere thanks to those who were involved in the various stages of this study to make it a success. My heartfelt gratitude goes to Prof. Tor Hemmingsen and the TN employment board for offering a qualifying position in the department while pursuing the PhD degree. I herewith convey my sincere gratitude to Prof. Per Skjerpe for the given opportunity to get engaged in research and teaching activities in the department since 2012 and recommending me for this position.

My deepest gratitude, heartiest appreciation and sincere thanks go to my esteemed supervisors Prof. Dimitrios Pavlou and Prof. Tor Hemmingsen for clear guidance and continuous encouragement given to me throughout this research. I can never ever forget their highly valuable comments on the research thought process, planning experiments and interpretation of results. Their advices always kept me on the right track and enabled me to overcome the difficulties arisen during the study. These great advices supported me to improve my research dissemination skills, data interpretation skills and commitment to the work. All these great guidance eventually directed towards the original research outcomes.

I really appreciate Emeritus Prof. Ove Tobias Gudmestad, Associate Prof. Samindi Samarakoon and Prof. Tore Markeset for their initial involvement in the PhD program. I thank Prof. Ove Tobias for the follow up and encouragement given during the PhD studies. Meanwhile I wish to express my heartiest appreciation and gratitude to Prof. Vidar Hansen, Dr. Wakshum Mekonnen Tucho, Dr. Karl Gunnar Solheim, Erlend Holm and Terje Årthun for given contribution, valuable advices and supports for experimental work in hydrogen embrittlement studies and writing the

paper 6. Special thank should go to Inge Brandstrup Hemmingsen for voluntary support given for the proof reading.

I would like to appreciate the given great support to conduct the experiments by Johan Andreas Thorkaas, John Grønli, Adugna Deressa Akessa, Jørgen Grønsund, Mona Wetrhus Minde, Emil Kristiansen, Tor Gulliksen and Jan Magne Nygård. Without your positive contribution, the experimental work would not be successful.

I convey my gratitude for all the support and positive encouragement given during my PhD study by Marianne Sun May Per, Samdar Kakay, Sheryl Josdal and Kathrine Lima Molde. I am also grateful to all my friends and colleagues in UiS for giving me positive motivation and sharing good times with me. I am also thankful to Cathrine Reilstad, Carolina Hara, Anne Karin Rafos and Nina Stava for administrative support. I herewith thank to PhD course coordinators and reviewers of the papers.

Last but not least, my unlimited gratitude goes to my husband, my loving daughter and son for their patience while I have spent immensely many extra hours and weekends working on my PhD. I am lucky to have the most lovable, patient and kind family. I would like to convey my heartfelt gratitude and thank to my mother, my father, my mother-in-law and father-in-law for their showers of blessings and continuous encouragement given to me throughout the study. Without their support, blessing and sacrifice, this research would not have been successfully completed.

Abstract

Steel bridges are generally subjected to degradation due to corrosive environments. Uniform corrosion, pitting corrosion, crevice corrosion, intergranular corrosion, microbiologically influenced corrosion and environment-assisted cracking (EAC) are commonly applicable to steel bridges. EAC is classified into corrosion fatigue (CF), stress corrosion cracking (SCC) and hydrogen embrittlement (HE). The recent failures and collapses of bridges show that EAC significantly affects the structural integrity of steel bridges. The found knowledge gaps are the lack of detailed guidelines for assessing structural integrity due to EAC, the unavailability of generalized S-N curves for structural details exposed to corrosive environments, and the lack of investigations into the EAC susceptibility of steel types used in bridges. This study aims to contribute these gaps. The objectives of the thesis are to (i) propose a conceptual framework to assess the structural integrity due to EAC of ageing steel bridges; (ii) derive a generalized formula of S-N curve for structural details which are corroded and/or exposed to corrosive environment; (iii) investigate the EAC susceptibility of ST52 steel in 3.5wt% NaCl media with different hydrogen-charging environments; (iv) investigate the HE susceptibility of a tempered martensitic steel by slow strain rate tensile testing of hydrogen pre-charged specimens under hydrogen charging while straining.

In the first part of the thesis, a framework is presented for assessing the structural integrity of steel bridges for EAC damage. The framework consists of four major steps, i.e. identification of factors affecting the corrosion and/or EAC; identification of forms of corrosion, their causes and effects, checking for structural integrity/estimation of remaining life, and proposing remedial measures to control EAC and/or strengthening techniques. The conceptual framework consists of proven bridge inspection and investigation methodologies, except for EAC.

As a major contribution, a formula for an S-N curve is proposed, to predict the fatigue life of members and joints of steel bridges exposed to corrosive environments. The concept is identified by the corrosion fatigue results of different types of steel specimens tested in air, fresh water and seawater. The corrosive parameters of the S-N curve are determined for marine and urban environments and tabulated for the detailed categories given in the Eurocode and the DNV GL code. The proposed S-N curve formula is compared with full-scale fatigue test results of several structural details, and the validity of the formula is confirmed. The formula does not require any material parameter other than the code-given fatigue curves. The fatigue life of a case-study bridge is estimated by using the new formula, and the results are compared with conventional approaches. The applicability and significance of the proposed curve are confirmed.

SCC and HE susceptibility of ST52 steel is experimentally investigated by slow strain rate tests (SSRT). Stress versus strain curves are plotted, and characteristic parameters are determined. Hence, EAC susceptibility indexes are calculated. Fracture surface analyses are conducted. The study reveals that the cathodic protection (CP) process accelerates the EAC susceptibility of ST52 steel in a 3.5 wt% NaCl water solution. The change in the mechanical properties of tempered high-strength carbon steel AISI 4130 due to HE is investigated by SSRT. Scanning electron microscopy (SEM) and transmission electron microscopy (TEM) are conducted for fracture surfaces, and such samples show a transition of failure mechanism from brittle intergranular cracking at the lowest tempering temperature to ductile microvoid coalescence at the highest temperature. The material was subjected to HE when the tempering temperatures were 400 ^{o}C and lower, corresponding to a hardness value of 450 HV and greater. Hence, the limiting tensile strength and fracture strain are determined.

Keywords: Corrosion fatigue, stress corrosion cracking, hydrogen embrittlement, steel bridges, structural integrity

Contents

Preface ii
Acknowledgments iv
Abstract vi
List of Papers* x
Abbreviations xii
Chapter 1 Introduction 1
1.1 Background 1
1.2 Problem statement-failures of steel bridges 2
1.3 Research gaps 3
1.4 Objectives and scope 11
1.5 Outline of the thesis 12
Chapter 2 Research Outcomes 15
2.1 Proposed conceptual framework for integrity assessment of steel bridges 17
2.2 S-N curve formula for steel bridges located in corrosive environment 20
2.2.1 S-N curve for steel specimens 20
2.2.2 S-N curve for structural members and joints 22
2.2.3 Verification of proposed S-N curve formula 26
2.2.4 Case study: Fatigue life estimation of a steel bridge 26
2.3 EAC susceptibility of structural steel in 3.5wt% NaCl media due to hydrogen charging 27
2.4 HE susceptibility of martensitic carbon steel 28
Chapter 3 Conclusions 33
3.1 Summary 33
3.2 Concluding remarks 35

3.3 Recommendations for future research 38
References 39
Appended Papers 47
Paper 1. Environmental assisted corrosion damage of steel bridges: A conceptual framework for structural integrity
Paper 2. Fatigue strength degradation of metals in corrosive environments
Paper 3. Fatigue strength degradation of corroded structural details: A formula for S-N curve
Paper 4. S-N curve for riveted details in corrosive environment and its application to a bridge
Paper 5. An experimental study on environmental assisted cracking of structural steel in 3.5 wt% NaCl solution
Paper 6. Effect of hydrogen on mechanical properties and fracture of martensitic carbon steel under quenched and tempered conditions

List of Papers*

1. Adasooriya ND, Hemmingsen T, Pavlou D. Environment-assisted corrosion damage of steel bridges: A conceptual framework for structural integrity. *Corrosion Reviews*. 2019; 1-17. https://doi.org/10.1515/corrrev-2019-0066
2. Adasooriya ND, Hemmingsen T, Pavlou D. Fatigue strength degradation of metals in corrosive environments. *Proceedings of First Conference of Computational Methods in Offshore Technology-COTech 2017, IOP Conference Series: Materials Science & Engineering*: IOP Publishing; Stavanger, Norway: 2017: Article number 276 012039.
3. Adasooriya ND, Pavlou D, Hemmingsen T. Fatigue strength degradation of corroded structural details: A formula for S-N curve. *Fatigue & Fracture of Engineering Materials & Structures.* 2019; 1-13. https://doi.org/10.1111/ffe.13156
4. Adasooriya ND, Hemmingsen T, Pavlou D. S-N curve for riveted details in corrosive environment and its application to a bridge. *Fatigue & Fracture of Engineering Materials & Structures*. 2020; 1-15. https://doi.org/10.1111/ffe.13193
5. Adasooriya ND, Hemmingsen T, Pavlou D. An experimental study on environment-assisted cracking of structural steel in 3.5 wt% NaCl Solution, *ISOPE -2019: The 29th International Ocean and Polar Engineering Conference*, 16-21 June, Honolulu, Hawaii, USA, ID: ISOPE-I-19-522, pp. 4154-4160.
6. Adasooriya ND, Tucho WM, Holm E, Årthun T, Hansen V, Solheim KG, Hemmingsen T. Effect of hydrogen on mechanical properties and fracture of martensitic carbon steel under quenched and tempered conditions, *Journal of Material Science & Engineering A* (under review).
7. Adasooriya ND, Samarakoon S, Gudmestad OT. Corrosion propagation phase and bond strength degradation of reinforced

concrete structures: State of the art. *International Journal of Computational Methods and Experimental Measurements*. 2018; 6; 499-514.

8. Adasooriya ND. Fatigue Reliability Assessment of Ageing Railway Truss Bridges: Rationality of Probabilistic Stress-Life Approach. *Case Studies in Structural Engineering*. 2016; 6; 1-10.
9. Adasooriya ND, Siriwardane SC. Remaining Fatigue Life Estimation of Corroded Bridge Members. *Fatigue & Fracture of Engineering Materials & Structures*. 2014; 33; 603-622.
10. Adasooriya ND, Siriwardane SC. Ohga M. A simplified approach to predict the failure of steel members under interaction effect of fracture and fatigue. *International Journal of Fatigue*. 2013; 47; 161-173.

*The research outcomes of Paper 1-6 are summarized in Chapter 2 and the major conclusions of this thesis in Chapter 3 are based the Paper 1-6. The Paper 1-6 are attached after page 48 of the thesis. Even though the scope of the papers 7-10 are in the areas of fatigue, corrosion and structural integrity, those papers are not to be considered as a part of this thesis as outcomes of those papers do not provide sufficient research outcomes related to environment-assisted cracking of steel bridges.

Abbreviations

AISI	American iron and steel institute
ASTM	American society for testing and materials
CF	Corrosion fatigue
COV	Coefficient of variation
CP	Cathodic protection
EAC	Environment-assisted cracking
EN	Europeans normalization
HCF	High cycle fatigue
HE	Hydrogen embrittlement
HV	Vicker’s hardness value
I	Susceptibility Index
ISO	International organization for standardization
LCF	Low cycle fatigue
NDT	Nondestructive testing
SCC	Stress corrosion cracking
SEM	Scanning electron microscopy
S-N	Stress-life
SSRT	Slow strain rate tensile tests
TEM	Transmission electron microscopy
VHCF	Very high cycle fatigue

Chapter 1 Introduction

1.1 Background

Bridge authorities are paying significant attention to the issues of ageing, as most of the bridges in the world are reaching their design life [1-5]. Replacement of all the ageing bridges is practically impossible, due to both the decommissioning and new building costs. Some of the ageing bridges are located in urban industrial or moderate marine settings, which have been classified as corrosive environments [6, 7]. Although many bridges are located far from the sea, de-icing salt may simulate a marine environment for bridges in snowy regions [6]. These bridges are generally subjected to deterioration and degradation due to corrosion [8-12].

Corrosion is one of the principal deterioration processes that affects the integrity of structures. Steel bridges are subjected to many forms of corrosion, such as uniform/patch corrosion, crevice corrosion, pitting corrosion, galvanic corrosion, intergranular corrosion, microbiologically influenced corrosion, and environment-assisted cracking (EAC) [8, 9, 13-16]. These forms of corrosion affect the degradation of steel bridges. Major effects from corrosion are change of structural stiffness due to thickness reduction, stress concentration due to pitting, surface irregularity and roughness, degradation of material strength due to the electrochemical process, and unexpected fixities due to the build-up of corrosion products caused by wastage. The cracking of members is especially started at highly stressed locations. Thickness reduction, surface roughness and cyclic loading accelerate crack initiation under different types of corrosion [17].

Guidelines for the inspection of corrosion, corrosion prevention, coating and surface treatments of bridges are given in different international

standards [16-17]. On some occasions, bridge owners fail to attend inspection or repair strategies on time for various reasons, such as lack of funding, knowledge, facilities, concern and guidelines for remedial measures to control EAC [8, 9, 12, 14]. Significant amounts of degradation and/or deterioration due to corrosion were recognized in some cases when the bridge owners focused their attention on inspection or repair works [8, 9].

Uncertainties in the skills of inspectors and accessibility issues hinder damage detection by visual inspection of bridges for some places of the structure. Although non-destructive testing-based damage detection approaches are more accurate, they are expensive and time-consuming. Recent research has observed that dynamic model parameters or vibration measurements-based structural health monitoring techniques may provide more realistic predictions regarding the state of damage to steel structures. However, the accuracy of vibration measurements-based structural health monitoring techniques is not sufficient to detect localized corrosion and EAC. Researchers are still highlighting the significance of further study on EAC [6, 7, 18], due to the combined effect of the inherent nature of the corrosive environment and the random loading behaviour of steel bridges.

1.2 Problem statement-failures of steel bridges

The case histories of steel bridge failures, including recent collapses of key structures, such as Silver Bridge in 1967, Mianus River Bridge in 1990, Minnesota Bridge in 2007, etc., emphasize the importance of more accurate simulation of EAC in different corrosive environments, with respect to different structural materials. There are three major types of EAC: stress corrosion cracking (SCC), hydrogen embrittlement (HE) and corrosion fatigue (CF), all of which significantly affect the degradation of metal structures [17]. Fractures due to cyclic stress in corrosive media are designated as CF. SCC is generally defined as failure caused by continuously applied stress in a corrosive media. The

cracking/damage caused by hydrogen atoms diffusing into the metal, due to a corrosive medium or cathodic polarization, are generally defined as HE [17]. The results of this may cause gradual weakening of the bridge over time, leading to either progressive collapse or sudden catastrophic failure of the bridge. Catastrophic failures are frequently published in the literature [1]. Some of the reported bridge failures are clearly due to corrosion [13, 19]. Generally, SCC and HE are more common for highly stressed bridge components, such as suspension cables, where dead load induced stress levels are significantly higher than the ordinary traffic loads. The combined influence of the severe corrosive environment and the cyclic stresses due to variable traffic loads initiates cracks in both corroded and uncorroded regions (i.e. corrosion-free areas and/or coating-lost areas) of the bridge members and joints [14, 20-22]. Fractures due to the cyclic stress in corrosive media are designated as corrosion fatigue (CF) [13, 19, 23, 24], which is a type of environmentally assisted cracking; hence, fatigue strength degradation can be observed. The fatigue performance of steel joints and members depends on the type of material, fabrication methods of joints, degree of coating, state of deterioration due to corrosion and the corrosive environment. A significant amount of full-scale fatigue testing has been carried out for structural details [5-7]. It is difficult to compare the degree/severity of the effect of CF for the above tests, without studying the distinction of mechanisms between corroded members tested in air, corroded members tested in a corrosive environment and uncorroded members tested in corrosive environments. The contradictory conclusions reported in the literature motivate more accurate simulation of the CF strength of riveted structural details in different corrosive environments [6, 18, 25].

1.3 Research gaps

Through the process of reviewing the literature on the causes, effects and remedial measures of EAC on ageing steel bridges, the following gaps were identified.

1. Lack of detailed provisions and guidelines for assessing structural integrity due to EAC

Codes or standards for bridge assessment are only provided in some nations [26, 27], such as the UK, USA, Canada, Germany and Switzerland. These guidelines/manuals are prepared for all types of bridges in general, and steel bridge corrosion damage comprises only a small portion of them [26-29]. The procedures to investigate loss of section/material and stress concentration effects due to corrosion and to simulate their consequences for structural stiffness are precisely given in these codes, manuals and standards [29, 30]. Generalizing these types of guidelines is a necessity for Europe [30-32]. As a result, a simplified approach was recently proposed for existing steel bridges, based on past research. The proposed approach consists of four levels. The assessment relies heavily on visual inspection [31]. None of the levels incorporated the effects of EAC on structural integrity and major attention for HE, SCC or CF has not been given in these documents. Recoating has been recommended as a remedial measure in many of the codes. The type of recoating should be determined, based on the types of EAC [17].

The most recent inspection manual [29] comprehensively discussed non-destructive damage inspection techniques, such as metal thickness test, magnetic particle testing, eddy current testing, ultrasonic flaw detection test and full-scale load tests. Further thickness loss and surface irregularities/cracks due to corrosion can be detected by the mentioned NDT methods. However, internal cracks/defects, reduction of ductility, toughness and strength, and accelerated crack growth rate due to EAC cannot be captured by the above techniques.

This indicates that detailed provisions and frameworks are not available for assessing structural integrity due to EAC, i.e. SCC, HE and CF [6, 7, 32]. Therefore, the majority of bridge inspectors have

a knowledge gap in respect of understanding/recognizing the mechanism, occurrence locations, causes and effects of EAC, as well as inspection and test methods and remedial measures for EAC. Bridge authorities have not properly identified the effects of EAC, as failures occur without any loss of materials. Therefore, it is essential that these concepts are included in the guidelines.

2. Generalized S-N curve formulas are not available in codes of practices for structural details of bridges which are exposed to corrosive environments

Corrosion pit induced stress concentration models and fatigue notch factor are commonly used to determine a structure's integrity [33-36]. Fatigue crack initiation life is determined when micro-cracks propagate to a certain critical length. Fatigue crack propagation life is determined by the fracture mechanics approach. Accurate determination of the modified corrosion-fatigue stress intensity threshold and the critical length has been reported as challenging and difficult [6, 7, 37]. Therefore, limited published works are found in the area of fatigue notch factor due to pitting corrosion [35, 36]. Recent investigations of non-passive metals such as carbon steel reveal that CF cracks are not initiated at pits, even where those are available. This statement concludes that CF crack initiation mostly occurs without the formation of pits (i.e. absence of pitting corrosion) and may occur in any corrosive media [38-41]. This mechanism is proved by means of a slip-band preferential dissolution model and hydrogen embrittlement theory [39-41]. As these models are unable to represent CF crack initiation below yield stress and in the absence of hydrogen, Zhao et al [38] investigated the CF crack initiation and propagation mechanism of a carbon steel in detail, through stress-controlled fatigue tests and microstructural analyses, by using scan electron microscopy, electron backscatter diffraction and transmission electron microscopy. The CF crack initiation and initial propagation mechanisms are highly governed by the peak stress level

[38]. A generalized model which precisely addresses the above mechanism is lacking in the literature for predicting the life of defect-free (i.e. without cracks or pits) structural details. Therefore, further research is required to develop models to predict the fatigue strength of corroded steel members, joints and connections (i.e. constructional details) that are subjected to different types of corrosion.

As a result, a strain-life model was proposed, based on the Smith–Watson–Topper model [6, 7], to simulate the CF behaviour of metals. The model takes into account the state of the corrosive environment, the stress level and the corrosive behaviour of the steel. In the same articles, further verification of the proposed function is recommended for future studies. The procedure for determining the model parameters requires a series of fatigue tests. The effect of pitting on the prediction of life is recommended for further studies [6, 7]. Transformation of stress ranges into strain ranges is required to use the model, by using cyclic properties of steel and fatigue notch factor. Due to the mentioned complexities of the model and uncertainties of the model parameters, few applications are reported. Therefore, a simple formula/approach, for modelling the fatigue strength of steel specimens/materials which are exposed to corrosive environments, is required.

Detailed provisions and models/formulas are not available in codes of practices to predict the fatigue strength of corroded structural details of land-based structures/onshore structures [4, 6, 7]. Testing of different full-scale details in simulated corrosive environments is complicated, especially in very high cycle fatigue (VHCF) regions (e.g. if the cyclic frequency is 1 Hz, for 10^8 cycles, it takes more than three years to finish a single test). Therefore, the test results are limited, and the fatigue endurance of the majority of available results is reported in the range from 10^4 to 10^6 cycles. The obtained results are also scattered, since the test process is subjected to many variables and uncertainties. Those results are not sufficient to warrant

the variable amplitude fatigue limits of the details. A few past studies recommend that the endurance limit is neglected (i.e. the S-N curve should be used without cut-off limit), to take into account the fatigue strength degradation due to the effect of the corrosive environment of structural details and unexpected localized corrosion (i.e. mild pitting or crevice corrosion) near the corroded details [4, 21, 22, 42]. The modified S-N curves do not match the available fatigue test results of corroded details. To overcome these shortcomings and research gaps, a generalized S-N curve formula is required for structural details of steel bridges which are corroded and/or exposed to corrosive environments.

3. The susceptibility to HE and SCC of most commonly used steel types of bridges (i.e. S355, ST52) with cathodically protected members has not been properly investigated

Tiwari et al. [43] studied internal HE of mild steel and maraging steel, while developing a novel technique for hydrogen charging. The specimen with extended portion is subjected to steady uniaxial load. The extended portion of the specimen acts as a cathode in an alkaline bath and electrolytic hydrogen-charging of the specimen. The significant effect of hydrogen is to enhance yield strength, ultimate tensile strength, tangent modulus, work hardening rate, and ductility reduction. Though different hydrogen-charging durations were considered, the test results were not sufficient to find a correlation or limiting mechanical properties.

Eliaz et al [44] studied the mechanism and failure recurrence that occurred through hydrogen embrittlement and stress corrosion cracking, for high strength AISI 4340 alloy steel. The behaviour of this material differs considerably from that of commonly used steel such as ST52 and S355.

Kim et al [45] investigated the hydrogen embrittlement of welded high-strength steel by SSRT. The optimum cathodic protection (CP)

potential has also been studied. Correlation between mechanical properties and hydrogen embrittlement was not observed. Failure strain decreased with the cathodic potential. This material is not related to mild steel, which is generally used for bridges. The effect of hydrogen-charging duration was not considered in this study.

Changes in the ductility parameters of ASTM A36 steel due to SCC were studied by means of SSRT tests by Venkatesh [46]. The study mainly concerns the crack growth rate and threshold stress intensity factor. Although the benefit of this paper is that the results can be used to develop a detailed engineering analysis, the effect of CP for EAC was not considered in this study.

Espinosa-Medina et al [47] investigated the effects of pH and temperature on stress corrosion cracking of 1018 low carbon steel in 0.5M NaCl solution at different pH values and temperatures of 25 ^{o}C, 50 ^{o}C and 70^{o}C, using SSRT. The SCC susceptibility index was first defined, based on the percentage reduction in the area and the time to failure. Hydrogen-assisted anodic dissolution seems to be the reason for the cracking of 1018 steel in NaCl solution. As there has not been sufficient observation, this may be the most likely mechanism.

Depover et al [48] studied the effect of HE on the mechanical properties of advanced high-strength steels. The embrittlement index was first defined in this study, to investigate the effect of HE on the ductility, and the huge effect of HE was examined. This effect may not be similar for commonly used mild steel for bridges as the HE mechanism of martensitic steel is different from low strength steels.

The effect of cathodic potentials on the SCC behaviour of bainitic high-strength E690 steel in simulated seawater was investigated by Hongchi Ma [49]. The SSRT was performed, and percentage reduction area, based on the SCC susceptibility index, was studied. The SCC susceptibility index increased drastically when the applied

potential was -950 mV and greater. Although this study considered well the effect of CP on EAC, this material's behaviour differs from that of the mild steel commonly used for bridges.

Rhode et al [50] studied HE effects on mechanical properties in T24 welds. The heat-affected zone and the weld metal in hydrogen-charged and uncharged conditions were subjected to a tensile test. The embrittlement index was used to obtain a correlation of the limiting values of mechanical properties. This study does not have a significant relation to the CP effects on EAC of commonly used bridge materials.

Rosenberg et al [51] evaluated the HE of micro alloyed pipeline (X70) and structural hot rolled steel strips (S355) by different test methods, such as static tensile testing, cyclic loading and Charpy V impact testing. The test specimens were exposed to the outdoor environment at room temperature for four years. This study reveals that four years of ageing specimens, followed by hydrogen charging, did not affect the values of yield strength and ultimate tensile strength. Although it is concluded that HE had a significant effect on the reduction in area, the limiting values or correlation of reduction of ductility and/or fracture strain were not quantitatively discussed for S355 steel.

The EAC susceptibility of structural steels, such as ST52, S355, etc., has not been properly investigated. Mild structural steels are sensitive to SCC, HD and CF in NO_3^- and OH^- environments, H_2S, HCl and H_2SO_4 environments and aqueous environments (i.e. seawater, fresh water, etc.), respectively [17]. However, failures caused by unexpected reduction in ductility have been reported in structures located in marine environments under continuously applied loading. During the process of cathodic protection (CP), hydrogen is charging, and electrochemical reaction is accelerated by the corrosive environment. This may lead to a reduction in the

ductility of the specimen without brittle fracture. The HE and SCC susceptibility of cathodically protected S355 steels has not been properly investigated, and more detailed investigations are required to confirm this failure/fracture mechanism.

4. The HE susceptibility of high-strength carbon steel has not been investigated under quenched and tempered conditions

Hydrogen embrittlement (HE) in metals leads to cracking and may cause catastrophic failures. HE is often classified as (i) internal hydrogen embrittlement, which occurs due to pre-existing hydrogen in the material, or (ii) hydrogen environment embrittlement, which occurs due to hydrogen picked up from the environment under cathodic protection or in the presence of hydrogen gases, or (iii) hydrogen embrittlement due to electroplating [43]. The HE of steel may reduce ductility, toughness and strength and accelerate crack growth [43].Three conditions are required for HE: (a) the presence and diffusion of hydrogen, (b) a susceptible material/microstructure and (c) mechanical stresses [18, 43, 52]. The HE susceptibility is material-dependent, and there are no generalized guidelines to control the HE of high-strength steels. In general, HE susceptibility decreases with increasing tempering temperature for martensitic steel (i.e. a decrease in hardness) [18].

Post heat treatments are common processes for improving the ductility of high-strength martensitic steel. Even though much improvement has been achieved through heat treatments, many failures of high-strength steel structures are still observed. The suspension cable wire fractures of Lysefjord Bridge [53], Lake Maracaibo Bridge and Hamburg Bridge [13, 19] are examples of these failures. About 40% of the failures of oil and gas pipelines are due to corrosion associated with environment-assisted cracking [4].

Quenching and tempering processes are commonly used for high-strength martensitic steel, to increase ductility. In some structural

materials manufactured as-quenched or under tempered conditions, precipitated carbide may reduce the hydrogen diffusivity in the materials and cause intergranular fracture [48]. The carbide precipitates are also dependent on factors such as carbon content, cooling rate, quenching media and tempering temperature [48, 54-56].

Several scholars have studied the effects of internal HE of mild steel and the loss of ductility with intergranular cracking and work hardening [18, 43, 57, 58]. These processes depend on the strain rate, the method of hydrogen charging and the microstructure of the material [18, 48, 59, 60]. The two most commonly used experimental hydrogen-charging methods are electrochemical (i.e. cathodic protection and electroplating) and exposure to hydrogen gas [18]. Slow strain rate tensile tests (SSRT) are often used for HE susceptibility investigations of steel [61]. As the HE susceptibility depends on the material, environment and application, case-specific investigations are required, in order to determine HE susceptibility limits.

Although several studies have been carried out for some high-strength carbon steels, according to the literature, there is a lack of investigations into the relationship between HE susceptibility and hardness and, thus, on tempering temperature for cathodically protected martensitic carbon steel. In addition, the limiting/conservative values for tensile strength and fracture strain (i.e. ultimate fracture strain) are not available for these cathodically protected steel types.

1.4 Objectives and scope

The aim of this study is to compensate for the above-mentioned lacks/deficiencies in current practices and to fill the knowledge gaps regarding structural integrity assessment of steel bridges due to EAC. In

order to achieve the aim, the following objectives are mainly considered in this thesis.

1. Propose a conceptual framework to assess the structural integrity of ageing steel bridges due to EAC. The concept of the framework is developed by reviewing EAC mechanisms, causes, effects and remedial measures, to control the EAC.

2. Derive a generalized formula for S-N curve to determine the fatigue strength of structural members, joints and connections (i.e. constructional details) which are corroded and/or exposed to corrosive media/environment. Also propose a methodology to integrate the derived S-N curve formula for both probabilistic and deterministic fatigue assessment approaches.

3. Investigate the EAC susceptibility of ST52 steel (i.e. a commonly used one of the steel types for bridges) in 3.5wt% NaCl media, with different hydrogen-charging environments.

4. Investigate the HE susceptibility of a tempered high-strength carbon steel, by SSRT of hydrogen pre-charged specimens under hydrogen charging while straining. Hence, a methodology is illustrated to determine conservative values for ultimate tensile strength and fracture strain for hydrogen pre-charged martensitic carbon steels.

1.5 Outline of the thesis

The thesis is organized in two major parts.

Part I briefly presents the introduction, research outcomes and conclusions. The research background, problem statement, literature review and main objectives are described in Chapter 1. Chapter 2 briefly outlines the structure of the thesis and presents an overview of the research approach. The main research outcomes are also stated in this chapter. Chapter 3 contains the present research and a list of conclusions

drawn from the study. The limitations and suggestions for future research are discussed in the latter part of this chapter.

Part II of the thesis consists of six relevant journal and conference papers. The research approaches, original research outcomes and their limitations and validity are presented in detail in these six papers, refer page 47.

Chapter 2 Research Outcomes

The research was conducted to fill the identified research gaps, and the research outcomes were published/presented in international journals and conference proceedings. The thesis is based on these six papers. An overview of the articles, with corresponding objectives of the thesis, is shown in Figure 1.

Paper 1: Environment-assisted corrosion damage of steel bridges: A conceptual framework for structural integrity. *Corrosion Reviews.* 2019; 1-17. https://doi.org/10.1515/corrrev-2019-0066.

Paper 2: Fatigue strength degradation of metals in corrosive environments. *COTech- 2017, IOP Conference Series: Materials Science & Engineering:* IOP Publishing; Norway: 2017: Article number 276 012039.

Paper 3: Fatigue strength degradation of corroded structural details: A formula for *S-N* curve. *Fatigue & Fracture of Engineering Materials & Structures.*2019; 1-13. https://doi.org/10.1111/ffe.13156

Paper 4: S-N curve for riveted details in corrosive environment and its application to a bridge. *Fatigue & Fracture of Engineering Materials & Structures*. 2020; 1-15. https://doi.org/10.1111/ffe.13193

Paper 5: An experimental study on environment-assisted cracking of structural steel in 3.5 wt% NaCl Solution. *ISOPE -2019 Conference,* 16-21 June, Honolulu, Hawaii, USA, ID: ISOPE-I-19-522, pp. 4154-4160.

Paper 6: Effect of hydrogen on mechanical properties and fracture of martensitic carbon steel under quenched and tempered conditions. *Journal of Material Science & Engineering A* (under review).

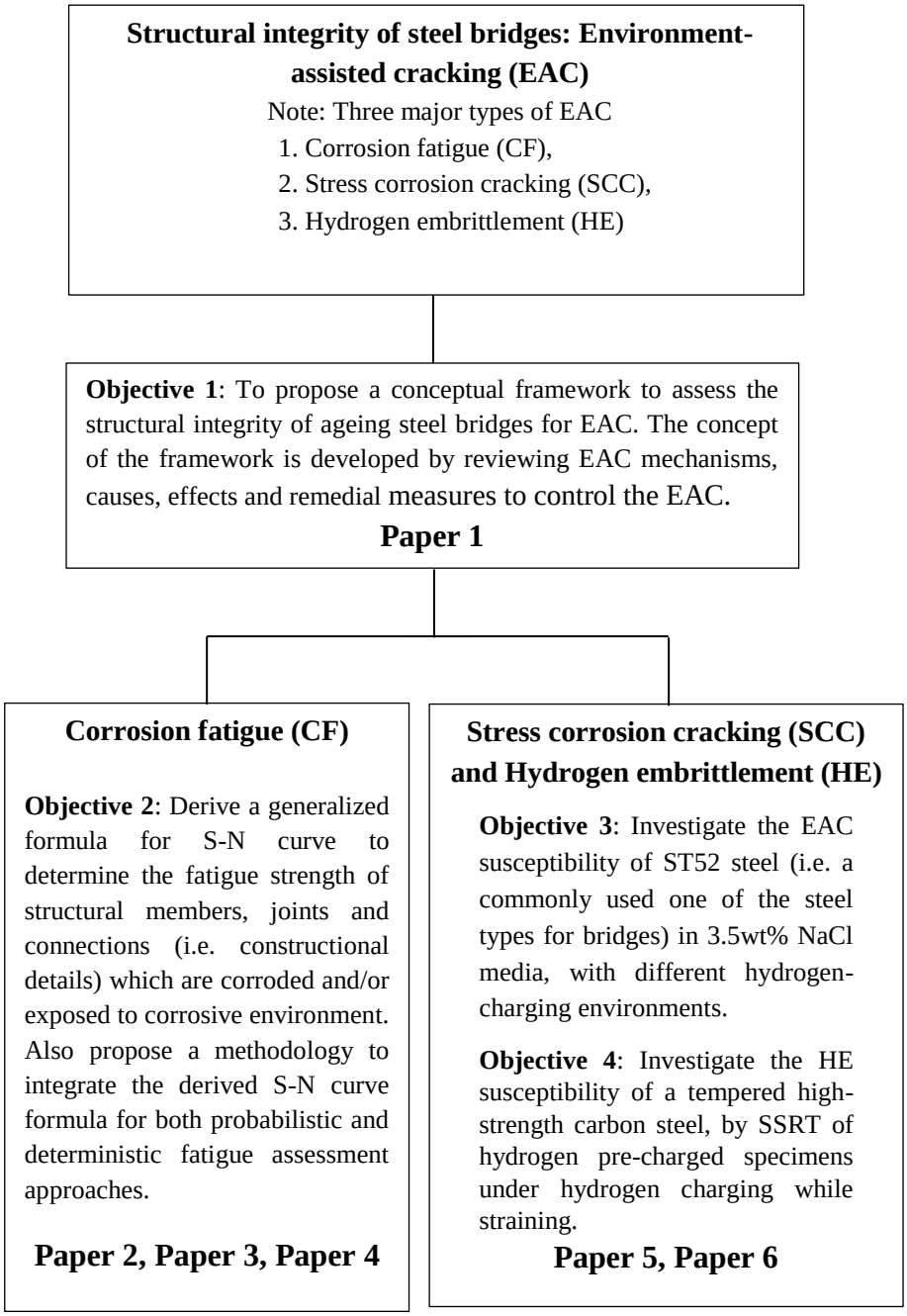

Figure 1. Research objectives and overview of the outcomes

2.1 Proposed conceptual framework for integrity assessment of steel bridges

A conceptual framework for identifying issues of corrosion and EAC of steel bridges is presented in Paper 1 [62]. The concept of the paper was developed by studying the mechanisms of different forms of corrosion, their effects, possible locations of occurrence, most appropriate inspection techniques, remedial measures and lessons learned from bridge failures in history. The checks for structural integrity for different limit states and the selection of remedial measures to ensure structural integrity against EAC are included in the proposed framework. The framework consists of four major steps, as shown in Figure 2. The first step is the identification of factors affecting the corrosion and/or EAC, which is discussed in Sections 2.2 and 2.5 of the paper. The classification of the forms of corrosion should be done by referring to Table 1 and Section 2.3 in the paper, as the next step. The forms are mainly classified as uniform/patch corrosion, localized corrosion, SCC/HE and CF. In the third step, the effects of corrosion are clearly classified, by following Section 2.4 and Section 3 in the paper. Checking the bridge for structural integrity and estimating the remaining life are considered in detail, as the next major step. This step includes global and local stress analysis, by considering the time-dependent corrosion wastage. The determination of mechanical properties, due to SCC/HE and fatigue strength degradation caused by CF, is also included in this step, by following the proposed experimental approaches in Section 4. If the structural integrity checks are not satisfied and/or the required remaining life cannot be achieved, remedial measures to control EAC and/or strengthening should be put in place, by following Table 3, which is the final step. The framework consists of proven bridge inspection and investigation methodologies, except for EAC [28, 29, 32]. Therefore, experimental methodologies to obtain the degraded mechanical properties due to EAC are discussed in the rest of the papers appended to the thesis.

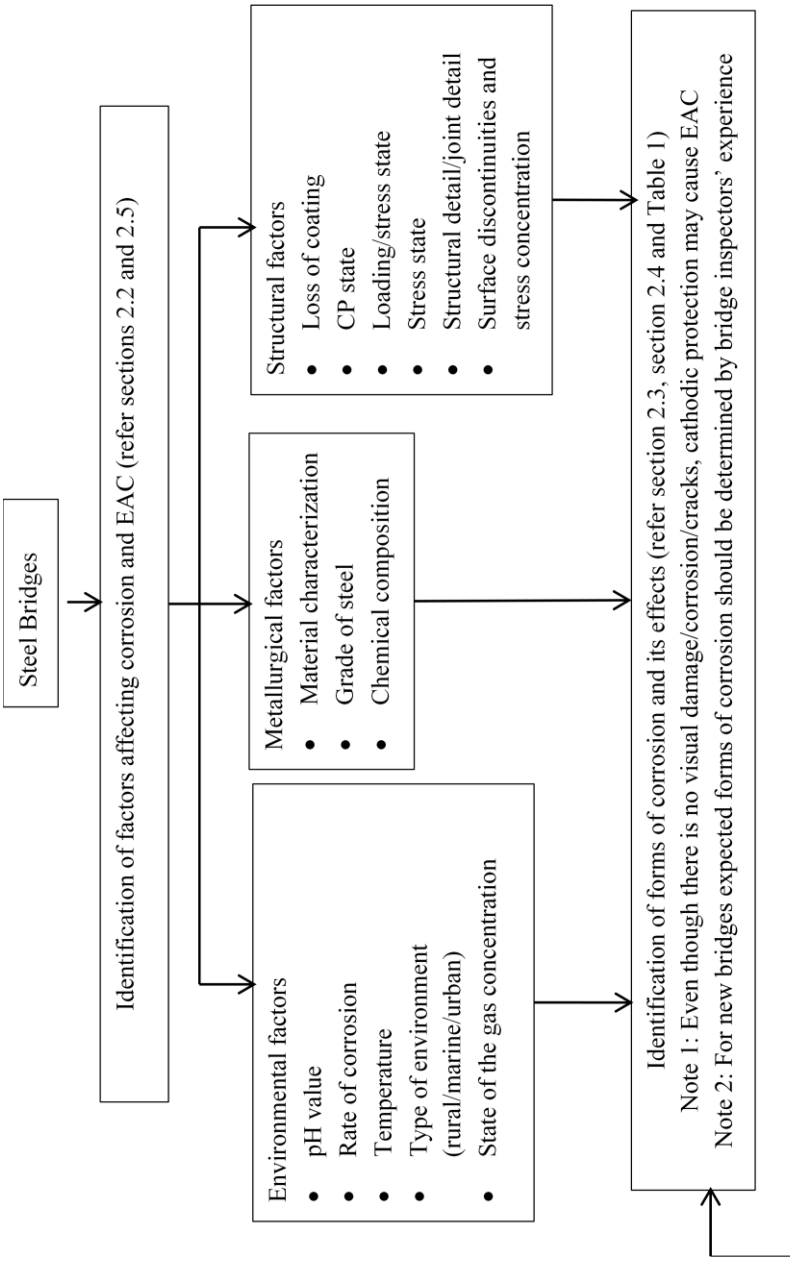
Steel Bridges
Identification of factors affecting corrosion and EAC (refer sections 2.2 and 2.5)
Environmental factors
pH value
Rate of corrosion
Temperature
Type of environment (rural/marine/urban)
State of the gas concentration
Metallurgical factors
Material characterization
Grade of steel
Chemical composition
Structural factors
Loss of coating
CP state
Loading/stress state
Stress state
Structural detail/joint detail
Surface discontinuities and stress concentration
Identification of forms of corrosion and its effects (refer section 2.3, section 2.4 and Table 1)
Note 1: Even though there is no visual damage/corrosion/cracks, cathodic protection may cause EAC
Note 2: For new bridges expected forms of corrosion should be determined by bridge inspectors' experience

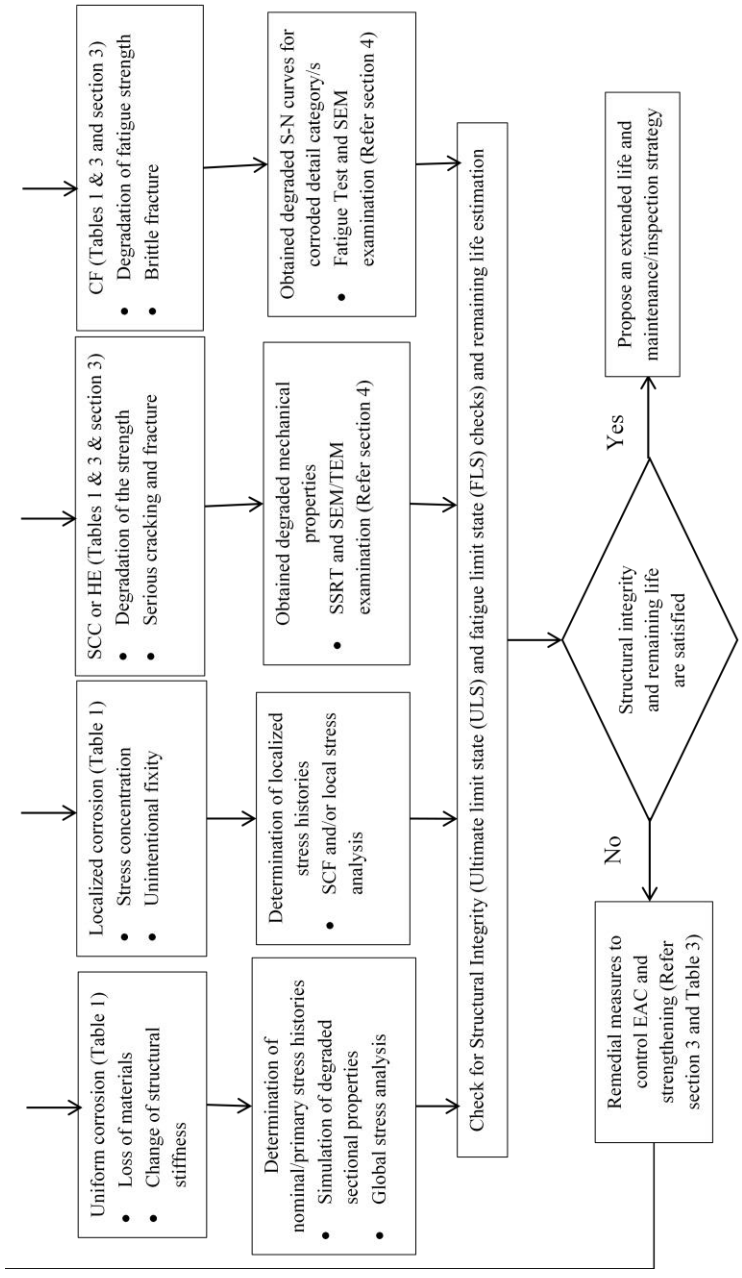

Figure 2. Proposed conceptual framework

2.2 S-N curve formula for steel bridges located in corrosive environment

A formula is proposed to estimate the fatigue life of members and joints of steel structures exposed to corrosive environments. The concept of the formula is first studied from the recently identified mechanism of corrosion fatigue. Hence, the corresponding stress-life curve (i.e. S-N curve) is presented for steel specimens in corrosive environments. It is further improved to derive a linear, bilinear or trilinear S-N curve for structural details of steel structures which are exposed to corrosive environments. The parameters of the S-N curve are proposed for the detail categories given in the Eurocode [66] and the DNV-GL code [67]. The proposed S-N curve formula is compared with full-scale fatigue test results of several structural details, and the validity of the formula is confirmed. The fatigue life of a railway bridge is estimated by using the proposed formula, and the results are compared with both deterministic and probabilistic conventional approaches.

2.2.1 S-N curve for steel specimens

Based on Basquin's law, the S-N curve formula for steel in corrosive environments is proposed. The environmental, metallurgical and structural factors are the governing parameters of the CF strength [8]. Negligible differences between low cycle fatigue (LCF) lives in corrosive and non-corrosive environments were observed in almost all the fatigue test results of steel specimens, with a significantly larger difference being observed in the very high cycle fatigue (VHCF) region [6, 17, 63, 64], and this is the main concept of the proposed curve. The degradation mechanism of CF and the derivation of the proposed formula are presented in Paper 2 [37], with the final formula shown in Eq. (1).

$$\sigma_{a.cor} = \left(\sigma_f' N_{f,LCF}^{c}\right) N_f^{(b-c)} \quad \text{where } c = \frac{\log \sigma_\infty - \log \sigma_{\infty,cor}}{\log N_{f,FL} - \log N_{f,LCF}} \tag{1}$$

where $\sigma_{a,cor}$ is the fatigue strength of corroded material, which corresponds to the number of cycles to fatigue failure, N_f as shown in Figure 3. The term σ_f' is the fatigue strength coefficient, and b is the Basquin exponent. The endurance limit (i.e. fatigue limit for HCF) is σ_∞, and $\sigma_{\infty,cor}$ is the endurance limit for the steel specimens in corrosive environments, which corresponds to a specified number of cycles, $N_{f,FL}$. When the stress amplitude is the yield strength, σ_y, the number of cycles to fatigue failure of the uncorroded material is $N_{f,LCF}$.

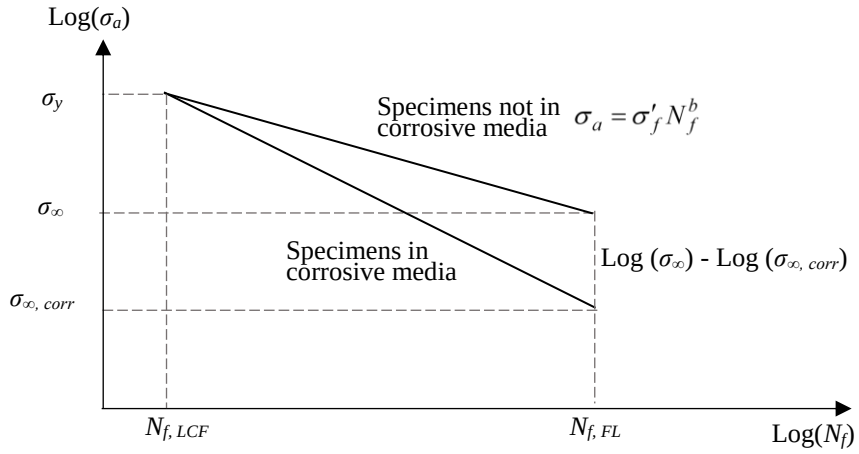

Figure 3. Schematic representation of fatigue strength degrdation of materials in corrrosive media

The values of σ_f', b, σ_∞, $N_{f,FL}$ and $N_{f,LCF}$ are determined from the *S-N* curve of steel specimens tested in air. The value of $\sigma_{\infty,cor}$ has to be determined by fatigue testing of pre-corroded and uncorroded steel specimens in a simulated corrosive environment in the VHCF region and is a complicated process. Therefore, Papers 2 and 3 in the thesis [37, 65] present a reasonably accurate relation to obtain $\sigma_{\infty,cor}$ for structural steels in natural water (i.e. similar to an urban environment) and seawater (i.e. similar to a marine environment). The determined mean and coefficient

of variation (COV) of the $\sigma_{\infty,cor}/\sigma_{\infty}$ ratio are 0.61 and 0.1, respectively, for steel in natural water. The conservative value for the $\sigma_{\infty,cor}/\sigma_{\infty}$ ratio is proposed as 0.5, by considering a 5% failure probability. Similarly, the mean and COV of the $\sigma_{\infty,cor}/\sigma_{\infty}$ ratio for steel in seawater are 0.46 and 0.59, respectively. The conservative value for the $\sigma_{\infty,cor}/\sigma_{\infty}$ ratio is proposed as 0.27.

2.2.2 S-N curve for structural members and joints

The formula for the S-N curve for steel specimens in corrosive media described above was further improved to develop *S-N* curves for structural details of steel structures (i.e. steel members, joints, connections, etc.) exposed to corrosive environments. The formula is obtained by modifying the design S-N curves of detail categories/detail classes of connections. The linear, bilinear or trilinear design S-N curves of details used in different fatigue codes can be modified to obtain the proposed S-N curve for structural details in corrosive environments. The derivation of the proposed formula is presented in Paper 3 [65]. The fatigue strength range of structural details in corrosive environments, $\Delta\sigma_{cor}$, and the corresponding number of cycles to fatigue failure, N_R, can be derived, if $\Delta\sigma_{cor} \geq \Delta\sigma_{D,cor}$,

$$\Delta\sigma_{cor} = \Delta\sigma_D \left[N_{f,LCF}^{c} N_{f,CAFL}^{1/m}\right] N_R^{(-c-1/m)} \quad (2)$$

$$\text{where } c = \frac{\log \Delta\sigma_D - \log \Delta\sigma_{D,cor}}{\log N_{f,CAFL} - \log N_{f,LCF}}$$

The $\Delta\sigma_D$ is the stress range at the fatigue curve slope changing point, which corresponds to the $N_{f,CAFL}$ cycles as shown in Figure 4. The $\Delta\sigma_D$ is defined as the constant amplitude fatigue limit [66]. The slope of the fatigue strength curve is -1/*m*. According to the Eurocode [66], *m* is equal to 3 when $\Delta\sigma \geq \Delta\sigma_D$, equal to 5 when $\Delta\sigma_D \geq \Delta\sigma > \Delta\sigma_L$ and infinite when $\Delta\sigma \leq \Delta\sigma_L$, where $\Delta\sigma_L$ is the fatigue endurance limit of the detail which corresponds to $N_{f,VAFL}$. The $N_{f,\,LCF}$ is the number of cycles to

fatigue failure of the details when stress range transits from the high cycle fatigue to the low cycle fatigue region. $\Delta\sigma_{D,cor}$ is the stress range at intersecting points of two slopes of fatigue curve of the details, exposed to corrosive environments, which is corresponding to $N_{f,CAFL}$ cycles. $\Delta\sigma_{L,cor}$ is the stress range corresponding to $N_{f,VAFL}$ cycles of the details, exposed to corrosive environments. These parameters and S-N curves of the structural details exposed to corrosive environments are clearly shown in Figure 4. If $\Delta\sigma_{cor} \leq \Delta\sigma_{D,cor}$, the fatigue strength range of structural details in corrosive environments has been derived as,

$$\Delta\sigma_{cor} = \Delta\sigma_{D,cor}\left[N_{f,CAFL}^{-\acute{c}}\right]N_R^{\acute{c}} \tag{3}$$

$$\text{where } \acute{c} = \frac{\log \Delta\sigma_{D,cor} - \log \Delta\sigma_{L,cor}}{\log N_{f,CAFL} - \log N_{f,VAFL}}$$

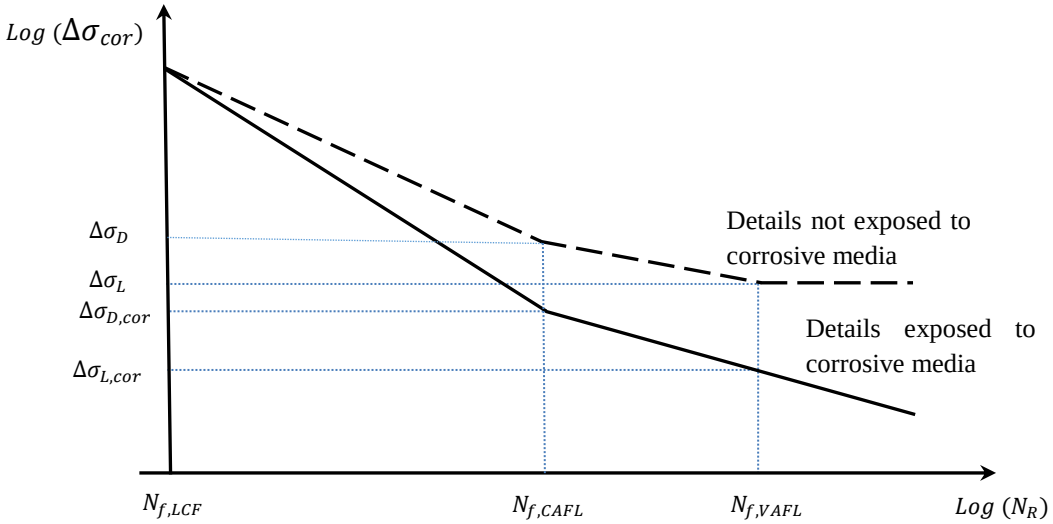

Figure 4. Schematic representation of S-N curve of structural details exposed to corrosive environments

The values of $\Delta\sigma_D, \Delta\sigma_L, m, N_{f,LCF}, N_{f,CAFL}$ and $N_{f,VAFL}$ are directly obtained from the code providing fatigue strength/S-N curves of structural details tested in air [66, 67]. The $\Delta\sigma_{D,cor}$ and $\Delta\sigma_{L,cor}$ are the corrosive state and the environment-dependent parameters of the detail. Papers 3 and 4 [65, 68] propose a reasonably accurate relation to obtain $\Delta\sigma_{D,cor}$ and $\Delta\sigma_{L,cor}$ for structural steels in the urban environment and in the marine environment, based on the parameters used in the proposed formula for steel specimens. The corresponding mean and conservative values (i.e. design value=mean-2×standard deviation) are listed in Table 1 for detail categories given in the Eurocode and DNV GL code.

Table 1. Parameters used in the proposed S-N curve for structural details exposed to corrosive environment

Parameter	Constructional details in Eurocode				Constructional details in DNV GL code			
$N_{f,LCF}$	10^4				10^4			
$N_{f,CAFL}$	5×10^6				10^7			
$N_{f,VAFL}$	10^8				10^8			
$\frac{\Delta\sigma_L}{\Delta\sigma_D}$	0.549				0.631			
Corrosion parameters	Marine environment		Urban environment		Marine environment		Urban environment	
	Mean value	Conservative value	Mean value	Conservative value	Mean value	Conservative value	Mean value	Conservative value
$\frac{\Delta\sigma_{D,cor}}{\Delta\sigma_D}$	0.497	0.308	0.641	0.536	0.46	0.27	0.61	0.50
$\frac{\Delta\sigma_{L,cor}}{\Delta\sigma_L}$	0.356	0.175	0.518	0.40	0.356	0.175	0.518	0.40

2.2.3 Verification of proposed S-N curve formula

The corrosion fatigue test results of full-scale structural details exposed to corrosive media are compared with predicted fatigue lives by the proposed formula (i.e. Eqs. (2) & (3)) to confirm its validity, in Papers 3 and 4 [65, 68]. The full-scale fatigue testing results of rolled plates fabricated from weathering steel [6, 69], corroded bridge girders extracted from Trolley Bridge [70], girth welded pipes [71], tubular joints [72], corroded rolled beams of A588 steel [6, 7], riveted joints, riveted plate and truss/lattice girders [73] are used for this experimental verification. The S-N curves predicted by the proposed formula are in a good agreement with the experimentally obtained fatigue lives of corroded structural details and the details exposed to corrosive environments. The curve prediction was also compared with the recently proposed strain-life model in Paper 4 [68] and a very good match was found between the proposed models.

2.2.4 Case study: Fatigue life estimation of a steel bridge

The fatigue assessment for a riveted railway bridge exposed to a urban environment was performed by both deterministic and probabilistic approaches in Paper 4 in the thesis [68]. The time-dependent loss of material due to uniform corrosion (i.e. corrosion wastage) changes the cross-sectional properties and, hence, the overall structural stiffness as well as the dynamic response of the bridge. The time-dependent nominal stress histories were obtained for the most critical riveted details of the bridge. The proposed S-N curve is directly used for fatigue life estimation by a deterministic approach. The formulation of a fatigue reliability index is modified by the corrosive parameters of the proposed S-N curve formula, to assess the fatigue lives through a probabilistic approach.

Three different methods were considered in this life estimation. In Method 1, lives were calculated based on a combination of nominal stress histories, without considering corrosion wastage, the uncorroded

S-N curve and Miner's rule [74]. A combination of the nominal stress ranges obtained by considering corrosion wastage, the S-N curve without cut-off limit (i.e. without constant amplitude fatigue limit) [21, 22, 42] and Miner's rule was used in Method 2. In Method 3 (i.e. proposed method), the calculation was performed based on a combination of the nominal stress ranges obtained by considering the corrosion wastage, the proposed S-N curve obtained by proposed formulas Eqs. (2) and (3) and Miner's rule. This comparison shows significant differences between the three methods and confirms the importance of using the proposed fatigue curve to perform safe life assessment of ageing steel bridges.

2.3 EAC susceptibility of structural steel in 3.5wt% NaCl media due to hydrogen charging

The susceptibility of ST52 steel and S355 steel to EAC was experimentally investigated by SSRT, and the results are presented in Paper 5 [75]. An experimental set-up was introduced and tensile test specimens prepared according to ASTM E8. The period of hydrogen charging and strain rates were the test variables. Stress versus strain curves were plotted and characteristic parameters were determined for 19 test specimens. Hence, EAC susceptibility/sensitivity indices were calculated, as shown in Table 2.

The table shows that the EAC susceptibility indices of all the stress-strain characteristic parameters (i.e. f_y, f_u, $L\%$ and $A\%$) are not very significant when ST52 steel is immersed in NaCl solution and subjected to SSRT. The susceptibility indices of all the stress-strain characteristic parameters are significant when specimens are immersed in NaCl solution, then subjected to hydrogen charging for a certain period and, thereafter, subjected to SSRT while charging hydrogen during straining. The table shows that there are increments of EAC susceptibility indices of $A\%$ and $L\%$ with the hydrogen pre-charged period. A clear pattern/scatter cannot be seen for these indices of f_y and f_u.

Fracture morphologies and scanning electron microscopy (SEM) analysis are presented in Paper 5 [75]. There is an obvious dimple morphology, which can be seen for fracture surfaces of the SSRT specimens tested in air and 3.5wt% NaCl media. Both fracture morphologies show the microvoid coalescence, which is the mechanism of ductile fracture. The morphologies of fracture surfaces of ST52 steel specimens tested under different corrosive environments with different hydrogen charging durations indicate a tendency for intergranular fracture, illustrating that the fracture surface shows the cleavage morphology. These observations and detailed analysis reveal that EAC susceptibility is low when ST52 is in 3.5wt% NaCl corrosive media (i.e. seawater). However, it is found that the CP process accelerates EAC susceptibility of ST52 steel by charging hydrogen, which decreases the ductility.

Table 2. EAC susceptibility indices with H pre-charged duration

Batch number	Hydrogen pre-charged duration (h)	EAC susceptibility index I_{EAC}%			
		A	L	f_y	f_u
1	0	0.66	3.67	0.94	0.14
2	2	8.54	15.51	3.03	2.56
3	3	9.95	10.90	3.48	1.48
4	5	9.91	16.84	2.25	1.02
5	10	13.79	22.29	1.64	1.45

2.4 HE susceptibility of martensitic carbon steel

Changes in the mechanical properties of AISI 4130 steel due to HE were investigated using SSRT and presented in Paper 6 in this thesis [76]. The heat treatment processes consisted of austenitization at 873 ^{o}C for about 45 minutes, quenching in a salt bath, and tempering at temperatures of between 350 ^{o}C and 550 ^{o}C for about one hour. Vickers hardness test was carried out and linear variation of tempering temperature was

observed with the Vickers hardness value. The SSRT were performed on both hydrogen pre-charged and uncharged samples, and stress-strain curves were plotted. Hence, a relative HE susceptibility index (I_{HE}) was calculated for the hydrogen-charged samples, as shown in Figure 5.

There was a reduction in cross-sectional area, *A*% of tensile tested samples decreased with the increasing hardness value (i.e. decreasing tempering temperature), as shown in Figure 5(a). The hydrogen-charged samples were subjected to a significant decrement of *A*%. Negligible *A*% reduction is observed for the material with hardness above 465 HV (i.e. tempered below 400 ^{o}C). There is a clear trend between tensile strength and hardness value for the samples tested in air, as shown Figure 5(b). In contrast, the tensile strength attained a constant value for the charged samples tempered below 460 $^{\circ}$C (hardness > 450 HV). Figure 5(c) shows the decrement in ductility (fracture strain) with increased hardness for the samples tested in air. The fracture strain reaches a constant value when hardness is greater than 465 HV (< 400 $^{\circ}$C) for charged samples.

The I_{HE} are calculated for each stress-strain curve of tempered states, with respect to the characteristic parameters of the tested samples. The I_{HE} of the fracture strain and the percentage reduction in cross-sectional area (*A*%) are plotted as a function of hardness in Figures 5 and 6, respectively.

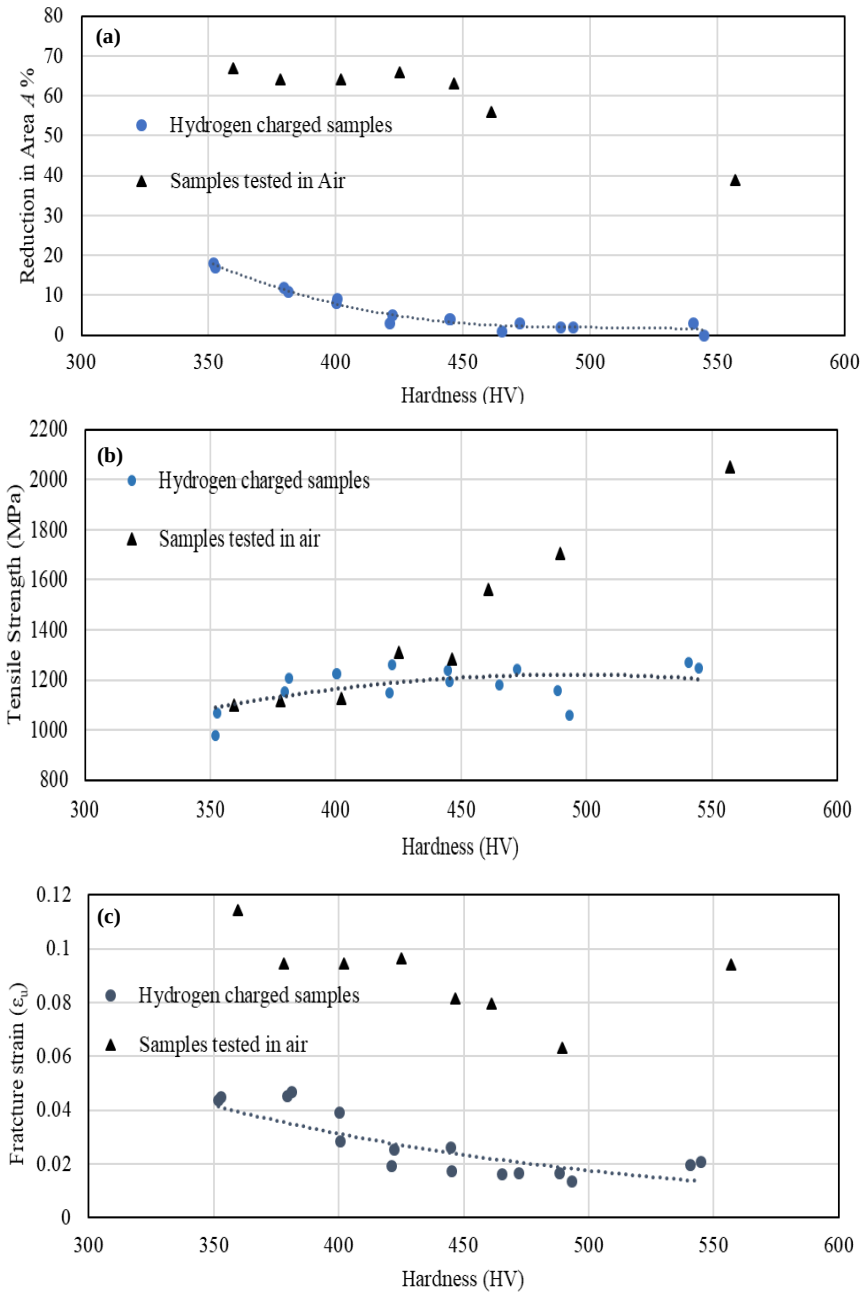

Figure 5. The relationship between hardness and (a) reduction of cross-sectional area, (b) tensile strength, (c) fracture strain

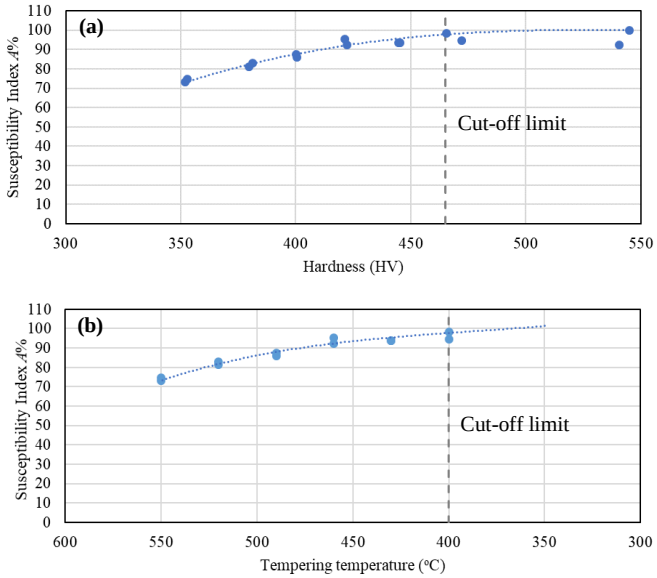

Figure 6. HE susceptibility index of reduction of cross-sectional area of the AISI 4130 samples versus (a) hardness, (b) tempering temperature

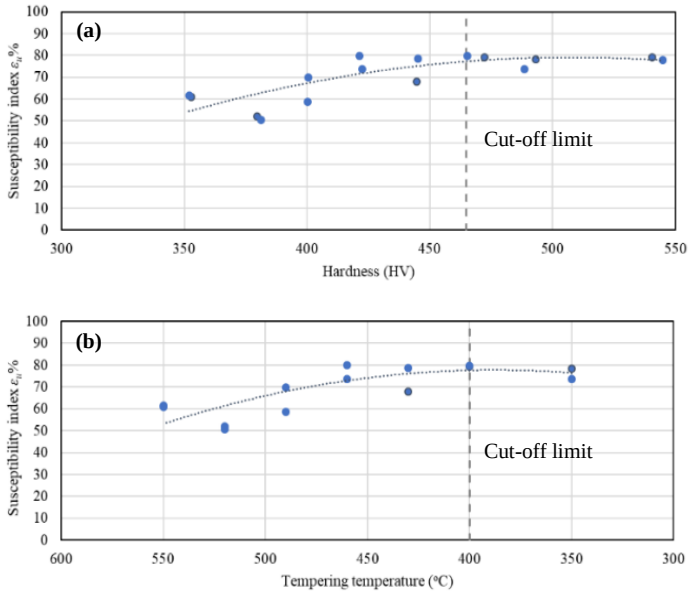

Figure 7. HE susceptibility index of fracture strain of the AISI 4130 samples versus (a) hardness, (b) tempering temperature

Figure 6(a) shows a significant increment in the HE susceptibility index of *A%* with the hardness value. HE susceptibility of more than 70% is observed for all the samples. For samples with hardness of 465 HV and above, 100% HE susceptibility is observed. Similarly, 100% HE susceptibility is also observed for samples heat-treated below 400 ^{o}C tempering temperature, as shown in Figure 6(b). Figure 7(a) shows the increment in the HE susceptibility index of fracture strain with the hardness. HE susceptibility of more than 50% is observed for all the samples. HE susceptibility of about 80% is observed for material with hardness greater than 465 HV. This suggests that the AISI 4130 material is most likely subjected to HE due to hydrogen charging when the hardness exceeds 465 HV. It is also accompanied by a loss of ductility. Similarly, Figure 7(b) shows that about 80% of the samples which were tempered at temperatures lower than 400 ^{o}C are susceptible to HE. In general, the study shows that AISI 4130 is susceptible to HE due to hydrogen charging when the tempering temperature is below 400 ^{o}C. Those samples which were quenched and subjected to tempering temperature of 400 ^{o}C and less are 100% susceptible to HE when considering the susceptibility of *A%*.

Microstructural characterizations and fracture surface analysis were performed by transmission electron microscopy (TEM) and SEM. The fracture surface analysis of such samples shows a transition of the failure mechanism from ductile microvoid coalescence to brittle intergranular cracking. TEM analysis reveals carbide precipitates at tempering temperatures of 490 $^{\circ}$C and higher. The AISI 4130 was subjected to HE due to hydrogen charging when the hardness value was 465 HV and greater, corresponding to tempering temperatures 400 $^{\circ}$C and lower.

Chapter 3 Conclusions

3.1 Summary

This research was conducted in three phases. A detailed review of environment-assisted corrosion damage of steel bridges was performed in the first phase and, hence, a conceptual framework for structural integrity was proposed (Paper 1). The second phase of the study focused on filling the research gap regarding CF of steel bridges. A generalized S-N curve was proposed for structural details of bridges which are exposed to corrosive environments, and this was applied to a case study bridge (Papers 2, 3 and 4). The proposed formula is novel and it provides a best practice for bridge engineers. The last phase of the study focused on experimentally investigating the HE and SCC susceptibility of commonly used steel types of bridges (Papers 5 and 6). This provides new knowledge/information for researchers and practising engineers.

A framework was presented in the first phase of the study to assess the structural integrity of steel bridges in respect of environment-assisted corrosion damage. Forms of corrosion of steel bridges, their effects, possible locations of occurrence and most appropriate inspection techniques are first studied, and lessons learned from past steel bridge failures are discussed. A review of the corrosion damage of steel bridges, including causes, effects and control measures, is presented, along with a guideline for the recognition and investigation of EAC of steel bridges. In the framework, experimental approaches were proposed, to investigate the EAC of structural steel. The framework aims to support the inspection and maintenance practices of steel bridges.

In the second phase of this study, a formula is proposed to predict the fatigue strength of joints and members of steel bridges located in corrosive environments. The concept of the formula is first studied from

the recently identified mechanism of CF. Hence, the corresponding fatigue strength curve (i.e. S-N curve) is presented for steel in corrosive environments. It is further improved, in order to derive a linear, bilinear or trilinear S-N curve for structural details of steel structures which are exposed to corrosive environments. The corrosive environment-dependent parameters of the S-N curve are determined, based on the CF testing results of different types of steel specimens in air, fresh water and seawater. The parameters are presented for the detailed categories given in the Eurocode and the DNV GL code. The proposed S-N curve formula is compared with full-scale fatigue test results of several structural details, and the validity of the formula is confirmed. The fatigue life of a riveted railway bridge is estimated by using the proposed formula, and the results are compared with both deterministic and probabilistic conventional approaches. The formulation of a fatigue reliability index is modified by the corrosive parameters of the proposed S-N curve formula, to assess the fatigue lives by a probabilistic approach. The applicability and significance of the proposed curve are then confirmed.

The susceptibility of ST52 steel to EAC is experimentally investigated by SSRT in Phase 3 of this research project. An experimental set-up is introduced, and tensile test specimens are prepared according to ASTM E8. The strain rate, duration of CP and NaCl concentration are the test variables. The stress-strain curve characteristic parameters (i.e. yield strength f_y, tensile strength f_u, percentage of elongation L%, and percentage reduction of cross-sectional area A%) are determined; hence, EAC susceptibility indices were calculated, by comparing the stress-strain characteristic parameters of specimens tested in the control environment. Hence, EAC susceptibility indexes are calculated. SEM analysis was performed for the fracture surfaces of the specimens, and the obtained fracture morphologies are analysed.

In another part of Phase 3 of the research, the change in the mechanical properties of tempered high-strength carbon steel (AISI 4130) due to HE was investigated, using SSRT. The heat treatment processes consisted of

austenitization at 873 ^{o}C for about 45 minutes, quenching in a salt bath, and tempering at temperatures between of 350 ^{o}C and 550 ^{o}C for about one hour. The SSRT were performed on both hydrogen pre-charged and uncharged samples. Vickers hardness test was carried out to study the variation in hardness with the tempering temperature. Microstructural characterizations and fracture surface analysis were carried out by the use of SEM and TEM. The fracture surface analysis of such samples shows a transition in the failure mechanism from brittle intergranular cracking at the lowest tempering temperature to ductile microvoid coalescence at the highest temperature.

3.2 Concluding remarks

The following general conclusions are made, based on the outcomes of this research study.

1. The detailed investigation of bridge failures and their causes reveals two main shortcomings in current bridge inspection/investigation practices: (i) lack of understanding and/or clear guidance in order to recognize the mechanisms of corrosion, locations where corrosion generally occur in steel bridges, their effects and inspection limitations; (ii) lack of resources for NDT and/or microscopic examinations.

   Although the interaction effect of SCC, HE and CF can be observed in existing bridges, failure finally happens due to EAC. This is commonly dependent on the rate of the effect of environmental, metallurgical and structural factors and the progress of corrosion. Therefore, inspectors should be capable of identifying the dominant EAC mechanism/s for the component, by identifying the material, stress state and environment. Uniform, pitting, galvanic, crevice and intergranular corrosion generally interact with EAC to degrade the mechanical properties and finally govern the failure/fracture of ageing steel bridges.

2. The proposed S-N curve formula of steel specimens exposed to corrosive environments shows a good match with fatigue test results of different steel types. This comparison concludes the validity of the proposed mean and conservative values for parameters used in the formula. The proposed curve does not require any material parameter or corrosive environment-specific parameter, except the S-N curve obtained in air.

   The derived S-N curves for steel members and joints exposed to corrosive environments are in good agreement with the experimentally obtained fatigue lives of corroded or uncorroded structural details which are exposed to corrosive environments. The physics behind the CF has been studied from the literature in a micro-structural level and specimen scale and finally incorporated into a structural member and joint scales. This is the main reason for having good agreement with the full-scale fatigue test results. The values of the curve parameters have been proposed only for detail categories given by Eurocode and DNV GL code. The same procedure can be utilized with the values proposed for the steel specimens, to determine the model parameters for other detail categories given in other codes. The main advantage of the proposed formula is that it requires only the S-N curve of the structural detail in air, which is given in relevant codes, to predict the corresponding S-N curve in corrosive media.

   The fatigue life of a riveted bridge is estimated by using the proposed S-N formula, and the results are compared with both deterministic and probabilistic conventional approaches. Fatigue lives calculated by a deterministic approach show a significant reduction when the effect of corrosion is considered. This reduction is not significant when probabilistic fatigue life

estimation is used, as this approach takes into account the uncertainties of the mean S-N curve and stress evaluation. These reductions in fatigue lives further highlight the importance of having accurate S-N curves for ageing bridges for conservative maintenance practices.

3. The observations and analysis of EAC susceptibility investigations reveal that EAC sensitivity/susceptibility is low when ST52 is in 3.5wt% NaCl corrosive media (i.e. simulated seawater). However, it is found that the CP process accelerates the EAC susceptibility of ST52 steel by charging hydrogen, which decreases the ductility. The duration of the CP process increases the tendency of fracture in ST52 steel. This conclusion may be common for other types of structural steels.

4. Investigation of the HE susceptibility of tempered high-strength carbon steel reveals that the hydrogen pre-charging causes embrittlement of AISI 4130 steel. The HE susceptibility index of the reduction in the cross-sectional area is 100% when the hardness value is greater than 465 HV. The HE susceptibility index of fracture strain (i.e. strain to failure) is about 80% when hardness is greater than 465 HV. The percentage reduction in the cross-sectional area is negligible when the hardness is above 465 HV. The fracture surface examinations showed the transition from ductile microvoid coalescence to brittle intergranular cracking where hardness is above 465 HV. Thus, high-strength carbon steel, AISI 4130, is subjected to HE due to hydrogen charging when the hardness value exceeds 465 HV.

   The maximum ultimate tensile strength and ultimate fracture strain can be conservatively considered as 1200MPa and 0.02, respectively, for hydrogen precharged high-strength carbon steel, AISI 4130. As-quenched samples have the highest hydrogen

embrittlement susceptibility and are subjected to intergranular cracking due to hydrogen charging when the hardness is above 465 HV. The fracture behaviour of AISI 4130 steel is ductile and hydrogen embrittlement susceptibility decreases when tempering temperature is higher than 400 ^{o}C.

3.3 Recommendations for future research

Problems identified for future studies are briefly mentioned below.

1. The S-N curve should be verified for the giga-cycle fatigue region, tested in corrosive media. Application of the proposed S-N curve for different types of steel bridges is required, to identify the significance of the proposed curve.
2. The effect of the strain rate and the cathodic potential for EAC susceptibility of structural steel will be studied in the future.
3. The HE susceptibility of tempered high-strength carbon steel and a few more types of long-span bridge materials should be investigated by SSRT of hydrogen-charged samples for limiting mechanical properties.
4. Improvement of existing S-N curve based non-linear fatigue damage models to take into account the corrosion effect.

References

1. Imam BM, Righiniotis TD. Fatigue evaluation of riveted railway bridges through global and local analysis. *J. Constr. Steel. Res*. 2010; 66: 1411-1421.
2. Helmerich R, Kuhn B, Nussbaumer A. Assessment of existing steel structures: A guideline for estimation of the remaining fatigue life. *J. Struct. Infrastruct. Eng*. 2007; 3: 245-255.
3. Adasooriya ND. Fatigue reliability assessment of ageing railway truss bridges: Rationality of probabilistic stress-life approach. *Case Studies in Struct Eng.* 2016; 6: 1-10.
4. Adasooriya ND, Siriwardane SC. Remaining fatigue life estimation of corroded bridge members. *Fat. Fract. Eng. Mater. Struct*. 2014; 37: 603-622.
5. Larsson T. *Fatigue assessment of riveted bridges.* PhD dissertation. Sweden: Luleå University of Technology; 2009.
6. Aghoury I El. *Numerical tool for fatigue life prediction of corroded steel riveted connections using various damage models.* PhD thesis. Canada, Montreal: Concordia University; 2012.
7. Aghoury I El, Galal K. Corrosion-fatigue strain-life model for steel bridge girders under various weathering conditions. *J. Struct. Eng*. 2014; 140 (6): Article number 04014026.
8. Yasser Y, Jeom KM. Ultimate strength reliability analysis of corroded steel-box girder bridges. *Thin Wall. Struct.* 2011; 49: 157-166.
9. Lima K, Robson N, Oosterhof S, Kanji S, DiBattista J, Montgomery CJ. Rehabilitation of a 100-year-old steel truss bridge. *CSCE 2008 Annual Conference*, June 10-13; 2008.
10. Nakamura S, Suzumurab K. Hydrogen embrittlement and corrosion fatigue of corroded bridge wires. *J. Constr. Steel. Res.* 2009; 65: 269-277.

11. Yukikazu Y, Makoto K. Maintenance of steel bridges on Honshu-Shikoku crossing. *J. Constr. Steel. Res.* 2002; 58: 131-150.
12. Li ZX, Chan THT. Fatigue criteria for integrity assessment of long span steel bridge health monitoring. *Theo. & App. Fracture Mechanics* 2006; 46: 114-127.
13. Kulicki JM, Prucz Z, Sorgenfrei DF, Young WT. Guidelines for evaluating corrosion effects in existing steel bridges, National Cooperative Highway Research Program Report 333, Transportation Research Board, National Research Council, Washington D.C.; 1990.
14. Kayser JR. *The effects of corrosion on the reliability of steel girder bridges*. PhD thesis, Michigan, USA: University of Michigan; 1988.
15. Paik JK, Lee JM, Ko MJ. Ultimate shear strength of plate elements with pit corrosion wastage. *Thin Wall. Struct.* 2004; 42: 1161-1176.
16. ECCS. WG-A, TC6, Assessment of Existing Steel Structures, final draft 08, ECCS: Brussels, 2004.
17. Revie RW, Uhlig HH. *Corrosion and Corrosion Control, An Introduction to Corrosion Science and Engineering*, 4th edn., Wiley and Sons; 2008.
18. Roberge PR. *Handbook of Corrosion Engineering*, 1st edn., McGraw Hill, New York; 2000.
19. Chung Y, Fulton LK. Environmental hydrogen embrittlement of G41400 and G43400 steel bolting in atmospheric versus immersion services. *J. Fail. Ana. Prev.* 2017; 17; 330-339.
20. Mohamed ELM, Thierry PL, Nicolas S, Olivier D. Effect of corrosion on the high cycle fatigue strength of martensitic stainless steel X12CrNiMoV12-3. *Int. J. Fatigue.* 2013; 47: 330-9.
21. Wahab MA, Sakano M. Corrosion and biaxial fatigue of welded structures. *J. Mat. Proc. Tech. 3.* 2003; 143-144: 410-415.

22. Nguyen KT, Garbatov Y, Soares CG. Spectral fatigue damage assessment of tanker deck structural detail subjected to time-dependent corrosion. *Int. J. Fatigue.* 2013; 48:147-155.
23. Thomas L. Lessons learned from the Bay Bridge bolt failure. *Structural Forensics.* 2017; 10-13.
24. Rolla EP. Stress-corrosion tests of bridge cable wire. *J. Res. Nat. Bure. Stand.* 1944; 33: 201-211.
25. Mikkelsen O, Rege K, Hemmingsen T, Pavlou D. Numerical estimation of the stop holes-induced fatigue crack growth retardation in offshore structures taking into account the corrosion effect. *Proceeding of International Society of Offshore and Polar Engineers Conference Series*. San Francisco: American Society of Mechanical Engineers; 2007: ISOPE-I-17-552: 451-458.
26. FHWA NHI 12-049, *Bridge Inspector's Reference Manual*, BIRM Vol. 1, Federal Highway Administration, US Department of Transportation and National Highway Institute; 2012.
27. BD 56/10, The assessment of steel highway bridges and structures, *Design manual for Road and Bridges*, Vol. 3, Section 4, Part II, UK Highway Agency; 2010.
28. Struzinsky M. *Bridge Inspection Manual*, Department of Transportation, New York; 2016.
29. JICA Report 12307708, *Bridge Inspection Manual*, General Directorate of Techniques, Road Infrastructure Department, Ministry of Public Works and Transport; 2018.
30. Pipinato A. Steel bridges: Codes, design specifications and construction issues. Bridge Maintenance, Safety, Management and Life Extension - *Proceedings of the 7th International Conference of Bridge Maintenance, Safety and Management*, IABMAS; 2014: 1891-1898.
31. Siviero E, Pavan R. Assessment of existing steel bridges: codes and standard. *IOP Conf. Series: Mat. Sci. Eng.* 2018; 419.
32. Adasooriya ND, Siriwardane SC. Remaining fatigue life estimation of corroded bridge members. *Fatigue Fract. Eng. Mater. Struct*. 2014; 37: 603-622.

33. Hoeppner DW, Chandrasekaran V, Taylor AMH. Review of pitting corrosion fatigue models. *Proceedings of ICAF International Conference*. Melbourne, Australia: 1995: 1-25.
34. Acuña N, González-Sánchez J, Ku-Basulto G, Domınguez L. Analysis of the stress intensity factor around corrosion pits developed on structures subjected to mixed loading. *Scripta Materialia.* 2006; 55: 363-366.
35. Ian T. *The effect of notches and pits on corrosion fatigue strength.* PhD thesis. UK: Sheffield Hallam University; 2004.
36. Sharifi Y, Rahgozar R. Fatigue notch factor in steel bridges due to corrosion. *Arch. Civil and Mech. Eng.* 2009; 9: 75-83.
37. Adasooriya ND, Hemmingsen T, Pavlou D. Fatigue strength degradation of metals in corrosive environments. *Proceedings of first conference of computational methods in offshore technology-COTech 2017, IOP Conf Ser: Mater Sci Eng*: IOP Publishing; Stavanger, Norway; 2017: Article number 276 012039.
38. Zhao T, Liu Z, Du C, Dai C, Li X, Bowei Z. Corrosion fatigue crack initiation and initial propagation mechanism of E690 steel in simulated sea water. *Mat. Sci. & Eng. A*. 2017; 708: 181-192.
39. Vucko F, Bosch C, Delafosse D. Effects of cyclic plastic strain on hydrogen environment assisted cracking in high-strength steel. *International Hydrogen Conference (IHC 2012): Hydrogen-Materials Interactions*. WY, United States: American Society of Mechanical Engineering; 2012.
40. Vucko F, Bosch C, Aoufi A, Delafosse D. *Palladium coating on quenched-tempered martensitic steel for hydrogen electrochemical permeation tests. Technical Reports-ENSMSE-SMS-2014-01*. France: EMSE-00951142; 2014.
41. Wang R. *Corrosion fatigue of metal materials*. Xi'an: Press of Northwestern Polytechnical University; 2001.
42. Gerhard S, Christian K, Bertram K, Hensen W. *Condition assessment and inspection of steel railway bridges, including stress measurements in riveted, bolted and welded structures:*

Sustainable Bridges-Background document SB3.4. Sweden: Digital Vetenskapliga Arkivet; 2007.

43. Tiwari GP, Bose A, Chakravartty JK, Wadekar SL, Fotedar RK. A study of internal hydrogen embrittlement of steels. *Mat. Sci. Eng.: A.* 2000; 286: 269-281.
44. Eliaz N, Shachar A, Tal B, Eliezer D. Characteristics of hydrogen embrittlement, stress corrosion cracking and tempered martensite embrittlement in high-strength steels. *Eng Fail. Anal.* 2002; 9(2):167-184.
45. Kim, SJ, Jang SK, Kim J. Electrochemical study of hydrogen embrittlement and optimum cathodic protection potential of welded high strength steel. *Met. Mat. Inter.* 2005; 11: 63-69.
46. Venkatesh A, Kane RD. Fracture analysis of slow strain rate test for stress corrosion cracking. *NACE Corrosion 2009 Conference and Expo*; 2009; Paper No. 092996.
47. Espinosa-Medina MA, Sosa E, Angles-Chavez C, Contreras A. Assessment of pH and temperature effects on stress corrosion cracking of 1018 low carbon steel. *Corr. Eng. Sci. Tech.* 2011; 46: 32-41.
48. Depover T, Pérez Escobar D, Wallaert E, Zermout Z, Verbeken K. Effect of hydrogen charging on the mechanical properties of advanced high strength steels. *Inter. J. Hyd. Energy* 2014; 39: 4647-4656.
49. Ma H, Liu Z, Du C, Wang H, Li X. Effect of cathodic potentials on the SCC behavior of E690 steel in simulated seawater. *Mat. Sci. Eng. A.* 2015; 642: 22-31.
50. Rhode M, Steger J, Boellinghaus T, Kannengiesser T. Hydrogen degradation effects on mechanical properties in T24 weld microstructures. *Weld World* 2016; 60: 201-216.
51. Rosenberg G, Sinaiova I. Evaluation of hydrogen induced damage of steels by different test method. *Mat. Sci. Eng. A*. 2017; 682: 410-422.
52. Lai CL, Tsay LW, Chen C. Effect of microstructure on hydrogen embrittlement of various stainless steels. *Mat. Sci. Eng. A.* 2013; 584: 14-20.

53. Gjerding-Smith K, Johnsen R, Lange HI, Leinum BH, Gundersen G, Isaksen B, Nærum G. Wire fractures in locked coil cables. *Bridge Stru. Ass., Design and Constr.* 2007; 2: 63-77.
54. Zheng Y, Wang F, Li C, Lin Y, Cao R. Effect of martensite structure and carbide precipitates on mechanical properties of Cr-Mo alloy steel with different cooling rate. *High Temp. Mat. Proc.* 2019; 28: 113-124.
55. Nanninga N, Grochowsi J, Heldt L, Rundman K. Role of microstructure, composition and hardness in resisting hydrogen embrittlement of fastener grade steels. *Corrosion Science* 2010; 52: 1237-1246.
56. Hernandez VHB, Nayak SS, Zhou Y. Tempering of martensite in dual-phase and its effect on softening behavior. *Metallur. Mat. Transactions A* 42 2011; Article number: 3115.
57. Marchetti L, Herma E, Laghoutaris P, Chêne J. Hydrogen embrittlement susceptibility of tempered 9%Cr–1%Mo steel. *Int. J. Hydr. Energy* 2011; 36: 15880-15887.
58. Das T, Rajagopalan SK, Brahimi SV, Wang X, Yue S. A study on the susceptibility of high strength tempered martensite steels to hydrogen embrittlement (HE) based on incremental step load (ISL) testing methodology, *Mat. Sci. Eng. A* 2018; 716: 189-207.
59. Djukic MB, Bakic GM, Zeravcic VS, Rajicic B, Sedmak A, Mitrovic R, Miskovic Z. Towards a unified and practical industrial model for prediction of hydrogen embrittlement and damage in steels. *Proc. Struc. Integrity* 2016; 2: 604-611.
60. Djukic MB, Zeravcic VS, Bakic GM, Sedmak A, Rajicic B. Hydrogen damage of steels: A case study and hydrogen embrittlement model, *Eng. Fail. Analy.* 2015; 58: 485-498.
61. Michler T, Naumann J. Microstructural aspects upon hydrogen environment embrittlement of various BCC steels, *Inter. J. of Hydr. Energy* 2010; 35: 821-832.
62. Adasooriya ND, Hemmingsen T, Pavlou D. Environmental assisted corrosion damage of steel bridges: A conceptual

framework for structural integrity. *J. Corrosion Reviews;* 2019; 1-17. https://doi.org/10.1515/corrrev-2019-0066

63. Glaser W, Wright LG. *Mechanically Assisted Degradation. ASM Handbooks*. ASM Internationals; 1992: 137-144.
64. Gangloff RP. Environmental cracking - corrosion fatigue, In: Baboian R, Dean Jr. SW, Hack HP, Hibner EL, Scully JR, eds. *Corrosion Tests and Standards Manual*. ASTM Internationals; 2005.
65. Adasooriya ND, Pavlou D, Hemmingsen T. Fatigue strength degradation of corroded structural details: A formula for S-N curve. *Fat. Fract. Eng. Mater. Struct.*2019; 1-13. https://doi.org/10.1111/ffe.13156
66. NS EN 1993-1-9. *Eurocode 3: Design of steel structures - Part 1-9: Fatigue*. Belgium: European Committee for Standardization; 2005.
67. DNV GL Recommended practices. *Fatigue design of offshore steel structures DNVGL-RP-0005*. Norway: Det Norske Veritas; April 2016.
68. Adasooriya ND, Hemmingsen T, Pavlou D. S-N curve for riveted details in corrosive environment and its application to a bridge. *Fat. Fract. Eng. Mater. Struct.* 2020; 1-15. https://doi.org/10.1111/ffe.13193
69. Kunihiro T, Inove K, Fukuda T. *Atmospheric exposure study of weathering steel*. *Research Lab. Report Br. 71-08*. Tokyo, Japan: Ministry of Construction; 1972.
70. Albrecht P, Shabshab CF, Wulin L. Remaining fatigue strength of corroded steel Beams, *IABSE reports*. International Association of Bridge and Structural Engineering Publications; 1990: 71-84.
71. Zhang YH, Maddox SJ. Fatigue testing of full-scale girth welded pipes under variable amplitude loading. *J. Offshore Mechanics and Arctic Eng*. 2014; 021401-1-10.
72. HSE OTH 92 390. *Background to new fatigue guidance for steel joints and connections in offshore structures, offshore technology report.* UK: Health Safety Executives; 1999.

73. Larsson T. *Fatigue assessment of riveted bridges.* PhD dissertation. Sweden: Luleå University of Technology; 2009.
74. Miner MA. Cumulative damage in fatigue. *J. Appl. Mech*. 1945; 12: 159-64.
75. Adasooriya ND, Hemmingsen T, Pavlou D. An Experimental Study on Environmental Assisted Cracking of Structural Steel in 3.5 wt% NaCl Solution, *ISOPE -2019: The 29th International Ocean and Polar Engineering Conference*, 16-21 June, Honolulu, Hawaii, USA, ID: ISOPE-I-19-522, pp. 4154-4160.
76. Adasooriya ND, Tucho WM, Holm E, Årthun T, Hansen V, Solheim KG, Hemmingsen T. Effect of hydrogen on mechanical properties and fracture of martensitic high strength carbon steel under quenched and tempered conditions, *J. Material Science & Engineering A* (Under review).

Appended Papers

Paper 1	Adasooriya ND, Hemmingsen T, Pavlou D. Environmental assisted corrosion damage of steel bridges: A conceptual framework for structural integrity. *Corrosion Reviews*. 2019; 1-17. https://doi.org/10.1515/corrrev-2019-0066.
Paper 2	Adasooriya ND, Hemmingsen T, Pavlou D. Fatigue strength degradation of metals in corrosive environments. *Proceedings of First Conference of Computational Methods in Offshore Technology-COTech 2017, IOP Conference Series: Materials Science & Engineering*: IOP Publishing; Stavanger, Norway: 2017: Article number 276 012039.
Paper 3	Adasooriya ND, Pavlou D, Hemmingsen T. Fatigue strength degradation of corroded structural details: A formula for S-N curve. *Fatigue & Fracture of Engineering Materials & Structures.* 2019; 1-13. https://doi.org/10.1111/ffe.13156.
Paper 4	Adasooriya ND, Hemmingsen T, Pavlou D. S-N curve for riveted details in corrosive environment and its application to a bridge. *Fatigue & Fracture of Engineering Materials & Structures.*2020; 1-15. https://doi.org/10.1111/ffe.13193
Paper 5	Adasooriya ND, Hemmingsen T, Pavlou D. An experimental study on environmental assisted cracking of structural steel in 3.5 wt% NaCl Solution, *ISOPE* -

	2019: The 29th International Ocean and Polar Engineering Conference, 16-21 June, Honolulu, Hawaii, USA, ID: ISOPE-I-19-522, pp. 4154-4160.
Paper 6	Adasooriya ND, Tucho WM, Holm E, Årthun T, Hansen V, Solheim KG, Hemmingsen T. Effect of hydrogen on mechanical properties and fracture of martensitic carbon steel under quenched and tempered conditions, *Journal of Material Science & Engineering A* (under review).

Paper 1

Environment-Assisted Corrosion Damage of Steel Bridges: A Conceptual Framework for Structural Integrity

Journal Paper

Corrosion reviews

Published Online 2019

Paper 2

Fatigue Strength Degradation of Metals in Corrosive Environments

Conferences Paper

Conference of Computational Methods in Offshore Technology, COTech 2017

Stavanger, Norway

Fatigue strength degradation of metals in corrosive environments

IOP Conf. Series: Materials Science and Engineering **276** (2017) 012039 doi:10.1088/1757-899X/276/1/012039

Fatigue strength degradation of metals in corrosive environments

N D Adasooriya*, T Hemmingsen and D Pavlou

Department of Mechanical and Structural Engineering and Materials Science, University of Stavanger, Norway

*Contact author: mudiyan.n.adasooriya@uis.no

Abstract. Structures exposed to aggressive environmental conditions are often subjected to time-dependent loss of coating and loss of material due to corrosion; this causes reduction in the cross-sectional properties of the members, increased surface roughness, surface irregularities and corrosion pits, and degradation of material strengths. These effects have been identified and simulated in different research studies. However, time and corrosive media dependent fatigue strength curves for materials have not been discussed in the design or assessment guidelines for structures. This paper attempts to review the corrosion degradation process and available approaches/models used to determine the fatigue strength of corroded materials and to interpolate corrosion deterioration data. High cycle fatigue and full range fatigue life formulae for fatigue strength of corroded materials are proposed. The above formulae depend on the endurance limit of corroded material, in addition to the stress-life fatigue curve parameters of the uncorroded material. The endurance limit of corroded material can either be determined by a limited number of tests in the very high-cycle fatigue region or predicted by an analytical approach. Comparison with experimentally measured corrosion fatigue behavior of several materials is provided and discussed.

1. Introduction

Corrosion is one of the principal deterioration processes that affect the integrity of structures. Major effects can be listed as thickness reduction, irregularities of the surfaces, surface roughness, and stress concentration due to the pitting and degradation of material due to the electrochemical process. The cracking of members especially starts at highly stressed locations. Thickness reduction, surface roughness and cyclic loading accelerate the crack initiation under different types of corrosion [1]. Cracks caused by corrosive media are mainly governed by environmental assisted cracking (EAC) such as stress corrosion cracking (SCC), corrosion fatigue (CF), sulfide stress cracking, etc. CF and SCC play a significant role in the degradation of metal structures. Fractures due to cyclic stress in corrosive media are designated as CF. SCC is generally defined as failure caused by continuously applied stress in corrosive media. Researchers are still highlighting the significance of further study on CF [2-4], due to the inherent nature of corrosion and its effects on random fatigue behavior.

Recent failures of key structures such as Silver Bridge in 1967, Mianus River Bridge in 1990, Minnesota Bridge in 2007, etc., emphasize the importance of more accurate simulation of CF in

different corrosive environments in respect to different structural materials. Therefore, the consideration of the corrosion effects on structural integrity is important [3,5].

This paper reviews the effects of CF in structural degradation. Initially, the paper describes the corrosion degradation process of metallic materials. Then methods for modeling CF are comprehensively reviewed. New formulae for determining the fatigue strength of corroded material are proposed as an original contribution of this paper. The proposed formulae are compared with published results of the experimentally measured CF behavior (i.e. fatigue test of corroded specimens) of several steel types.

2. Corrosion degradation process of metalic materials

Corrosion of steel is an electrochemical process, which starts with the presence of oxygen and water. Common agents such as carbon dioxide, sodium chloride and hydrogen sulfide affect this process. The corrosion mechanism of iron can be described as follows: oxidation of iron takes place when dissolution of iron produces ferrous iron (Fe^{2+}) at the anode with the presence of various impurities. At the cathode, oxygen produces hydroxide irons(OH^-).Then Fe^{2+} and OH^- iron combine to form ferrous hydroxide ($Fe(OH)_2$).Further oxidation of ferrous hydroxide produces rust ($Fe_2O_3.H_2O$). Corrosion pits, corrosion products on surfaces, uneven surfaces, loss of material and degradation of material strength can be seen as outcomes of the above electrochemical process [3,6]. Generally, structures are subjected to five of the most important forms of corrosion [6,7], the most common of which is general (uniform) corrosion, which is uniformly distributed on the surface. General corrosion often occurs in locations where water accumulates [6,8]. Pitting corrosion is a localized form of corrosion which is restricted to a small area and usually begins with an irregularity on the surface. This type is dangerous because it may cause local stress concentrations. Crevice corrosion is also a form of localized corrosion, occurring where different components of the structure are close together, leading to narrow spaces. Galvanic corrosion takes place when two different metals are placed in an electrolyte and are electrically connected, as is possible at bolted or welded connections. The last dominant form of corrosion is CF, which is the mechanical degradation of a material under the combined action of localized corrosion and cyclic loading [8]. Fractures due to corrosion fatigue are often transgranular. The effect of CF on structural integrity is reported as significant for most situations [2,3,6-8,10].

The effects of corrosion deterioration to metal structures yields; (i) reductions of the effective cross-sectional area, moment of inertia, torsional and warping constants [6,11-14]. This may change the overall stiffness of the structures and hence change the stress state in the remaining part of the material/member; (ii) Interaction of corrosion (i.e. mostly pitting and crevice) and cyclic loading affects the mechanical properties of metal and, hence, cracks initiate from the corrosion-induced surface (i.e. CF); thereby a significant decrease in the fatigue strength (i.e. degrade the S-N curve in air) can be observed [7, 15-17] as shown in Figure 1. Finally, these may cause a reduction of the fatigue life of metal structures which are subjected to loss of coating, rust or corrosion wastage.

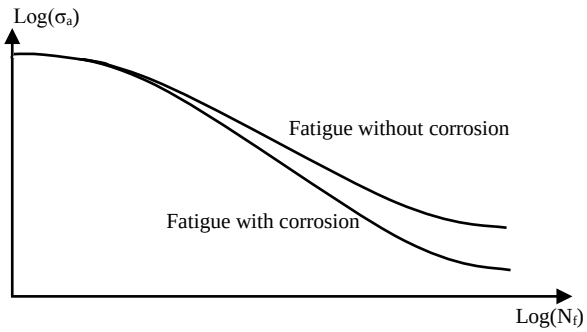

Figure 1. Fatigue behaviour of metals with and without corrosion

The behavior of the fatigue strength of corroded metals depends on various parameters such as types of corrosion, type and state of corrosive environment, rate of corrosion, chemical composition of the metal, etc. [18]. Generally, laboratory fatigue testing of corroded samples is popular for simulating the fatigue strength behavior of corroded materials [3]. However, it is obvious that testing corroded specimens is a time-consuming process, and it is still complicated to simulate a real corrosion situation in the environment. For this reason, a limited number of experimental studies are found, especially in the field of civil engineering, related to structural steels [2,3]. Therefore, there is a need for simple models or methodologies to model the fatigue strength of corroded materials. To fulfill this need, the major objective of this review paper is to illustrate/check the possibilities of proposing an interpolation formula for the fatigue strength of corroded material.

3. Modeling of fatigue damage due to corrosion

Approaches for modeling the fatigue damage of materials/structures due to corrosion can be mainly divided into two parts. The first is geometrical simulation of thickness loss and pitting. The other part is to model the degradation of material properties due to the corrosive environment (CF) by a stress-life fatigue model that simulates the fatigue strength of corroded material. The following subsections will review the aforementioned two parts of the modeling. At the latter part of this section, modeling of corrosion rate (i.e. intensity of corrosivity) is discussed, as it has a relation to the corresponding stress-life fatigue behavior of the corroded material.

3.1. Modeling of fatigue damage due to degradation of material properties

Fatigue damage due to corrosion pits and cracks is analytically modeled by fracture mechanics theories. Pitting corrosion damage models are widely used, based on stress intensity factor [19,20]. Moreover, fatigue crack propagation is determined by using stress intensity factor based fracture mechanics approaches [21, 22]. Using the modified corrosion-fatigue stress intensity threshold, ΔK_{th}, for the material to determine critical length L for corroded materials is reported as one method of modeling CF. Many researchers [2, 3] report that it is very difficult to get a clear value for ΔK_{th} in corrosive environments, in which the fatigue limit is not usually clear. The determination of critical length has not been well defined, as it is not clear in corrosive environments. Therefore, detailed research should be performed to fill this gap. A new strain-life model, based on the Smith–Watson–Topper model, was proposed in 2012 [2] to simulate the CF behavior of metals. The model takes into account the state of corrosive environment, the stress level, and the corrosive behavior of the material [2]. The parameters of the above CF model, which are modified Basquin's exponent and Coffin-Manson exponent, should be determined by a series of fatigue tests of materials in 3.5 wt/wt% NaCl which is a highly corrosive environment. As these model parameters are material dependent, and due to the complexity of fatigue tests, fewer applications of this model are found. This again emphasizes the importance of having a simple formula or methodologies to model the fatigue strength of corroded materials

3.2. Geometrical simulation of thickness loss and pitting

In order to estimate fatigue damage, it is essential to determine the stress histories generated by random loading of the structure. Therefore, it is necessary to know the stress cycles of all the corroded members in the past, present and future. The stress histories of the corroded members are evaluated by considering (i) past, present and future loadings and (ii) time-dependent change of cross-sectional shapes due to loss of material caused by the corrosion deterioration and related change in rigidities (i.e. change of axial, bending, torsional and warping rigidities), which finally cause change to the overall stiffness of the structure. These simulations associated fatigue damage/life assessment methods were discussed in recent literature [6, 11-14]. The proposed procedure with related theoretical formulae for structural elements has been comprehensively presented in recent literature [23]. For precise prediction of time-dependent stress histories, it is necessary to accurately model the time-dependent growth of corrosion wastage (i.e. rate of corrosion).

3.3. Modeling of corrosion rate

The environment makes a huge contribution to corrosion and changes the rate of corrosion. Corrosion rate is the speed of deterioration of material (loss of metal). It is the thickness reduction per year and can be calculated in general by metal loss divided by time. As corrosion rate is one of the key parameters, it is necessary to study the way corrosion effects in the integrity of steel structures and then the CF. Corrosion rate is one of the main factors affecting the service life of the structure. The intensity of the corrosivity depends on the corrosive environment. The corrosion rate is also presented for five categories of steel [23].

The experimental studies on corrosion rates include the following: (i) corrosion rates of low carbon steels in potable water conducted in this study, and (ii) effects of environmental factors on corrosion rates of previous research [24-29]. El Aghoury [2] proposed a new relationship between the logarithm of the penetration versus the proposed environmental corrosivity intensity factor (γcorr). The corrosive environments of the materials have been divided into corrosivity categories in ISO 9224, based on average corrosion rate [2].

4. Proposed formulae for fatigue strength of corroded material

Two S-N curve formulae for corroded metals are proposed, based on Basquin's law [21] and the full-range curve proposed by Kohout and Vechet [30]. Conventional S-N curves for uncorroded steel have been used for assessing structures and components in a non-corrosive environment. Vacuum is the perfect non-corrosive environment. The difference in the fatigue strength of metals such as mild steel in the vacuum and in dry air is less than 5% [1]. Therefore, dry air can also be considered as non-corrosive and, hence, Basquin's law and Kohout and Vechet's proposed full-range S-N curve can be used in dry air without any modifications. It is necessary to use degraded S-N curves, when fatigue life is estimated for structures and components in a corrosive atmosphere (rain, various gases, water, marine, etc.).

4.1. Concept used for the proposed formulae

Gliding may occur in some of the grains when materials are subjected to alternating stresses. Gliding is halted when dislocation reaches a grain boundary. In the presence of corrosion, disorganized atoms are in motion along a gliding plane with less activation energy than in the absence of corrosion. This phenomenon may reasonably be expected, even below the fatigue limit. This means that there is no safe stress level at which the fatigue life is infinite, as shown in Figure 1 [18]. However, it is convenient to determine an endurance limit for corroded steel corresponding to a specified number of cycles by assuming the material will endure some specified number of cycles which must be stated. Previously experimentally obtained fatigue lives show that the difference between fatigue strengths in corrosive and non-corrosive environments in the low-cycle fatigue (LCF) region is very low, compared to the high-cycle fatigue (HCF) and very-high-cycle fatigue (VHCF) regions [1,9,22]. The difference is significantly large in the HCF and VHCF regions.

4.2. Proposed formula for high-cycle fatigue region

The relation between the applied stress amplitude, σ_a, and the corresponding number of cycles to fatigue failure, N_f, follows Basquin's law, as presented in (1), for uncorroded material when the stress is below the yield strength, σ_y [21],

$$\sigma_a = \sigma'_f N_f^b \tag{1}$$

where σ'_f is the fatigue strength coefficient and b is Basquin's exponent.

The linear variation in the difference between the fatigue strengths in the uncorroded and corroded materials has been observed in previous fatigue test results [18], and the relative difference in log scale

is linearly deducted, as shown in Figure 2, from the corrosion-free material fatigue strength to obtain the corroded material fatigue strength. The difference between corroded and uncorroded S-N curves at the stress amplitude just above yield strength (σ_y) can be neglected, when compared to the difference at the very-high-cycle fatigue region. Hence, it is assumed that corroded and uncorroded S-N curves are intercepted when stress amplitude is equal to yield strength, as shown in Figure 2.

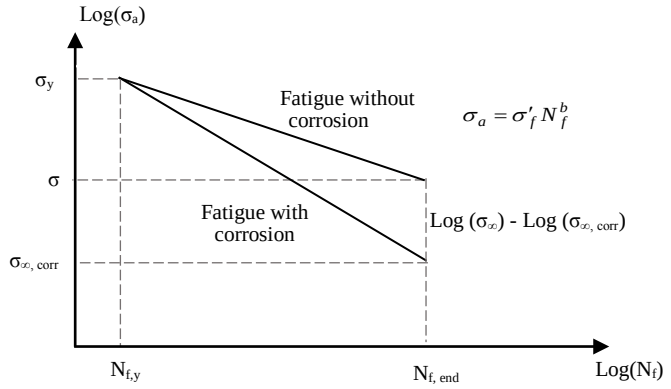

Figure 2. Schematic representation of fatigue strength degradation of corroded materials in HCF region

Hence, the fatigue strength of corroded material, $\sigma_{a,corr}$, which corresponds to number of cycles to fatigue failure, Nf, can be derived as,

$$\log(\sigma_{a,corr}) = \log(\sigma_a) - \frac{(\log\sigma_\infty - \log\sigma_{\infty,corr})}{(\log N_{f,end} - \log N_{f,y})}(\log N_f - \log N_{f,y}) \tag{2}$$

where σ_∞ is endurance limit (i.e. fatigue limit for high-cycle fatigue) and $\sigma_{\infty,corr}$ is endurance limit for corroded material, which corresponds to a specified number of cycles, $N_{f,end}$. The $N_{f,y}$ is the number of cycles to fatigue failure of uncorroded materials when stress amplitude is σ_y. The σ_a is fatigue strength of uncorroded material, which corresponds to the number of cycles to fatigue failure, N_f,, as defined in Eq. (1). The proposed formula for fatigue strength of corroded materials can be simplified as,

$$\log(\sigma_{a,corr}) = \log(\sigma_a) - \frac{\log\left(\sigma_\infty / \sigma_{\infty,corr}\right)}{\log\left(N_{f,end} / N_{f,y}\right)}(\log N_f - \log N_{f,y}) \tag{3}$$

or

$$\log(\sigma_{a,corr}) = \log(\sigma_a) - c(\log N_f - \log N_{f,y}) \tag{4}$$

where c is constant for a given material corresponding to the current state of corrosion and is given as,

$$c = \frac{\log\left(\sigma_\infty / \sigma_{\infty,corr}\right)}{\log\left(N_{f,end} / N_{f,y}\right)} \tag{5}$$

The proposed formula for fatigue strength can be obtained as,

$$\sigma_{a,corr} = (\sigma'_f N_{f,y}^c) N_f^{(b-c)} \tag{6}$$

The only parameter required for the above formulae is the endurance limit for the corroded material, $\sigma_{\infty,corr}$, which can be either experimentally obtained by a limited number of tests in the VHCF region

or can be predicted if there is a relationship between fatigue endurance degradation and rate of corrosion of the material.

4.3. Proposed formula for full range

The relationship between the applied stress amplitude, σ_a and number of cycles to fatigue failure, N_f, in full range (i.e. S-N curve for ultra-low cycle fatigue, LCF, HCF and VHCF regions) for uncorroded material is given as [31],

$$\sigma_a = \sigma_\infty \left(\frac{N+B}{N+C} \right)^b \tag{7}$$

where B and C are the number of cycles corresponding to the points of intersection of the tangent for the region of finite life described by Basquin's law, with the horizontal line across the ultimate strength and horizontal line across the endurance limit, respectively.

The linear variation in the difference between the fatigue strengths of uncorroded and corroded materials has been observed in the previous fatigue test results as described in the previous section. The relative difference is then linearly deducted to obtain corroded material fatigue strength for full range as follows:

$$\sigma_{a,corr} = \sigma_a - \frac{(\sigma_\infty - \sigma_{\infty,corr})}{\log C} \log N_f \tag{8}$$

The only parameter which is required for this formula is also the endurance limit for corroded material, $\sigma_{\infty,corr}$, which can be determined in the same way as described in the previous sub-section.

5. Experimental Verification of Proposed formulae

The proposed fatigue strength formulae for corroded materials are verified by comparing the experimental fatigue lives of corroded specimens of different materials, as shown below. The corrosion fatigue test results of three different steel types [18] and one type of aluminum alloy [31] are selected and compared with the predicted fatigue lives by the proposed formulae, as shown in the following sections. The fatigue tests have been conducted for constant corrosion rate.

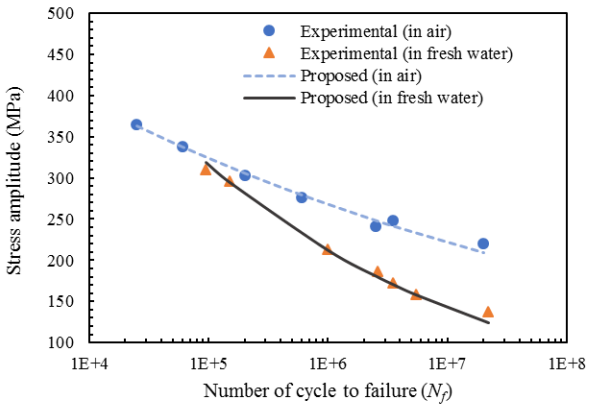

Figure 3. Comparison of proposed S-N curve with experimental test made in air and fresh water for annealed copper steel.

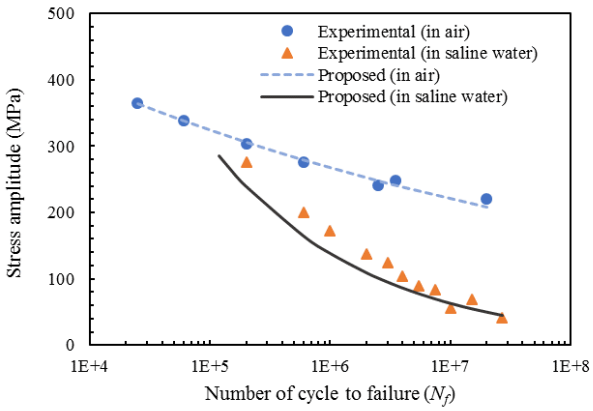

Figure 4. Comparison of proposed S-N curve with experimental test made in air and saline water for annealed copper steel.

5.1. Experimental verification of proposed formula for HCF

Figures 3 to 8 show the comparison of experimental fatigue lives of annealed copper steel (0.14% C, 0.98% Cu), hardened and tempered 0.16% carbon steel, hardened and tempered chrome-vanadium steel (0.88% Cr, 0.14% Va, 0.46% C) [18] and 6061-T6 aluminum alloy [31] specimens in different

corrosive environments with interpolated fatigue lives by the proposed interpolation formula for the high-cycle fatigue region shown in Eq (6).

Figures 3 to 7 show a good agreement between interpolated fatigue lives and experimentally observed lives for all three types of steel. This shows that the proposed formula in HCF provides a conservative rule regarding the fatigue strength of corroded steels. However, there are not conservative results for the aluminum alloy, as shown in Figure 8. One reason is the lack of an experimental data point to determine the endurance limit for corroded specimens. However, the proposed formula gives a better calculation of the mean fatigue strength of corroded aluminum alloy specimens.

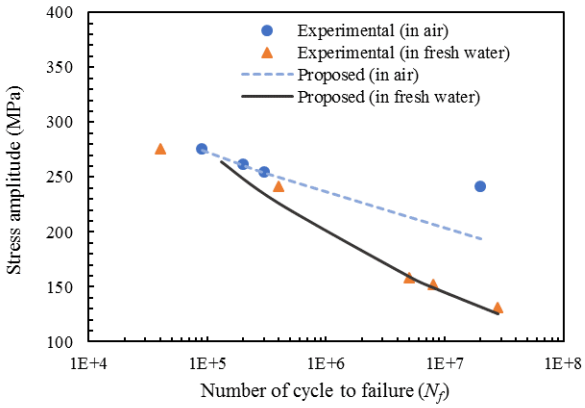

Figure 5. Comparison of proposed S-N curve with experimental test made in air and fresh water for 0.16% carbon steel (hardened and tempered).

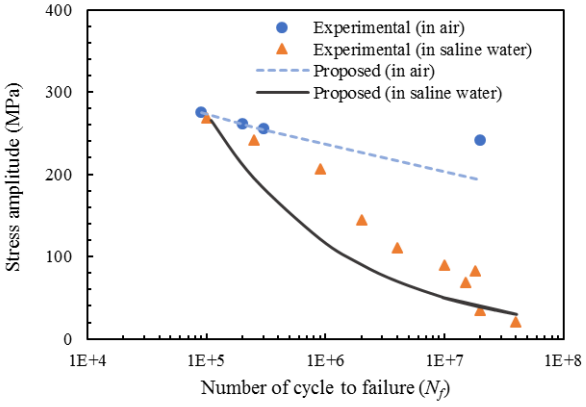

Figure 6. Comparison of proposed S-N curve with experimental test made in air and saline water for 0.16% carbon steel (hardened and tempered).

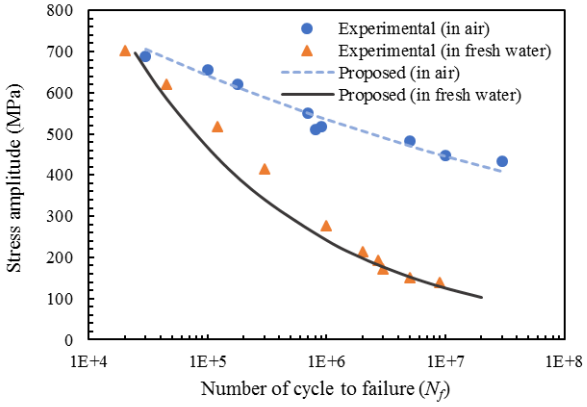

Figure 7. Comparison of proposed S-N curve with experimental test made in air and fresh water for chrome-vanadium steel (hardened and tempered).

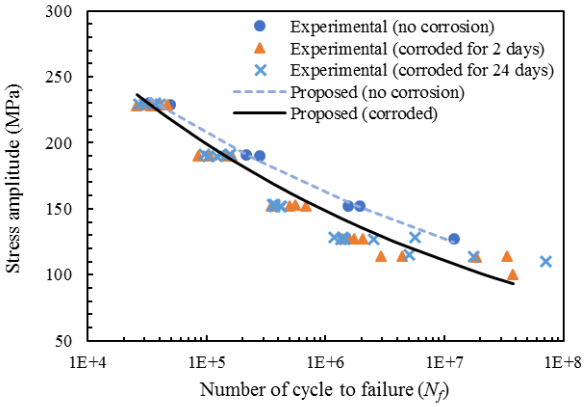

Figure 8. Comparison of proposed S-N curve with experimental test made with corrosive and non-corrosive situations of 6061-T6 aluminum alloy.

5.2. Experimental verification of proposed formula for full range

Figures 9 to 14 show the comparison of experimental fatigue lives of annealed copper steel (0.14% C, 0.98% Cu), hardened and tempered 0.16% carbon steel, hardened and tempered chrome-vanadium steel (0.88% Cr, 0.14% Va, 0.46% C) [18] and 6061-T6 aluminum alloy [31] specimens in different corrosive environments with interpolated fatigue lives by the proposed formula for full range shown in Eq. (8). Figures 9 to 14 show that the proposed formula for full range provides a conservative calculation of the fatigue strength of corroded materials. The proposed formula does not give better results when material is subjected to severe corrosion. This concludes that improvement of the proposed formula is required.

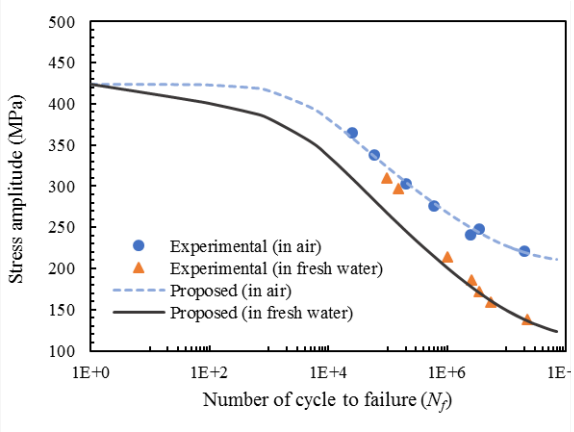

Figure 9. Comparison of proposed S-N curve with experimental test made in air and fresh water for annealed copper steel.

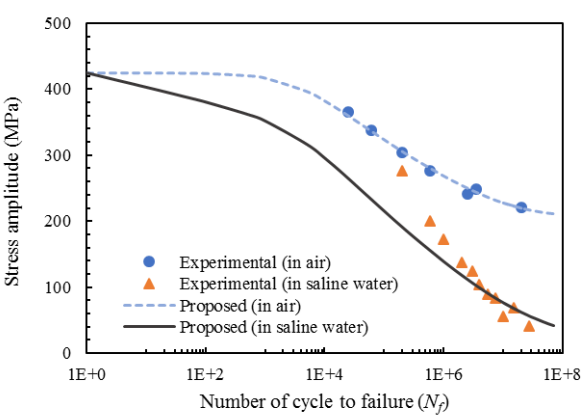

Figure 10. Comparison of proposed S-N curve with experimental test made in air and saline water annealed copper steel

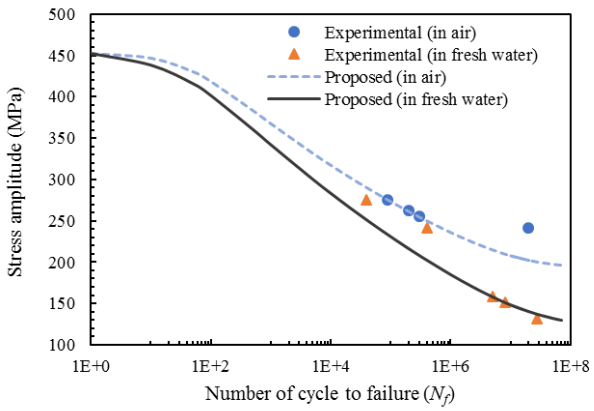

Figure 11. Comparison of proposed S-N curve with experimental test made in air and fresh water for 0.16% carbon steel (hardened and tempered).

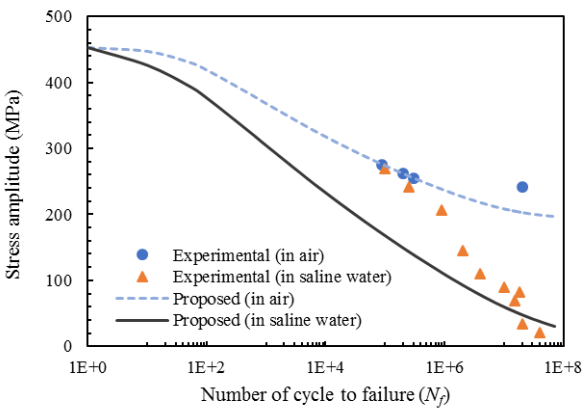

Figure 12. Comparison of proposed S-N curve with experimental test made in air and saline water for 0.16% carbon steel (hardened and tempered).

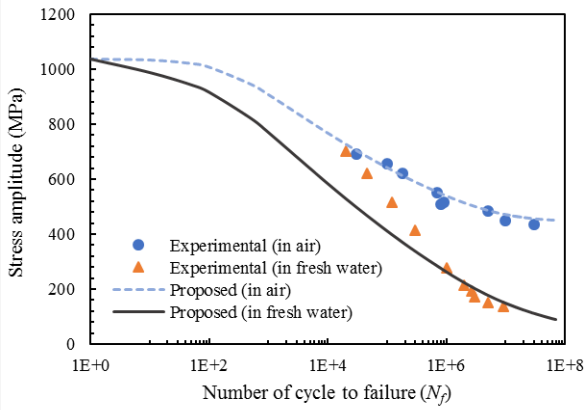

Figure 13. Comparison of proposed S-N curve with experimental test made in air and fresh water for chrome-vanadium steel (hardened and tempered).

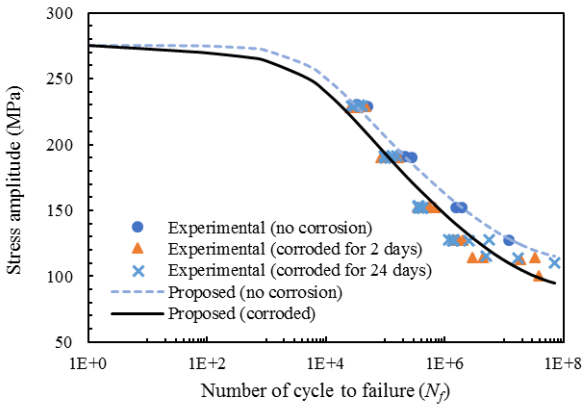

Figure 14. Comparison of proposed S-N curve with experimental test made with corrosive and non-corrosive situations of 6061-T6 aluminum alloy.

6. Discussion and conclusions

The corrosion degradation process of metallic materials has been reviewed by highlighting the mechanism of corrosion fatigue. Time-dependent geometrical changes in structural components and degradation of material strength are identified as key effects of corrosion. Corrosion fatigue, which is the degradation of materials under the combined action of localized corrosion and cyclic loading, significantly affects the integrity of structures. The fatigue damage due to corrosion pits and cracks can be modeled by fracture mechanics theories. Many researchers have reported the shortcomings of this approach in corrosive environments, as fatigue limit is not usually clear in corrosive environments. Generally, laboratory fatigue testing of corroded samples is popular for simulating CF. Testing corroded specimens is costly, and experimentally simulating the real corrosion situation in the environment is also complicated. A new strain-life model was proposed in 2012. Some of the model parameters should be determined by a series of complicated fatigue testing and, therefore, very few applications of this model have been reported.

Finally, new formulae for the fatigue strength of corroded materials were proposed in the paper. The proposed formulae only depend on the endurance limit of corroded material ($\sigma_{\infty,corr}$), in addition to the stress-life fatigue curve parameters of the uncorroded material. The $\sigma_{\infty,corr}$ can be either determined by a limited number of tests in the VHCF region or predicted by analytical approach. The interpolation formulae give fatigue lives were compared with experimentally obtained fatigue lives of a few materials in different corrosive environments. The comparisons show that the proposed formula for the HCF region gives a conservative calculation to the fatigue strength of corroded materials. It also reveals that the new formula for full range provides a better agreement with the fatigue strength of corroded materials. Knowledge of corrosion rates in the region where the structure is located is extremely important for damage assessments. Further verification of the proposed formulae is required for variable corrosion rates, as verification of the proposed formulae has been performed by comparing the results of fatigue tests conducted at a constant corrosion rate.

References

[1] Revie R W and Uhlig H H 2008 *Corrosion and Corrosion Control, An Introduction to Corrosion Science and Engineering* (Hoboken New Jersey: 4th edn., Wiley and Sons)
[2] Aghoury I El 2012 *Numerical tool for fatigue life prediction of corroded steel riveted connections using various damage models* (PhD thesis, Concordia University, Montreal)
[3] Aghoury I M El and Galal K 2014 Corrosion-fatigue strain-life model for steel bridge girders under various weathering conditions *J. Struct. Eng.* **140(6)** pp
[4] Roberge P R 2000 *Handbook of Corrosion Engineering* (New York: 1st ed., McGraw Hill)
[5] Mikkelsen O, Rege K, Hemmingsen T H and Pavlou D 2007 Numerical estimation of the stop holes-induced fatigue crack growth retardation in offshore structures taking into account the corrosion effect, *Proc. of 27th International Ocean and Polar Engineering Conference* (San Francisco, California)
[6] Yasser Y and Jeom K.M 2011 Ultimate strength reliability analysis of corroded steel-box girder bridges *Thin Wall. Struct* **49** pp 157-166
[7] Kayser J R 1988 *The effects of corrosion on the reliability of steel girder bridges* (PhD thesis, University of Michigan, Ann Arbor, Michigan, USA)
[8] Paik J K, Lee J M and Ko M J 2004 Ultimate shear strength of plate elements with pit corrosion wastage *Thin Wall. Struct* **42** pp 1161-1176
[9] Glaser W and Wright L G 1992 *Mechanically assisted degradation* (Ohio: ASM Handbooks, ASM Internationals) pp 137-144
[10] Wang Y Z 2011 *Corrosion fatigue, Corrosion Handbook* 3rd edn, ed R W Revie and H H Uhligs (New York: John Wiley and Sons)
[11] Li Z X and Chan T H T 2006 Fatigue criteria for integrity assessment of long span steel bridge health monitoring *Theo. & App. Fract. Mech.* **46** pp 114-127
[12] Lima K, Robson N, Oosterhof S, Kanji S, DiBattista J and Montgomery C J 2008 Rehabilitation

of a 100-year-old steel truss bridge *Proc. of Canadian society for civil engineering. annual conference* (Quebec: Canada)
[13] Nakamura S and Suzumurab K 2009 Hydrogen embrittlement and corrosion fatigue of corroded bridge wires *J. Constr. Steel. Res*. **65** pp 269-277
[14] Yukikazu Y and Makoto K 2002 Maintenance of steel bridges on Honshu- Shikoku crossing *J. Constr. Steel. Res.* **58** pp 131-150
[15] Mohamed E L M, Thierry P L, Nicolas S and Olivier D 2013 Effect of corrosion on the high cycle fatigue strength of martensitic stainless steel X12CrNiMoV12-3 *Int. J. Fatigue* **47** pp. 330-339
[16] Wahab M A and Sakano M 2003 Corrosion and biaxial fatigue of welded structures *J. Mat. Proc. Tech*. **3** pp 410-415
[17] Nguyen K T, Garbatov Y and Soares C G 2013 Spectral fatigue damage assessment of tanker deck structural detail subjected to time-dependent corrosion *Int. J Fatigue* **48** pp 147-155
[18] Boyer H E 1986 *Atlas of Fatigue Curves* (Ohio: USA, ASM Internationals)
[19] Hoeppner D W, Chandrasekaran V and Taylor A M H 1999 Review of pitting corrosion fatigue models *Proc. of ICAF International Conf*. pp 549
[20] Acuña N, González-Sánchez J, Ku-Basulto G and Domınguez L 2006 Analysis of the stress intensity factor around corrosion pits developed on structures subjected to mixed loading *Scripta Materialia* **55** pp 363-366
[21] Suresh S 1998 *Fatigue of Materials* (Cambridge: 2nd ed. Cambridge University Press, Cambridge, UK)
[22] Gangloff R P 2005 *Environmental cracking - corrosion fatigue* eds. R Baboian, S W Dean Jr., H P Hack, E L Hibner and J R Scully (Pennsylvania: USA ASTM Internationals, Corrosion Tests and Standards Manual)
[23] Adasooriya N D and Siriwardane S C 2014 Remaining fatigue life estimation of corroside bridge members *Fatigue Fract. Eng. Mater. Struct*. **37** pp 603-622
[24] Roberge P R 2011 *Atmospheric corrosion, Uhligs Corrosion Handbook* ed. R W Revie (New York: USA 3rd edn. John Wiley and Sons)
[25] Vashi R T, Kadiya H K and Champaneri V A 2008 Corrosion study of metals in rural atmosphere *J. Env. Research and Dev*. **3** pp 1
[26] Natesan M, Selvaraj S and Manickam T 2008 Corrosion behaviour of metals and alloys in marine – industrial environment *Science and Technology of Advance Materials* **9**, Page no. 045002 (7pp)
[27] Matsushima I 2011 *Carbon steel corrosion by sea water, Uhligs Corrosion Handbook* ed. R W Revie, (New York: 3rd edn. John Wiley and Sons) pp 601-608
[28] Parekh S P, Pandya A V and Kadiya H K 2012 Progressive atmospheric corrosion study of metals like mild steel, Zn and Al in urban station of Ahmedabad district *Int. J. Chemtech. Res*. **4(4)** pp 1770-1774
[29] Marref A, Basalamah S and Al Ghamdi R 2013 Evolutionary computation technique for predicting atmospheric corrosion *Int. J Corrosion* **2013** Article ID 805167
[30] Kohout J and Vechet S 2001 A new function for fatigue curve characterization and its multiple merits *Int. J. Fatigue* **23** pp175-83
[31] Matthew W, Paul D E, Huseyn O and Murat T 2017 The effect of surface corrosion damage on the fatigue life of 6061-T6 aluminum alloy extrusions *Mater. Sci. Eng.: A-Struct*. **690** pp 427-432

Paper 3

Fatigue Strength Degradation of Corroded Structural Details: A Formula for S-N Curve

Journal Paper

Fatigue & Fracture of Engineering Materials & Structures

Published Online 2019

Received: 16 September 2019 | Revised: 25 October 2019 | Accepted: 28 October 2019

DOI: 10.1111/ffe.13156

ORIGINAL CONTRIBUTION

WILEY FFEMS Fatigue & Fracture of Engineering Materials & Structures

Fatigue strength degradation of corroded structural details: A formula for *S-N* curve

N.D. Adasooriya | **D. Pavlou** | **T. Hemmingsen**

Department of Mechanical and Structural Engineering and Materials Science, University of Stavanger, Stavanger N-4036, Norway

Correspondence
N. D. Adasooriya, Department of Mechanical and Structural Engineering and Materials Science, University of Stavanger,Stavanger N-4036, Norway.
Email: mudiyan.n.adasooriya@uis.no

Abstract

A formula is proposed to predict fatigue strength of corroded members and joints of steel structures. The concept of the formula is first studied from recently identified mechanism of corrosion fatigue. Hence, the corresponding fatigue strength curve (i.e. S-N curve) of corroded steel is presented. It is further improved to derive linear, bilinear or trilinear S-N curve for corroded constructional details of steel structures. The parameters of the corroded steel S-N curve are determined based on the corrosion fatigue testing results of different types of steel specimens in air, fresh water and seawater. Hence, the parameters for the derived S-N curve of corroded constructional details are predicted based on the above parameters and tabulated for the detail categories given in the Eurocode and DNVGL code. The proposed S-N curve formula is compared with full-scale fatigue test results of several constructional details, and the validity of the formula is confirmed.

KEYWORDS

corrosion fatigue, joints and connections, S-N curve, steel structures

1 | INTRODUCTION

Corrosion is one of the main structural degradation processes that affect integrity. Fractures due to cyclic stress in corrosive media are designated as corrosion fatigue (CF) which is a type of environmental assisted cracking. The forty percent failures in oil and gas pipelines and 8% of failures in offshore steel structures are reported to be caused degradation/deterioration due to corrosion. Corrosion commonly takes place in the splash zone area of offshore structures as the coating in this area disappears a few years after installation.[1] Recent collapses of steel bridges due to corrosion are reported and some examples are the Silver Bridge in 1967, the Mianus River Bridge in 1990 and the Minnesota Bridge in 2007.[2-4] Though many bridges are located onshore, de-icing salt may simulate marine environment to the bridges in snowy regions.[2] These failures emphasize the importance of more accurate simulation of CF strength of structural joints and connections (i.e. constructional details) in different corrosive environments.[3,5,6]

Corrosion pit induced stress concentration models and fatigue notch factor are commonly used to determine structures integrity.[7-10] Fatigue crack initiation life is determined when micro-cracks propagate to certain critical length. Fatigue crack propagation life is determined by fracture mechanics approach. Accurate determination of modified corrosion-fatigue stress intensity threshold and the critical length has been reported as challenging and difficult.[2-4] Therefore, limited amount of published

works is found in the area of fatigue notch factor due to pitting corrosion.[9,10] Recent investigations of non-passive metals such as carbon steel reveals that CF cracks do not initiate at pits even though those are available. This statement concludes that CF crack initiation greatly occurs without the formation of pits (i.e. absence of pitting corrosion) and it may occur in any corrosive media.[11-14] This mechanism is proved by means of a slip-band preferential dissolution model and hydrogen embrittlement theory.[12-14] As these models are unable to represent CF crack initiation below yield stress and in the absence of hydrogen, Zhao et al[11] investigated the CF crack initiation and propagation mechanism of a carbon steel in details by stress controlled fatigue tests and microstructural analyses with scan electron microscopy, electron backscatter diffraction and transmission electron microscopy. The CF crack initiation and initial propagation mechanisms are highly governed by the peak stress level. In the high cycle fatigue region of steel, a high possibility of crack initiation in seawater is observed at the austenite grain boundaries than at the pits or from initial cracks.[11] A generalized model which precisely addresses the above mechanism is lacking in the literature for predicting life of the defect free (i.e. without cracks or pits) steel structural details. Therefore, further research is required to develop models to predict fatigue strength of the corroded steel members, joints and connections (i.e. constructional details) which are subjected to different types of corrosion.

As a result, a strain-life model was proposed based on the Smith–Watson–Topper model[2,3] to simulate the CF behaviour of metals. The model takes into account the state of corrosivity of environment, the stress level and the corrosive behaviour of the steel. Further verification of the proposed function is recommended in the same articles as future studies. The procedure for determining the model parameters requires a series of fatigue tests. The effect of pitting on the prediction of life is recommended for further studies.[2,3] To use the model, transformation of stress ranges into strain ranges is required to use the model by using cyclic properties of steel and fatigue notch factor. Due to mentioned complexities of the model and uncertainties of the model parameters, few applications are reported. A stress-life fatigue strength curve for corroded material is recently published.[4] The proposed curve depends on corrosion parameter, $\sigma_{\infty,cor,}$ which should be determined by CF tests in very high cycle fatigue (VHCF) region in relevant corrosive media. The determination of $\sigma_{\infty,cor}$ is complex as fatigue tests in the VHCF region is extremely time consuming. The discussed methods/models are limited for determination of the $\sigma_{\infty,cor}$ in the specimen scale. Therefore, it is required to have a simple formula/approach to model the fatigue strength of material, full-scale steel members and joints (i.e. constructional details).

Detailed provisions and models/formulas are not available in codes of practices to predict fatigue strength of corroded structural details of land-based structures/onshore structures.[2,3,15] Testing of different full-scale details in simulated corrosive environment is complicated especially in VHCF region (e.g. if the cyclic frequency is 1 Hz, for 10^8 cycles, it takes more than 3 years to finish a single test). Therefore, the test results are limited and the fatigue endurance of the majority of available results are reported in the range from 10^4 to 10^6 cycles. The obtained results are also scattered as the test process is subjected to many variables and uncertainties. Those results are not sufficient to warrant variable amplitude fatigue limits of the details. A few past studies recommend the endurance limit to be neglected (i.e. S-N curve should be used without cut off limit) to take into account the fatigue strength degradation due to the unexpected localized corrosion (i.e. mild pitting or crevice corrosion) near the corroded details.[15-18] The modified S-N curves do not match the available fatigue test results of corroded details.

Health and Safety Executive (HSE) provisions and guidelines for fatigue strength have been presented for the corroded structural details in offshore structures.[19] The fatigue strength curve for the welded tubular joints in seawater-free corrosion was obtained by applying environmental reduction factor (ERF) to the relevant curve in air. The ERF is determined by the ratio of the number of cycles to fatigue failure in air to that in seawater/marine environment for tubular joints at the same stress range. Average ERF value has been determined by very scattered CF test results (results varies from 0.8 to 5.2). The variation of defined test failure criteria (i.e. stopping criteria), damage histories of the joints and other environmental factors may scatter the obtained fatigue lives. The results were obtained in the range from 6×10^4 to 2×10^6 cycles and it does not include either constant amplitude fatigue limit (CAFL) or variable amplitude fatigue limit (VAFL) (i.e. 10^7 and 10^8 cycles respectively). A constant slope is proposed for the whole region of the corroded S-N curve. The same report has also mentioned the doubtfulness of the proposed ERF due to lack of data.[19] The modified corroded curve has the same slope with the air curve until 10^7 cycles. This violates CF behaviour of steels, which has negligible difference between fatigue lives in corrosive and non-corrosive environments in the low-cycle fatigue (LCF) region when compared to VHCF region.[2-4,19-22]

To overcome the previously mentioned problems, the main objective of this paper is to derive a generalized formula to determine the fatigue strength of structural joints/constructional details exposed to corrosive

media/environment. The concept of the proposed formula has been studied by means of the fatigue test results of different types of corroded steel specimens in different corrosive environments. The parameters used in the formula are mainly dependent on corrosive environment (i.e. urban and marine) and the corresponding constructional detail (i.e. detail category), which can easily be found in the fatigue design codes. The corrosive environment dependent parameters have already been conservatively defined based on the corrosion fatigue testing results of different types of steel in different environments. The proposed formula can be easily used with the trilinear or bilinear fatigue curves/S-N curves of detailed categories provided in any fatigue design codes of steels structures only in the high cycle fatigue (HCF) region. Initially the mechanism and the concept of the fatigue strength degradation of the material is discussed and hence the proposed relation is derived for steels exposed to corrosive media. The verification of the corroded parameters is done by comparing CF tests of different types of steel specimens tested in air, fresh water and seawater. The relation for the fatigue strength curve is then developed for corroded constructional details. The verification of the proposed formula is done by comparing experimental results of many full-scale tests of corroded structural details.

2 | MECHANISM OF FATIGUE STRENGTH DEGRADATION OF CORRODED STEEL

Gliding can be seen in some of the grains due to alternating stresses. When dislocations reach a grain boundary, gliding is ceased.[22,23] When the stress is reversed, the movement of the grains retraces along the gliding plane. Slight irregularities may prevent the smooth gliding and it roughens along original gliding plane. Roughness restricts the movement and develops another parallel gliding plane. Finally, these disorganized bands of material cause separation between gliding planes while producing gaps and eventually developing cracks at high stress ranges (i.e. above the endurance limit) or cease the gliding at low stress ranges (i.e. bellow fatigue endurance limit). Under corrosion, disorganized atoms are moving along a gliding plane with less activation energy than without corrosion. The CF crack initiation can occur without the presence of pits and the corrosion-fatigue cracks are expanded by post reaction of corrosion for carbon steel.[11] The slip-bands preferentially dissolution model and the hydrogen embrittlement theory[11-14] describe this mechanism properly above the yield strength. The mechanism of CF crack initiation and propagation is mainly governed by the peak stress level and the stress range. Higher probability of crack initiation has been observed in parent austenite grain boundaries in HCF region. The crack propagation has been reported along the parent austenite grain and ferrite lath boundaries.[11] This phenomenon may be observed even below the fatigue endurance limit and hence there is no safe stress level at which the fatigue life is infinite. The cracks are usually transgranular[4,23] and, therefore, the specified number of cycles are stated as an endurance for the corroded steel by assuming the material will endure. The degraded fatigue strength/endurance of the corroded steel depends on the environmental, metallurgical and structural factors. These factors have direct effects on the corrosion rate which governs both strength degradation and the overall stiffness of the structure.[15,24] The fatigue endurance/strength of corroded material reaches a threshold after a certain period of exposure to corrosive environment. Fatigue test results of steel specimens show that the difference between fatigue lives in corrosive and non-corrosive environments LCF region is negligible and a significant larger difference is observed in VHCF region.[2,4,20-22]

3 | FATIGUE STRENGTH CURVE FOR CORRODED STEEL MATERIAL

A fatigue strength formula for corroded steel is presented based on previously published work.[4] Values for corrosive parameters used in the formula are proposed in this paper to further simplify the previously published formula. The validity of the proposed parameters is confirmed by comparing CF test results of different types of steel.

3.1 | Formula for high cycle fatigue region

The formula presented in this section exists in a previous publication[4] by the same authors. Based on Basquin's law, the S-N curve formula for corroded steel is proposed.[4] The concept of the proposed formula is based on the degradation mechanism discussed in the section 2 and the derivation is presented in a previous paper.[4] The final formula is shown in Eq. (1).

$$\sigma_{a.cor} = \left(\sigma_f' N_{f,LCF}^{c}\right) N_f^{(b-c)} \quad \text{where } c = {}^{log}\left[\frac{\sigma_\infty}{\sigma_{\infty,cor}}\right] \Big/ {}_{log}\left[\frac{N_{f,FL}}{N_{f,LCF}}\right] \tag{1}$$

where $\sigma_{a,cor}$ is the fatigue strength of corroded material, which corresponds to the number of cycles to fatigue

failure, N_f. The term σ_f' is the fatigue strength coefficient and b is the Basquin's exponent. The endurance limit (i.e. fatigue limit for high-cycle fatigue) is σ_∞ and $\sigma_{\infty,cor}$ is the endurance limit for the corroded material, which corresponds to a specified number of cycles, $N_{f,FL}$. When the stress amplitude is the yield strength, σ_y, the number of cycles to fatigue failure of the uncorroded material is $N_{f,LCF}$.

3.2 | Proposed values of the parameters

The values of σ_f', b, σ_∞, $N_{f,FL}$ and $N_{f,LCF}$ are determined from the S-N curve of uncorroded materials. The value of $\sigma_{\infty,cor}$ has to be determined by fatigue testing in the VHCF region and it is a complicated process. Therefore, this section presents a reasonable accurate relation to obtain $\sigma_{\infty,cor}$ for structural steels in natural water (i.e. similar to urban environment) and sea water (i.e. similar to marine environment).

Revie and Uhlig[20,23,25] performed fatigue testing for several grades of medium and low strength corroded and uncorroded steels. Corrosive process was carried out in natural water. The values of σ_∞ and $\sigma_{\infty,cor}$ were determined corresponding to $N_{f,FL} = 10^7$ cycles. The ratios $\sigma_{\infty,cor}/\sigma_\infty$ are listed in Table 1a which shows that the ratio varies in the range of 0.53-0.70. The mean and coefficient of variation (COV) values of the ratio are 0.61 and 0.1. Taking into account the 5% failure probability (i.e. 95% safe prediction), the design value of the $\sigma_{\infty,cor}/\sigma_\infty$ ratio can be proposed as 0.5 for conservative prediction of fatigue strength of medium and low strength structural steels which are subjected to corrosion in natural water media. It is recommended to use mean and/or design value depending on the importance of the case studied.

Boyer[23] and Adasooriya et al.[4] presented previous fatigue test results in both air and saline/seawater. The related S-N curves were plotted for several grades of medium and low strength steels. The σ_∞ and $\sigma_{\infty,cor}$ were determined corresponding to $N_{f,FL} = 10^7$ cycles. The ratios $\sigma_{\infty,cor}/\sigma_\infty$ are tabulated in Table 1b which shows that the ratio varies in the range of 0.36-0.59. The mean and the coefficient of variation (COV) values of the ratio are 0.46 and 0.21. Taking into account the 5% failure probability (i.e. 95% safe prediction), the design value of $\sigma_{\infty,cor}/\sigma_\infty$ ratio can be proposed as 0.27 for conservative prediction of fatigue strength of medium and low strength structural steels which are subjected to corrosion in sea water media. The CF endurance limit of high strength steel reduces to 90% when it is exposed to sea water and hence the ratio is found to be 0.1.[26] Yantao et al.[27] concluded that the CF life was reduced to 1/2 to 1/3 of the life in air. This difference was greater when the stress level was low.

TABLE 1A Corrosion fatigue limits of steel tested in natural water[4,23,25]

Material	Fatigue endurance limit for uncorroded material, σ_∞ (MPa)	Fatigue endurance limit for corroded material, $\sigma_{\infty,cor}$ (MPa)	$\sigma_{\infty,cor}/\sigma_\infty$
0.11% C steel, annealed	172	110	0.64
0.16%C steel, quenched and tempered	241	138	0.57
1.09%C steel, annealed	289	158	0.55
3.5%Ni, 0.3%C steel, annealed	338	200	0.59
0.9%Cr, 0.1%V, 0.5%C steel, annealed	289	152	0.53
13.8%Cr, 0.1%C steel, quenched and tempered	345	241	0.70
0.14%C,0.88%Cu steel, annealed	234	149	0.64
12.9%Cr, 0.11%C steel, hardened and tempered	379	264	0.70

3.3 | Experimental verification of the proposed parameters

The corrosion fatigue test results of three different steel types[23] and one type of aluminium alloy[28] have been compared with the predicted fatigue lives by the proposed formulae and published by authors.[4] The major objective of this section is to verify the fatigue strength formula related proposed parameters by comparing the experimental fatigue lives of the corroded specimens of different materials in different corrosive environments.

Figure 1 shows the comparison of predicted fatigue strength with test results of three types of carbon steel: the mild steel (MS), cold twisted deformed steel (CTD) and quenched and self-tempered steel (QST). The pre-corroded specimens were subjected to fatigue testing in 50Hz and stress ratio, R, equal to -1.[25] The surface of the uncorroded specimens were polished to a roughness of

TABLE 1B Corrosion fatigue limits of steel tested in sea water[4,23]

Material	Fatigue endurance limit for uncorroded material, σ_∞ (MPa)	Fatigue endurance limit for corroded material, $\sigma_{\infty, cor}$ (MPa)	$\sigma_{\infty,cor}/\sigma_\infty$
0.14%C,0.88%Cu steel, annealed	234	84	0.36
0.16%C steel, hardened and tempered	241	89	0.37
27%Cr, 0.2%C high chromium steel	309	183	0.59
12.9%Cr, 0.11%C steel, hardened and tempered	379	194	0.51

R_z = 6 μm and enclosed in the natural water for 60 days. Both the design and the mean values of the $\sigma_{\infty,cor}/\sigma_\infty$ ratio were used for these verifications as shown in Fig. 1.

Figure 2a shows the comparison of predicted S-N curves with the test results of E690 steel in air and simulated sea water.[11] The E690 steel was newly developed for marine structures. The chemical composition, mechanical properties and the test specification were clearly discussed by Zhao et al..[11] The round bar specimens were subjected to stress-controlled fatigue testing in simulated sea water (i.e. 3.5wt% NaCl solution) at 1 Hz frequency. The CF test results of medium strength shaft steel are compared with proposed S-N formula in Fig. 2b. The sample preparation, test specifications and the mechanical properties have been clearly presented else where.[29] The fatigue tests were conducted at R=-1 at the frequency of 22 Hz. The corrosive media has been simulated by 3.5 wt% NaCl and pH value 5 solution. The corrosion fatigue test results of butt-welded joints of steel which is commonly used for offshore platforms are compared with proposed *S-N* formula in Fig. 2c. The sample preparation, test specifications and mechanical properties have been clearly presented else where.[27] Four point bending cyclic loading test was performed in the frequency of 0.5 Hz and the R = -1. The sea water circulation system was used during the testing and 24.53 wt% NaCl solution was used. The pH value of the solution ranged from 7.5 to 8.5. Both the design and the mean values of $\sigma_{\infty,cor}/\sigma_\infty$ ratio were used for these verifications as shown in Fig. 2.

Figures 1 and 2 show a good match between the fatigue strength curve related proposed values of $\sigma_{\infty,cor}/\sigma_\infty$ and corrosion fatigue test results of different types of steel.

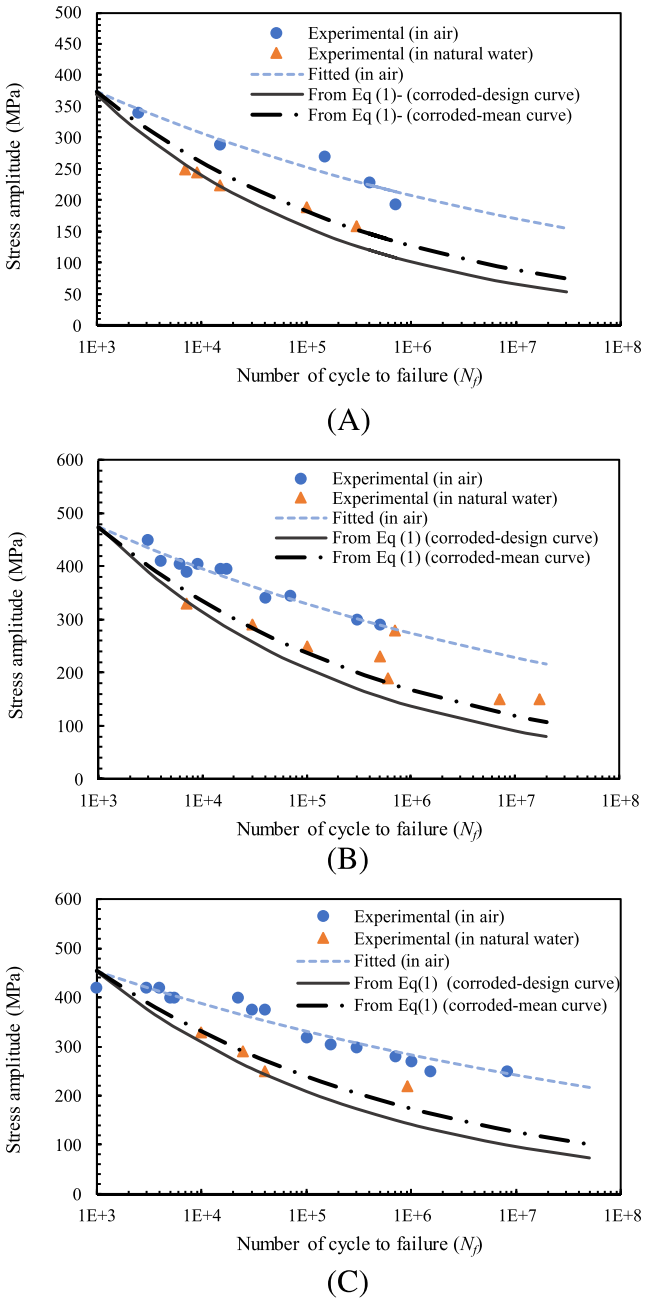

FIGURE 1 Comparison of the proposed S-N curve with experimental test carried out in natural water: (a) for mild steel (MS), (b) for cold twisted deformed steel (CTD), (c) for self tempered steel (QST) [Colour figure can be viewed at wileyonlinelibrary.com]

4 | PROPOSED FATIGUE STRENGTH CURVE FOR CORRODED CONSTRUCTIONAL DETAILS

The corroded material fatigue strength curve described above was further improved to develop *S-N* curves for corroded constructional details/detail categories. The proposed curve is obtained by modifying the design fatigue strength curves of categories/detail class of connections.

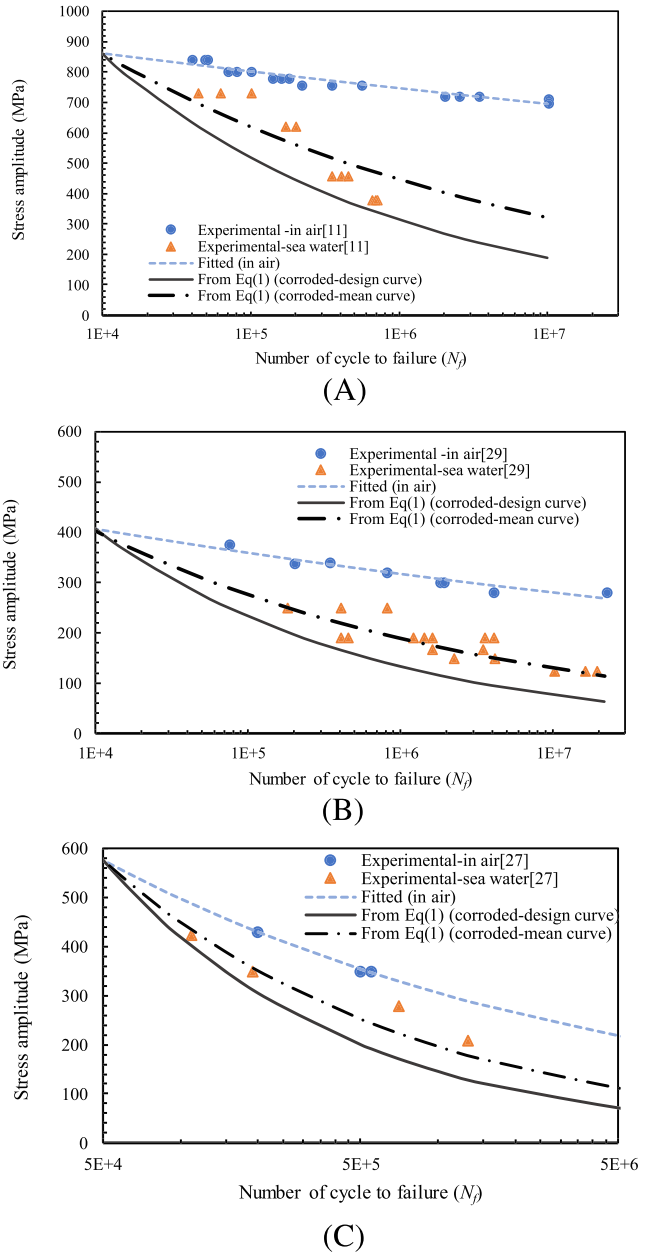

FIGURE 2 Comparison of the proposed S-N curve with experimental test carried out in simulated sea water: (a) for E690 steel, (b) for Shaft steel, (c) for steel butt welded joints [Colour figure can be viewed at wileyonlinelibrary.com]

The reduction factors, which represent environmentally assisted corrosion fatigue, are utilized for this modification. The linear, bilinear or trilinear design fatigue curves of details used in different fatigue codes can be modified to obtain the proposed fatigue curve for corroded details.

4.1 | Derivation of fatigue strength curve for corroded details

The trilinear fatigue strength curve of uncorroded constructional detail is presented in Fig. 3.[30] The relation between the stress range, $\Delta\sigma$ and the corresponding number of cycles to fatigue failure, N_R, presented by Eq. (2) for the uncorroded (i.e. fatigue design code given details) curve.

$$\Delta\sigma = \left(\Delta\sigma_D N_{f,CAFL}^{1/m}\right) N_R^{(-1/m)} \tag{2}$$

where $\Delta\sigma_D$ is the stress range at the fatigue curve slope changing point which corresponds to the $N_{f,CAFL}$ cycles. In some fatigue design codes, $\Delta\sigma_D$ is defined as the constant amplitude fatigue limit.[1,30] The slope of the fatigue strength curve is -1/m. According to the Eurocode[30] m is equal to 3 when $\Delta\sigma \geq \Delta\sigma_D$, is equal to 5 when $\Delta\sigma_D \geq \Delta\sigma > \Delta\sigma_L$ and it is infinite when $\Delta\sigma \leq \Delta\sigma_L$, where $\Delta\sigma_L$ is the fatigue endurance limit of the detail which corresponds to $N_{f,VAFL}$. This is also defined as the fatigue cut-off limit or variable amplitude fatigue limit in some fatigue design codes.[1,30] Some of the fatigue curves of the details do not have such a cut-off limit.

According to the verified mechanism and the concept of corroded fatigue endurance of steel mentioned in sections 2 and 3, the linear variation in the difference between the fatigue strengths of the uncorroded and corroded details has been observed as shown in Fig. 3. The relative difference in log scale is linearly deducted from the corrosion-free fatigue strength to obtain the fatigue strength of the corroded detail. Hence the fatigue strength range of corroded constructional detail, $\Delta\sigma_{cor}$, corresponding to N_R, can be derived, if $\Delta\sigma_{cor} \geq \Delta\sigma_{D,cor}$,

$$\log(\Delta\sigma_{cor}) = \log(\Delta\sigma) - {}^{log}\left[\frac{\Delta\sigma_D}{\Delta\sigma_{D,cor}}\right] \Big/ {}_{log}\left[\frac{N_{f,CAFL}}{N_{f,LCF}}\right] \left(\log N_R - \log N_{f,LCF}\right) \tag{3}$$

where $\Delta\sigma_{D,cor}$ is the stress range corresponding to $N_{f,CAFL}$ cycles at the intersection of the two corroded fatigue curves. Here, $N_{f,LCF}$ is the number of cycles to fatigue failure of uncorroded details at the intersection point of their HCF and LCF regions. This has been generally considered as 10^4 cycles, which is the lowest value of N_R given in fatigue design codes.[1,30] The proposed formula for the fatigue strength of corroded detail categories can be simplified as,

$$\frac{\Delta\sigma_{cor}}{\Delta\sigma} = \left(\frac{N_R}{N_{f,LCF}}\right)^{-c} \text{ where } c = {}^{log}\left[\frac{\Delta\sigma_D}{\Delta\sigma_{D,cor}}\right] \Big/ {}_{log}\left[\frac{N_{f,CAFL}}{N_{f,LCF}}\right] \tag{4}$$

By substituting $\Delta\sigma$ from Eq. (2), the proposed formula for the fatigue strength for the corroded detail can be obtained as

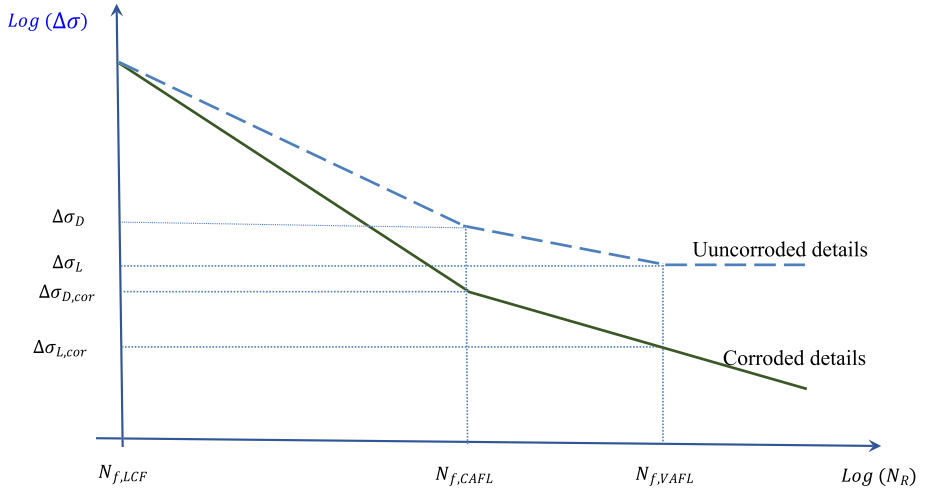

FIGURE 3 Schematic representation of fatigue strength curve of uncorroded and corroreded detail categories [Colour figure can be viewed at wileyonlinelibrary.com]

$$\Delta\sigma_{cor} = \Delta\sigma_D \left[N_{f,LCF}^{c} N_{f,CAFL}^{1/m} \right] N_R^{\left(-c-1/m\right)} \tag{5}$$

If $\Delta\sigma_{cor} \le \Delta\sigma_{D,cor}$, the fatigue strength of corroded constructional detail can be obtained,

$$\log\left(\Delta\sigma_{D,cor}\right) - \log\left(\Delta\sigma_{cor}\right) = \frac{\left[\log\Delta\sigma_{D,cor} - \log\Delta\sigma_{L,cor}\right]}{\left[\log N_{f,CAFL} - \log N_{f,VAFL}\right]} \times \left(\log N_{f,CAFL} - \log N_R\right) \tag{6}$$

or,

$$\frac{\Delta\sigma_{cor}}{\Delta\sigma_{D,cor}} = \left(\frac{N_R}{N_{f,CAFL}}\right)^{\acute{c}} \text{ where } \acute{c} = {}^{log}\left[\frac{\Delta\sigma_{D,cor}}{\Delta\sigma_{L,cor}}\right] \Big/ {}_{log}\left[\frac{N_{f,CAFL}}{N_{f,VAFL}}\right] \tag{7}$$

When $\Delta\sigma_{cor} \le \Delta\sigma_{D,cor}$, the proposed formula for fatigue strength for corroded details can be obtained as,

$$\Delta\sigma_{cor} = \Delta\sigma_{D,cor} \left[N_{f,CAFL}^{-\acute{c}} \right] N_R^{\acute{c}} \tag{8}$$

The parameters c and $\acute{c}$ depend on the CF endurance of the construction details and their determination are discussed in the following sub section.

4.2 | Parameters used in the proposed curve

The values of $\Delta\sigma_D$,$\Delta\sigma_L$,m,$N_{f,LCF}$,$N_{f,CAFL}$ and $N_{f,VAFL}$ are directly obtained from the code providing fatigue strength/S-N curves of constructional details tested in air.[1,30] The $\Delta\sigma_{D,cor}$ and $\Delta\sigma_{L,cor}$ are the corrosive state and the environment dependent parameters of the detail. These parameters are commonly determined by full-scale fatigue tests in the VHCF region and it is costly in terms of both resources and time as the loading frequency is very low for full scale testing. The test results (i.e. experimental fatigue lives) are scattered as the test process is subjected to many variables and uncertainties. These $\Delta\sigma_{D,cor}$ and $\Delta\sigma_{L,cor}$ can be determined by fracture mechanics theories when there are corrosion pits. Recent investigations of carbon steel reveals that CF cracks initiate in any corrosive media due to a different mechanism and the presence of the pits is not necessary.[11-14] Therefore, this section proposes a reasonably accurate relation to obtain $\Delta\sigma_{D,cor}$ and $\Delta\sigma_{L,cor}$ for structural steels in fresh water (i.e. similar to urban environment) and sea water (i.e. similar to marine environment) based on the parameters used in the proposed formula for corroded material as described in section 3.2.

The values of $\Delta\sigma_D$,$\Delta\sigma_L$,m,$N_{f,LCF}$,$N_{f,CAFL}$ and $N_{f,VAFL}$ are presented in Table 2 to determine Eurocode[30] given fatigue curves. The following relations are obtained to determine the values of $\Delta\sigma_{D,cor}$ and $\Delta\sigma_{L,cor}$ by interpolations and extrapolations of $\sigma_{\infty,cor}/\sigma_\infty$ ratios corresponding to $N_{f,CAFL}$ and $N_{f,VAFL}$.

$$\frac{\Delta\sigma_{D,cor}}{\Delta\sigma_D} = \left(\frac{\sigma_{\infty,cor}}{\sigma_\infty}\right)^{0.9} \text{ and } \frac{\Delta\sigma_{L,cor}}{\Delta\sigma_L} = \left(\frac{\sigma_{\infty,cor}}{\sigma_\infty}\right)^{1.33} \tag{9}$$

The corresponding mean and conservative values (i.e. design value= mean-2×standard deviation) are listed in Table 2. Similarly, for DNV code, the following relations can be derived. The corresponding values are listed in Table 2.

TABLE 2 Parameters used in the proposed fatigue strength curve of corroded details

Parameter	Constructional details in Eurocode				Constructional details in DNV code			
$N_{f,LCF}$	10^4				10^4			
$N_{f,CAFL}$	5×10^6				10^7			
$N_{f,VAFL}$	10^8				10^8			
$\frac{\Delta\sigma_L}{\Delta\sigma_D}$	0.549				0.631			
Corrosion parameters	Marine environment		Urban environment		Marine environment		Urban environment	
	Mean value	Conservative value	Mean value	Conservative value	Mean value	Conservative value	Mean value	Conservative value
$\frac{\Delta\sigma_{D,cor}}{\Delta\sigma_D}$	0.497	0.308	0.641	0.536	0.46	0.27	0.61	0.50
$\frac{\Delta\sigma_{L,cor}}{\Delta\sigma_L}$	0.356	0.175	0.518	0.40	0.356	0.175	0.518	0.40

$$\frac{\Delta\sigma_{D,cor}}{\Delta\sigma_D}=\frac{\sigma_{\infty,cor}}{\sigma_\infty}\ \text{and}\ \frac{\Delta\sigma_{L,cor}}{\Delta\sigma_L}=\left(\frac{\sigma_{\infty,cor}}{\sigma_\infty}\right)^{1.33} \quad (10)$$

The proposed values in Table 2 are compared with environmental reduction factors (ERF), which are obtained from experimental results of welded plate and tubular joints in marine environment. The ERF is the inverse of the ratios $\frac{\Delta\sigma_D}{\Delta\sigma_{D,cor}}$ and $\frac{\Delta\sigma_L}{\Delta\sigma_{L,cor}}$. The value varies from 1 to 5.2. An average ERF value of 3 has been recommended for both 16 mm welded plate and tubular joints at 10^6 cycles of endurance in freely corroding environment.[19] The proposed values have a good match with the ERF values. Even though this paper only presents the parameters for the Eurocode and DNV codes, the same procedure can be applied to determine the parameters for obtaining corroded S-N curves in any detail category given in any fatigue codes.

4.3 | Experimental verification of the proposed curve

The corrosion fatigue test results of structural details exposed to corrosive media are compared with predicted fatigue lives by the proposed formula to confirm its validity in this section. Full-scale fatigue testing results of rolled plates fabricated from SMA weathering steel[2,31] are compared with the prediction of Eqs 5 and 8 as shown in Fig. 4. This steel is commonly used in Japan for bridges, agricultural vehicles, railway wagons, water pipes and etc. The tests were performed in tension compression constant amplitude loading. Corroded and uncorroded

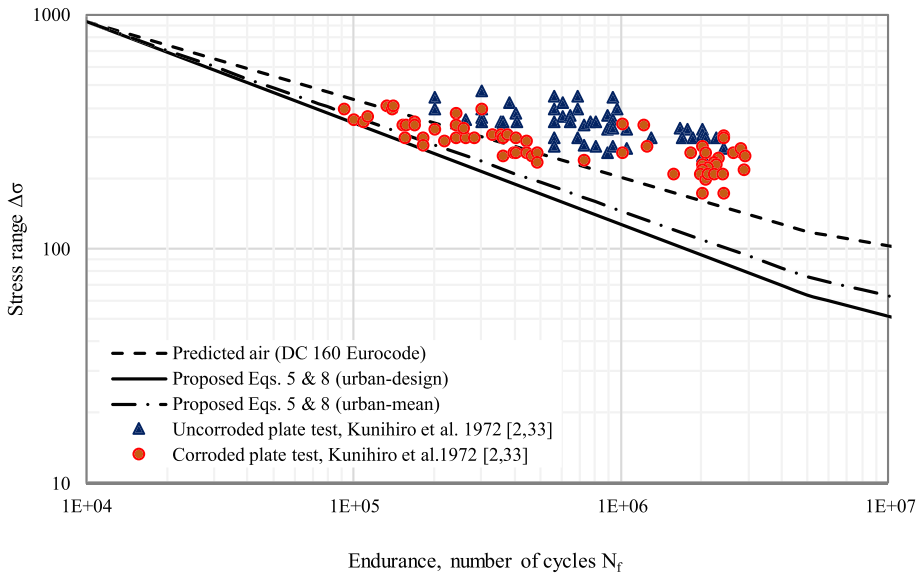

FIGURE 4 Comparison of proposed S-N curve with fatigue tests of 2 years weathered rolled SMA plates [Colour figure can be viewed at wileyonlinelibrary.com]

test results correspond respectively to plates taken after two years of weathering and unweathered plates. In lower stress levels, corroded specimens fatigue endurance is closer to uncorroded plates fatigue endurance as there were no severe rust pits formed after two years of weathering. The weathered steel is allowed to rust in order to form protection coating and the severity of rust pits governs the fatigue endurance.[3] Therefore, lower stress level is not sufficient to increase the stress concentration of rust pits and this is the reason why the same fatigue life for weathered and unweathered plates can be observed. The Eurocode detail category 160 represents fatigue strength of rolled steel plates.[30] As the plate was subjected to weathering in air and tests were performed in a sheltered environment, urban environment parameters conservatively were selected from Table 2 for predicting the S-N curves. The predicted S-N curve shows a good match with the test results as shown in the Fig. 4.

Fatigue test results of corroded bridge girders extracted from Trolley Bridge[32] are compared with the prediction of the proposed formula as shown in Fig. 5. The beams were standard rolled, 4.72 m long and made of carbon steel after 85 years of corrosion. The bridge was located urban environment and subjected to moderate corrosivity. The 22 beams which had not been subjected fatigue in service (i.e. operating stress were well below fatigue limit) were

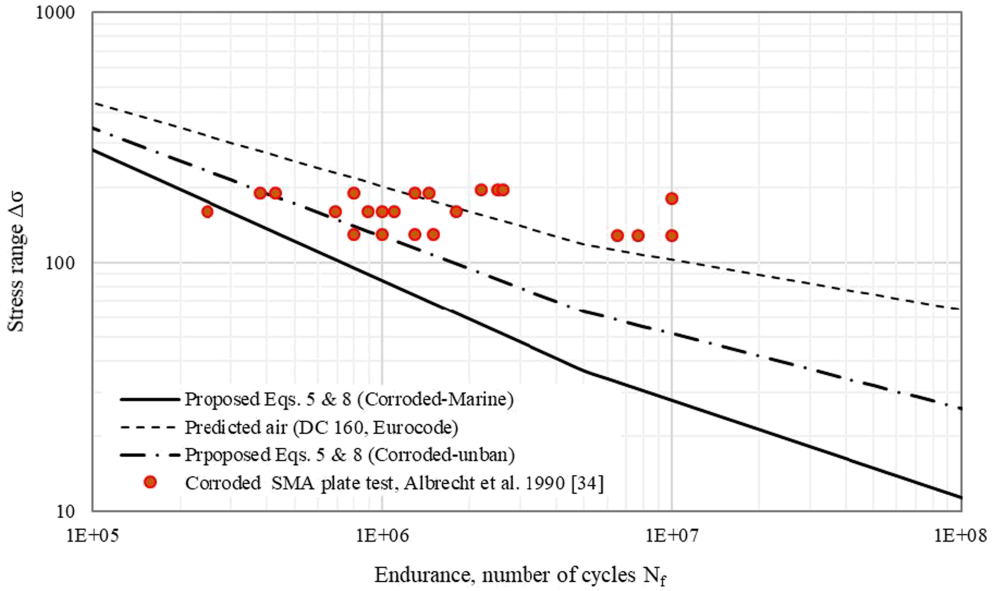

FIGURE 5 Comparison of proposed S-N curve with fatigue test of corroded carbon steel beams [Colour figure can be viewed at wileyonlinelibrary.com]

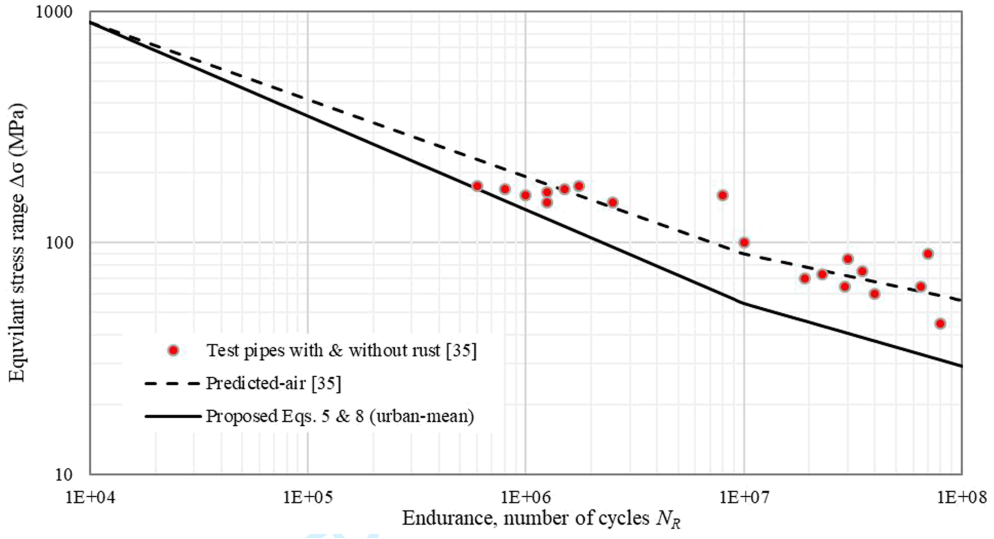

FIGURE 6 Comparison of proposed S-N curve with full-scale fatigue test of girth welded pipes under variable amplitude loading [Colour figure can be viewed at wileyonlinelibrary.com]

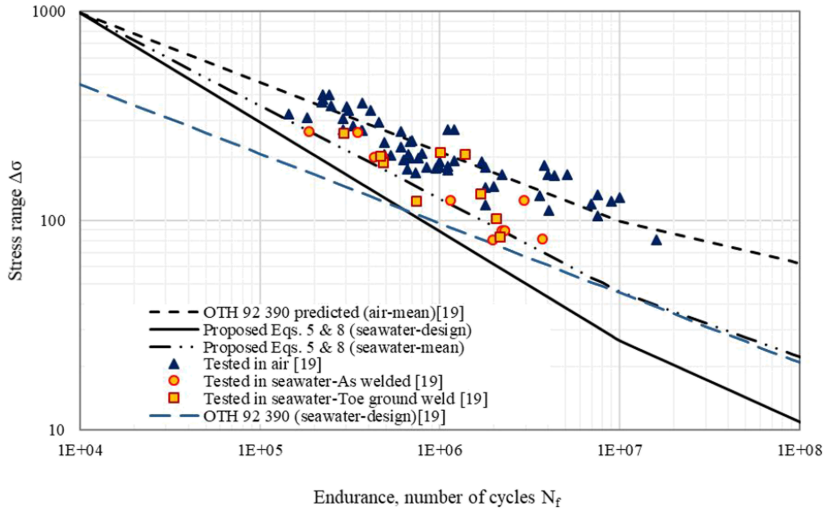

(A)

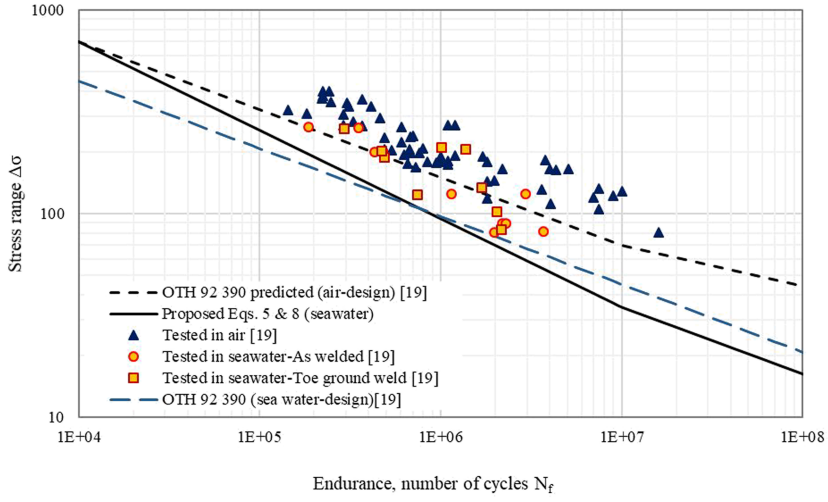

(B)

FIGURE 7 Comparison of proposed S-N curve with fatigue test of tubular joints in seawater-free corrosion, thickness 16 mm: (a). parameters obtained from mean S-N curve in air, (b). parameters obtained from design S-N curve in air [Colour figure can be viewed at wileyonlinelibrary.com]

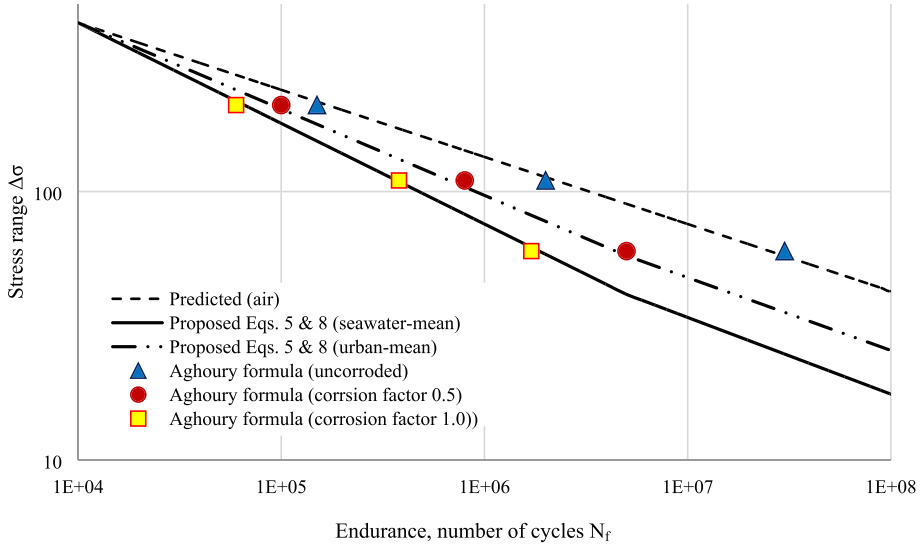

FIGURE 8 Comparison of proposed S-N curve with Aghoury's strain-life model [2,3] predicted fatigue endurances for different corrosion factors [Colour figure can be viewed at wileyonlinelibrary.com]

subjected to bending fatigue test. The Eurocode detail category 160 represents the fatigue strength of rolled carbon steel.[30] The proposed S-N curve for both marine and urban environments was plotted in Fig. 5 by using Eqs 5 and 8. The model parameters were selected from Table 2 to correspond detail category 160. Figure 5 shows a good agreement with the proposed formulae for 70% of the test results.

Figure 6 shows a similar verification with the fatigue testing results of full-scale girth welded pipes tested under variable amplitude loading.[33] The resonance fatigue testing technique was used for those full-scale pipes. Rotating redial force was applied to one end to excite the pipe close to its first mode of vibration. A bending moment was, then, generated to induce a variable amplitude stress state. Alternatively, girth welded pipe strips were also tested by ordinarily hydraulic test machine. Considerable amount of corrosion and rusting were observed in girth welded region only for few pipes and specimens. The S-N curve for uncorroded girth welded details were taken from the same reference and the predicted air curves are shown in Fig. 6. The model parameters for the proposed S-N curve of the corroded girth welded pipes were obtained from the predicted air curve and Table 2. Similarly, Eqs 5 and 8 are used to predict S-N curve of the corroded items as shown in Fig. 6 compared with the corresponding experimental results.

HSE offshore technology report[19] has provided free corrosion fatigue strength tubular joints used in offshore structures based on surveying some fatigue test results. The determination of ERF was also mentioned in the report. Fatigue tests of tubular joints with both the toe ground weld and as welded were considered for the test. Proposed S-N curves for the marine environment were

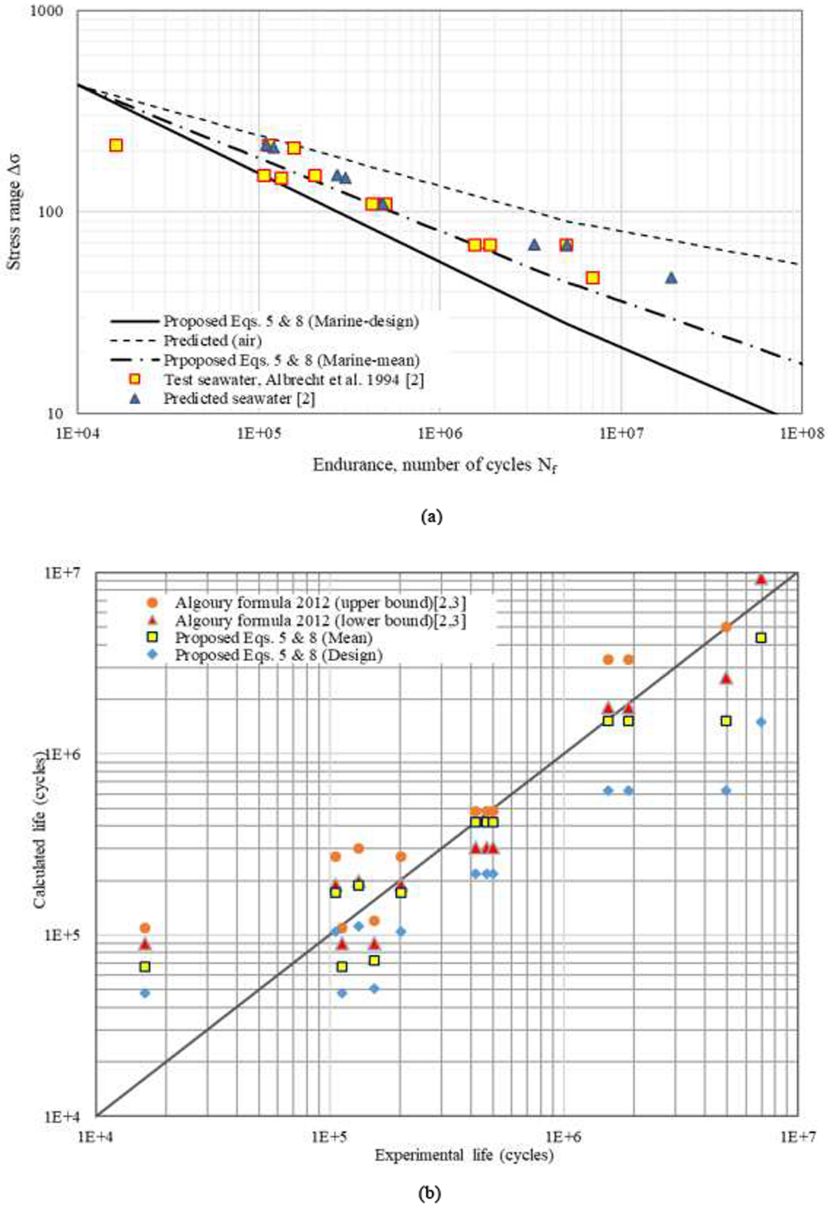

FIGURE 9 Comparison of Aghoury's strain-life model [2,3] predicted fatigue endurances and experimental fatigue lives of sheltered steel beams tested in moist saltwater environment with: (a). proposed S-N curve plots, (b). proposed S-N curve formula predicted fatigue lives [Colour figure can be viewed at wileyonlinelibrary.com]

plotted using the formulae given in Eqs 5 and 8 for thickness 12mm tubular joints as shown in Fig. 7. The proposed S-N curve in Fig. 7a was based on the parameters of mean S-N curve of tested tubular joints in air while Fig. 7b was based on the design curve. The marine environment model parameters were taken from Table 2 and hence both the design and the mean S-N curves are plotted for corroded tubular joints. Measured hot spot stresses were used for this comparison. The S-N curves has a very good agreement with the corresponding experimental fatigue lives. The previously proposed free corrosion (FC) fatigue curve[19] seems to be over conservative when the endurance is lower than 10^6 cycles. However, it is doubtful in VHCF region. The previous FC curve intersects the new curves between 10^5 and 10^6, where the test results were used for ERF determination. This indirectly indicates that the determined model parameters shown in Table 2 have a good agreement with the ERF values.[19]

As discussed in the introduction, Aghoury proposed a strain-life model based on the Smith–Watson–Topper model[2,3] to simulate the CF behaviour of metals. The S-N curves predicted by that model for three different corrosion rates are compared in Fig. 8 with the corresponding S-N curves predicted by Eqs 5 and 8 for marine and urban environments. The S-N curve for air was predicted based on corrosion factor zero. The figure shows good agreement between proposed models.

Aghoury[2,3] compared his model estimated fatigue lives with the experimental fatigue behaviour of the corroded rolled beams of A588 steel. The beams were boldly exposed for 67 months under metal deck in moist salt water (i.e. sheltered in marine environment). The fatigue lives predicted by both models are compared with experimental lives in Fig. 9. The figures confirm the validity of Eqs 5 and 8 and its parameters listed in Table 2.

5 | CONCLUSIONS

The comparisons of the predicted fatigue curves with fatigue test results of corroded steel in different corrosive media conclude the validity of a proposed formula and the validity of the proposed mean and conservative values for parameters used in the formula. The proposed curve does not require any material parameter or corrosive media specific parameter except the fatigue strength curve (i.e. S-N curve) obtained in air.

The S-N curves predicted by the derived formula are in a very good agreement with experimentally obtained fatigue lives of corroded constructional details considered in the present study. The physics behind the CF has been studied from the literature in a micro structural level, specimen scale and finally incorporated into structural member and joint scale. This is the main reason of having a good agreement with the full-scale fatigue test results. The values of the curve parameters have been proposed only for detail categories given by Eurocode and DNV code. The same procedure can be utilized with the values proposed for the corroded steel to determine the model parameters for any detail category given in any code. The main advantage of the proposed formula is that it requires only the fatigue strength curve of the constructional detail in air, which is given in relevant codes, to predict the corresponding S-N curve in a corrosive media.

NOMENCLATURE

b	Basquin's exponent
m	negative inverse slope of the *S-N* curve
N_f	number of cycles to fatigue failure
$N_{f,FL}$	endurance number of cycles
$N_{f,LCF}$	number of cycles to fatigue failure of the uncorroded materials at the yield strength
$N_{f,CAFL}$	number of cycles at constant amplitude fatigue limit
$N_{f,VAFL}$	number of cycles at variable amplitude fatigue limit
N_R	number of cycles to fatigue failure
$\Delta\sigma$	stress range
$\Delta\sigma_{cor}$	fatigue strength range of corroded constructional detail
$\Delta\sigma_D$	stress range at constant amplitude fatigue limit
$\Delta\sigma_{D,cor}$	stress range at intersecting points of two slopes of corroded fatigue at number of cycles at constant amplitide fatigue limit
$\Delta\sigma_L$	stress range at variable amplitude fatigue limit
$\Delta\sigma_{L,cor}$	stress range at number of cycles ar variable amplitude fatigue limit
$\sigma_{a,cor}$	fatigue strength of corroded material
σ_y	yield strength
$\sigma_f^{'}$	fatigue strength coefficient
σ_∞	endurance limit (i.e. fatigue limit for high-cycle fatigue)
$\sigma_{\infty,cor}$	endurance limit for corroded material.

ORCID

N.D. Adasooriya https://orcid.org/0000-0001-8412-8009

REFERENCES

1. DNV GL Recommended practices. *Fatigue design of offshore steel structures DNVGL-RP-0005*. Norway: Det Norske Veritas; April; 2016.

2. El Aghoury I. *Numerical tool for fatigue life prediction of corroded steel riveted connections using various damage models, PhD thesis*. Canada, Montreal: Concordia University; 2012.
3. El Aghoury I, Galal K. Corrosion-fatigue strain-life model for steel bridge girders under various weathering conditions. *J Struct Eng*. 2014;140(6):Article number 04014026.
4. Adasooriya ND, Hemmingsen T, Pavlou D. Fatigue strength degradation of metals in corrosive environments. Proceedings of first conference of computational methods in offshore technology-COTech 2017, IOP Conf Ser: Mater Sci Eng: IOP Publishing; Stavanger, Norway: 2017: Article number 276 012039.
5. Roberge PR. *Handbook of Corrosion Engineering*. 1st ed. New York: McGraw Hill; 2000.
6. Mikkelsen O, Rege K, Hemmingsen T, Pavlou D. Numerical estimation of the stop holes-induced fatigue crack growth retardation in offshore structures taking into account the corrosion effect. Proceeding of International Society of Offshore and Polar Engineers conference series. San Francisco: American Society of Mechanical Engineers, 2007: ISOPE-I-17-552: 451-458.
7. Hoeppner DW, Chandrasekaran V, Taylor AMH. Review of pitting corrosion fatigue models. Proceedings of ICAF International Conference. Melbourne, Australia: 1995: 1-25.
8. Acuña N, González-Sánchez J, Ku-Basulto G, Domınguez L. Analysis of the stress intensity factor around corrosion pits developed on structures subjected to mixed loading. *Scr Mater*. 2006;55:363-366.
9. Ian T. The effect of notches and pits on corrosion fatigue strength, PhD thesis. UK: Sheffield Hallam University; 2004.
10. Sharifi Y, Rahgozar R. Fatigue notch factor in steel bridges due to corrosion. *Arch Civ Mech Eng*. 2009;9(4):75-83.
11. Zhao T, Liu Z, Du C, Dai C, Li X, Bowei Z. Corrosion fatigue crack initiation and initial propagation mechanism of E690 steel in simulated sea water. *Mat Sci Eng A*. 2017;708:181-192.
12. Vucko F, Bosch C, Delafosse D. Effects of cyclic plastic strain on hydrogen environment assisted cracking in high-strength steel. International hydrogen conference (IHC 2012): hydrogen-materials interactions. WY, United States: American Society of Mechanical Engineering; 2012.
13. Vucko F, Bosch C, Aoufi A, Delafosse D. *Palladium coating on quenched-tempered martensitic steel for hydrogen electrochemical permeation tests. Technical Reports- ENSMSE-SMS-2014-01*. France: EMSE-00951142; 2014.
14. Wang R. *Corrosion fatigue of metal materials*. Xi'an: Press of Northwestern Polytechnical University; 2001.
15. Adasooriya ND, Siriwardane SC. Remaining fatigue life estimation of corroded bridge members. *Fatigue Fract Eng Mater Struct*. 2014;37(6):603-622.
16. Wahab MA, Sakano M. Corrosion and biaxial fatigue of welded structures. *J Mat Proc Tech 3*. 2003;143–144:410-415.
17. Nguyen KT, Garbatov Y, Soares CG. Spectral fatigue damage assessment of tanker deck structural detail subjected to time-dependent corrosion. *Int J Fatigue*. 2013;48:147-155.
18. Gerhard S, Christian K, Bertram K, Hensen W. *Condition assessment and inspection of steel railway bridges, including stress measurements in riveted, bolted and welded structures: Sustainable Bridges-Background document SB3.4*. Sweden: Digital Vetenskapliga Arkivet; 2007.
19. HSE OTH 92 390. *Background to new fatigue guidance for steel joints and connections in offshore structures, offshore technology report*. UK: Health Safety Executives; 1999.
20. Revie RW, Uhlig HH. *Corrosion and Corrosion Control, An Introduction to Corrosion Science and Engineering*, 4th edn. US: Wiley and Sons; 2008.
21. Glaser W, Wright LG. Mechanically assisted degradation. *ASM Handbooks ASM Internationals*. 1992;1992:137-144.
22. Gangloff RP. Environmental cracking - corrosion fatigue. In: Baboian R, Dean SW Jr, Hack HP, Hibner EL, Scully JR, eds. *Corrosion Tests and Standards Manual*. US: ASTM Internationals; 2005.
23. Boyer HE. *Atlas of Fatigue Curves*. USA: ASM International; 1986.
24. Yasser Y, Jeom KM. Ultimate strength reliability analysis of corroded steel-box girder bridges. *Thin-Walled Struct*. 2011;49:157-166.
25. Bandara CS. *Fatigue damage assessment of steel structures and components, Improvements in stress-life approach*. Germany: LAP Lambert Academic Publishing; 2015.
26. Luiz OAA. *Corrosion, Chapter 7, Machinery Failure Analysis Handbook*. Texas: Gulf Publishing Company; 2006:83-99.
27. Li Y, Hou B. Corrosion fatigue of welded joints of steel for marine platform. *Indian J Eng Mat Sci*. 2003;13:467-470.
28. Matthew W, Paul DE, Huseyn O, Murat T. The effect of surface corrosion damage on the fatigue life of 6061-T6 aluminum alloy extrusions. *Mater Sci Eng A*. 2017;690:427-432.
29. Li S-X, Akid R. Corrosion fatigue life prediction of a steel shaft material in sea water. *Eng Fail Anal*. 2013;34:324-334.
30. NS EN 1993-1-9. *Eurocode 3: Design of steel structures - Part 1-9: Fatigue*. Belgium: European Committee for Standardization; 2005.
31. Kunihiro T, Inove K, Fukuda T. *Atmospheric exposure study of weathering steel. Research Lab. Report Br. 71-08*. Tokyo, Japan: Ministry of Construction; 1972.
32. Albrecht P, Shabshab CF, Wulin L. Remaining fatigue strength of corroded steel Beams, IABSE reports. International Association of Bridge and Structural Engineering publications; 1990: 71-84.
33. Zhang YH, Maddox SJ. Fatigue testing of full-scale girth welded pipes under variable amplitude loading. *J Offshore Mech Arctic Eng*. 2014;136(2):Article number 02140-1.

How to cite this article: Adasooriya ND, Pavlou D, Hemmingsen T. Fatigue strength degradation of corroded structural details: A formula for *S-N* curve. *Fatigue Fract Eng Mater Struct*. 2019;1–13. https://doi.org/10.1111/ffe.13156

Paper 4

S-N Curve for Riveted Details in Corrosive Environment and its Application to a Bridge

Journal Paper

Fatigue & Fracture of Engineering Materials & Structures

December 2019, Accepted

S-N curve for riveted details in corrosive environment and its application to a bridge

Journal:	*Fatigue & Fracture of Engineering Materials & Structures*
Manuscript ID	FFEMS-8494.R1
Manuscript Type:	Original Contribution
Date Submitted by the Author:	25-Dec-2019
Complete List of Authors:	Adasooriya, Nirosha D; University of Stavanger, Structural and Mechanical Engineering and Material Science Hemmingsen, Tor; University of Stavanger, Mechanical and Structural Engineering and Materials Science Pavlou, Dimitrios G; University of Stavanger

S-N curve for riveted details in corrosive environment and its application to a bridge

Nirosha D. Adasooriya[1,*], Tor Hemmingsen[2], Dimitrios Pavlou[2]

[1] *University of Stavanger, Department of Mechanical & Structural Engineering and Materials Science, Stavanger N-4036, Norway.*

[2] *University of Stavanger, Department of Mechanical & Structiral Engineering and Materials Science, Stavanger N-4036, Norway.*

** Corresponding author: Nirosha D. Adasooriya; mudiyan.n.adasooriya@uis.no Tel.: +47 51831909*

Abstract

A formula for stress-life curve is proposed to predict the fatigue life of riveted bridges located in corrosive environments. The corrosive environment dependent parameters of the S-N curve are determined based on the corrosion fatigue testing results of different types of steel specimens in air, fresh water and seawater. Eurocode detail category 71 and UK WI-rivet detail category represent the fatigue strength of riveted members. The proposed S-N curve formula is compared with full-scale fatigue test results of riveted joints, plate girders and truss girders which were tested in a corrosive environment. Thus, the validity of the formula is confirmed. The formula does not require any material parameter other than the code-given fatigue curve of riveted details. The fatigue life of a riveted railway bridge is estimated by using the proposed formula, and the results are compared with conventional approaches. The applicability and significance of the proposed curve are confirmed.

Keywords: corrosion fatigue; S-N curve; riveted joints; steel bridges

Nomenclature: CF, corrosion fatigue; $C(t)$, average corrosion penetration in millimetres; DC, detail category; HCF, high cycle fatigue; LCF, low cycle fatigue; m, negative inverse slope of the *S-N* curve; N_R, number of cycles to fatigue failure; $N_{f,FL}$, endurance number of cycles; $N_{f,LCF}$, number of cycles to fatigue failure of the uncorroded materials at the yield strength; $N_{f,CAFL}$, number of cycles at constant amplitude fatigue limit; $N_{f,VAFL}$, number of cycles at variable amplitude fatigue limit; t, age in years; t_0, time in years of the first appearance of general corrosion; VHCF, very high cycle fatigue; WI, wrought iron; $\Delta\sigma$, stress range; $\Delta\sigma_{cor}$, fatigue strength range of corroded constructional detail; $\Delta\sigma_D$, stress range at constant amplitude fatigue limit; $\Delta\sigma_{D,cor}$, stress range at intersecting points of two slopes of corroded fatigue curve at $N_{f,CAFL}$ cycles; $\Delta\sigma_L$,

stress range at variable amplitude fatigue limit; $\Delta\sigma_{L,cor}$, stress range at $N_{f,VAFL}$ cycles; β, reliability index; Δ, Miner's critical damage accumulation index; D_{cor}, Miner's damage accumulation index in corrosive environment; S_{re}, equivalent constant amplitude stress ranges calculated using bilinear *S-N*; s, slope of the *S-N* curve; *N(t)*, subjected number of cycles of the considered detail at age *t*; A_{cor}, fatigue detail coefficient; n_i^o , the number of cycles in i^{th} stress range when S_{ri} is greater than the $\Delta\sigma_{D,cor}$; n_j^o, number of cycles in j^{th} stress range when S_{rj} is less than the $\Delta\sigma_{D,cor}$; β_{target}, target reliability index.

1. Introduction

Bridge authorities are paying significant attention to the ageing issues of bridges, as most railway bridges in the world are reaching their design life[1-5]. Replacement of all of these is practically impossible, due to both the decommissioning and new building costs, as there are many ageing bridges. Most of the structural members of these bridges were constructed by riveted members (i.e. built up by riveting the plates). Riveting was widely used to assemble metal structures before 1940[5,6]. Drilling, punching and reaming are major processes used for making rivet holes. Then hot rivets drive through the holes of the two plates and hammer the shank to form the second rivet head[5]. The clamping force develops in between plates when cooling the rivets. The release of clamping force increases the bearing, and this may have a significant effect in reducing the fatigue strength[5]. Some degree of corrosion has always been present in these old bridges, due to the difficulty of maintaining the coating/corrosion protection system in between layered parts/plates of riveted built-up sections[5-7]. Some of these bridges are located in urban industrial and moderate marine environments which have been classified as severely corrosive environments[8,9]. Although many bridges are located onshore, de-icing salt may simulate a marine environment for bridges in snowy regions[8]. The combined influence of the severe corrosive environment and the cyclic stresses due to variable traffic loads initiate cracks in both corroded and uncorroded regions (i.e. corrosion-free areas and/or coating-lost areas) of the riveted members and joints[10-13]. Fractures due to the cyclic stress in corrosive media are designated as corrosion fatigue (CF), which is a type of environmentally assisted cracking; hence, fatigue strength degradation (i.e. degradation of the S-N curve) can be observed. The fatigue performance of riveted joints and members depends on the type of material, production methods of rivet holes, clamping force, degree of coating, state of deterioration due to corrosion and the corrosive environment.

A significant amount of full-scale fatigue testing has been carried out for riveted details[5,8,9]. It is difficult to compare the degree/severity of the effect of CF for the above tests, without studying the distinction of mechanisms between corroded members tested in air, corroded members tested in a corrosive environment and uncorroded members tested in corrosive environments. The contradictory conclusions reported in the literature motivate more accurate simulation of the CF strength of riveted structural details in different corrosive environments[8,14,15].

Detailed provisions and models/formulas are not available in codes of practices to predict the fatigue strength of the riveted details of land-based structures which are exposed to corrosive environments[4,8,9]. As bolted and/or welded joints are popular for modern bridge applications, new fatigue standards have not paid major attention regarding S-N curves for riveted details. A few past studies recommend neglecting the endurance limit (i.e. the S-N curve should be used without a cut-off limit), to take into account the fatigue strength degradation due to the effect of a corrosive environment[4,12,13,16]. The modified S-N curves do not match the available fatigue test results of riveted details exposed to corrosive environments.

To overcome the previously mentioned problems, the main objective of this paper is to propose a formula for an S-N curve for riveted joints and members exposed to corrosive environments. The parameters used in the formula are mainly dependent on a corrosive urban environment and the riveted detail categories of both steel and wrought iron. The urban environment-dependent parameters of the S-N curve formula are conservatively determined, based on the corrosion fatigue testing results of different types of steel presented in a previous publications[3,17]. The proposed S-N curve formula is verified by comparing the full-scale fatigue test results of uncorroded (i.e. corrosion-free), weathered and deteriorated riveted girders (i.e. both plate and truss girders) tested in an urban environment. The fatigue life of a riveted bridge is estimated by using the proposed S-N formula, and the results are compared with conventional approaches.

2. Proposed S-N curve for riveted bridges exposed to a corrosive environment

The fatigue strength curve for specimens in a corrosive environment, which was proposed by authors' previous studies[3, 17], is further developed to obtain an *S-N* curve for riveted joints and members which are exposed to corrosive environments. The fatigue design standards, currently used in Europe, have defined only two detail categories for

riveted structural details. Those are detail category 71, which is given in Eurocode[18] and WI-rivet detail category, which is given in the UK railway assessment code[4,19,20]. The curve has been obtained by modifying the design S-N curves of both detail category 71[18] and WI-rivet detail category, which is given in the UK railway assessment code[4,19,20], respectively. The environmentally assisted CF behaviour of the tested laboratory specimens was utilized for this modification.

2.1. The concept used for the proposed curve

The stress range and peak stress level are the governing parameters of CF crack initiation and propagation. The CF crack initiation may occur without the presence of pits and the CF cracks are expanded by the post reaction of corrosion for carbon steel [21]. Gliding can be seen in some of the grains due to cyclic stresses. When dislocations reach a grain boundary, gliding is ceased[22]. When the stress is reversed, the movement of the grains retraces along the slip plane. Slight irregularities restricts the movement and develops another parallel slip plane. Finally, these disorganized bands of material cause separation between slip planes while initiating the cracks at high stress ranges. Due to the interaction of a corrosive environment, disorganized atoms are moving along slip planes with less activation energy unlike with corrosion. This behavior may be observed even in lower stress ranges (i.e. bellow the fatigue endurance limit)[3,17] and hence there is no safe stress level at which the fatigue life is infinite. The environmental, metallurgical and structural factors are the governing parameters of the CF strength[4,23]. Negligible differences between low cycle fatigue (LCF) lives in corrosive and non-corrosive environments were found in almost all the fatigue test results of steel specimens, and a significantly larger difference is found in the very high cycle fatigue (VHCF) region[3,8,22,24,25].

2.2. Derivation of fatigue strength curve for the riveted details in corrosive environments

The fatigue strength curve is presented in Fig. 1 for riveted details which are not exposed to a corrosive environment [18,19,20] (i.e. design S-N curves given in fatigue codes), and the corresponding formula can be presented in general for both detail category 71[18] and WI-rivet detail category[4,19,20] as shown in Eq. (1).

$$\Delta\sigma = \left(\Delta\sigma_D N_{f,CAFL}^{1/m}\right) N_R^{(-1/m)} \quad (1)$$

The $\Delta\sigma$ is the stress range and N_R is the corresponding number of cycles to fatigue failure.

The $\Delta\sigma_D$ is the stress range at the fatigue curve slope changing point, which corresponds to the $N_{f,CAFL}$ cycles. The $\Delta\sigma_D$ is defined as the constant amplitude fatigue limit[18]. The slope of the fatigue strength curve is -1/m. According to the Eurocode[18], m is equal to 3 when $\Delta\sigma \geq \Delta\sigma_D$, equal to 5 when $\Delta\sigma_D \geq \Delta\sigma > \Delta\sigma_L$ and infinite when $\Delta\sigma \leq \Delta\sigma_L$, where $\Delta\sigma_L$ is the fatigue endurance limit of the detail which corresponds to $N_{f,VAFL}$. This is also defined as the fatigue cut-off limit or variable amplitude fatigue limit in Eurocode given detail category 71[18]. These fatigue curves are generally referred to as trilinear S-N curves. The fatigue curves of the WI-rivet detail category, which is given in the UK railway assessment code[4,19,20], do not have such a cut-off limit and are commonly named bi-linear S-N curves. The curve parameters, slopes and details of knee points (i.e. $N_{f,CAFL}$, $N_{f,VAFL}$, $\Delta\sigma_D$ and $\Delta\sigma_L$) are listed in Table 1 for both detail categories by referring to the relevant standards[18, 4, 19, 20].

Fig. 1. Schematic representation of fatigue strength curve of riveted details exposed to corrosive environments

According to the CF mechanism and the concept of fatigue endurance of laboratory specimens mentioned in Section 2.1, the linear variation in the difference between the fatigue strengths of riveted details which are not exposed to corrosive environments has been observed, as shown in Fig. 1. The previously published CF test results of steel specimens[3,17], which were tested in corrosive environments, show a non-linear behavior of the S-N curve. This can be conservatively assumed as a bilinear S-N curve. For most of the steel specimens, the intersecting points of the two slopes of the assumed bilinear S-N curves were found between 10^6 to 10^7 cycles. This range coincides with the number of cycles at the first intersecting points of the two slopes of S-N curves of specimens tested in non-corrosive environment, i.e $N_{f,CAFL}$. Therefore, the $N_{f,CAFL}$is considered as the number of cycles at the intersecting point of the two slopes of the S-N curve of riveted details exposed to corrosive environments. This value may not be valid for the structural details which are subjected to severe pitting/localized corrosion as it has a negligible crack initiation life relative to the crack propagation life. The relative difference in log scale is linearly deducted from the S-N curves of riveted details given in fatigue codes, to obtain the S-N curves of riveted details which are exposed to corrosive environments. The detailed derivation is presented in authors' previous publications[3,17]. Hence, the fatigue

strength range of riveted details in corrosive environments, $\Delta\sigma_{cor}$, corresponding to N_R, can be derived, if $\Delta\sigma_{cor} \geq \Delta\sigma_{D,cor}$,

$$\log(\Delta\sigma_{cor}) = \log(\Delta\sigma) - \left[\frac{\log\Delta\sigma_D - \log\Delta\sigma_{D,cor}}{\log N_{f,CAFL} - \log N_{f,LCF}}\right](\log N_R - \log N_{f,LCF}) \quad (2)$$

where $\Delta\sigma_{D,cor}$ is the stress range corresponding to $N_{f,CAFL}$ cycles at the intersection of the two slopes of fatigue curves for corrosive environments. Here, $N_{f,LCF}$ is the number of cycles to fatigue failure of riveted details at the intersection point of their high cycle fatigue (HCF) and LCF regions. This has been generally considered as 10^4 cycles, which is the lowest value of N_R given in fatigue design codes[18,19]. The proposed formula for the fatigue strength of riveted detail categories in corrosive environments can be simplified as,

$$\frac{\Delta\sigma_{cor}}{\Delta\sigma} = \left(\frac{N_R}{N_{f,LCF}}\right)^{-c} \text{ where } c = \frac{\log\Delta\sigma_D - \log\Delta\sigma_{D,cor}}{\log N_{f,CAFL} - \log N_{f,LCF}} \quad (3)$$

By substituting $\Delta\sigma$ from Eq. (1), the proposed formula for the fatigue strength for the riveted detail exposed to a corrosive environment can be obtained as,

$$\Delta\sigma_{cor} = \Delta\sigma_D\left[N_{f,LCF}^{c} N_{f,CAFL}^{1/m}\right] N_R^{(-c-1/m)} \quad (4)$$

If $\Delta\sigma_{cor} \leq \Delta\sigma_{D,cor}$, the fatigue strength of riveted details exposed to corrosive environments can be obtained,

$$\log(\Delta\sigma_{D,cor}) - \log(\Delta\sigma_{cor}) = \frac{[\log\Delta\sigma_{D,cor} - \log\Delta\sigma_{L,cor}]}{[\log N_{f,CAFL} - \log N_{f,VAFL}]}(\log N_{f,CAFL} - \log N_R) \quad (5)$$

or,

$$\frac{\Delta\sigma_{cor}}{\Delta\sigma_{D,cor}} = \left(\frac{N_R}{N_{f,CAFL}}\right)^{\acute{c}} \text{ where } \acute{c} = \frac{\log\Delta\sigma_{D,cor} - \log\Delta\sigma_{L,cor}}{\log N_{f,CAFL} - \log N_{f,VAFL}} \quad (6)$$

When $\Delta\sigma_{cor} \leq \Delta\sigma_{D,cor}$, the proposed formula for the fatigue strength of riveted details exposed to corrosive environments can be obtained,

$$\Delta\sigma_{cor} = \Delta\sigma_{D,cor}\left[N_{f,CAFL}^{-\acute{c}}\right] N_R^{\acute{c}} \quad (7)$$

Parameters c and $\acute{c}$ depend on the CF endurance of the riveted details, and values of the parameters are given in the following section.

2.3 Corrosive environment dependent parameters of the proposed curve

The values of $\Delta\sigma_D$, $\Delta\sigma_L$, m, $N_{f,LCF}$, $N_{f,CAFL}$ and $N_{f,VAFL}$ are directly obtained from the code providing fatigue strength/S-N curves of riveted structural details[4,18,19,20]. Eurocode detail category 71 represents the fatigue strength of riveted members[5]. In addition to detail

category 71, the WI-rivet detail category also represents riveted details, as proposed in the UK railway assessment code[4,19,20]. The $\Delta\sigma_{D,cor}$ and $\Delta\sigma_{L,cor}$ are the corrosive state and the environment-dependent parameters, and full-scale fatigue tests should be performed in the VHCF region to determine these parameters. The full-scale tests of riveted members and joints in simulated corrosive environments are challenging, in terms of both resources and time. Fracture mechanics approaches were very popular in the past for determining the above parameters in the presence of corrosion pits. However, recent investigations of carbon steel reveal that CF cracks initiate in any corrosive media, due to a different mechanism and not necessarily due to the presence of pits[21,26-28].

Reasonable accurate values of c, $\acute{c}$ $\Delta\sigma_{D,cor}$ and $\Delta\sigma_{L,cor}$ for riveted details in urban environments are presented in this section. These parameters directly relate to the CF endurance of structural steel specimens tested in natural water. The fatigue limit for specimens tested in air, σ_{∞}, and the endurance limit for the specimens tested in natural water, $\sigma_{\infty,cor}$, were determined as corresponding to 10^7 cycles of fatigue tests of several grades of pre-corroded and uncorroded steel specimens, which were tested in natural water[24,29,30]. The ratio $\sigma_{\infty,cor}/\sigma_{\infty}$ varies in the range of 0.53-0.70. The mean and coefficient of variation (COV) of the ratio are 0.61 and 0.1. The conservative value for $\sigma_{\infty,cor}/\sigma_{\infty}$ ratio is proposed as 0.5, by considering a 5% failure probability. Hence, the values for $\Delta\sigma_{D,cor}$ and $\Delta\sigma_{L,cor}$ are obtained by inter- and extrapolations of the $\sigma_{\infty,cor}/\sigma_{\infty}$ ratios corresponding to $N_{f,CAFL}$ and $N_{f,VAFL}$ for Eurocode detail category 71. The corresponding mean and conservative values (i.e. design value = mean-2×standard deviation) are calculated and listed in Table 1. Similarly, for the WI-rivet detail category, the corresponding values are calculated as shown in Table 1. Hence, the mean and design c and $\acute{c}$ values are calculated for both detail categories, as shown in Table 1. There is no discrepancy in the number of cycles at the curve slope changing point, $N_{f,CAFL}$ between the two S-N curves of riveted details (one which is exposed to air and another which is exposed corrosive environments).

Table 1. Parameters used in the proposed fatigue strength curve of riveted details in corrosive environments

3. Experimental verification of the proposed curve

The proposed S-N curves of riveted detail categories are compared with full-scale

fatigue tests of riveted joints, plate girders and truss girders, to confirm the validity of the proposed curve. The formulas in Eq. (4) and (7) along with specific parameters given in Table 1 are used to obtain the S-N curve of riveted details exposed to corrosive environments. The formula given in Eq. (1) with the parameters in Table 1 are utilized to predict the corresponding S-N curve in air of the same detail. Commonly used fatigue codes in Europe has defined only two detail categories for riveted structural details, i.e. detail category 71, which is given in Eurocode[18] and WI-rivet detail category, which is given in the UK railway assessment code[4,19,20]. As shown in Eq. (1), slope (s) of the S-N curves in air is $-1/m$. The slopes before and after the knee point (i.e. S-N curve slope changing point) of S-N curve for riveted details exposed to corrosive environments are $-c-{}^{1}/_{m}$ and $\acute{c}$ respectively as shown in Eq. (4) and (7). The corresponding values of the plotted curves are shown in Figs. 2-4 and Fig. 8.

Larsson[5] collected fatigue test results of riveted bridge components from the literature. These results were obtained from full-scale testing of riveted plate girders. Most of the components were subjected to a four-point bending test. One of the reports states the frequency of the fatigue tests as 520 cycles/min[6]. The frequency is vital for CF tests as the effect of corrosive environment to the steel is time dependent. As mentioned in the section 2.1 and 2.3, the concept of the S-N curve and curve parameters were studied from the standard CF results of different types of steel specimens (both pre-corroded and un-corroded) tested in corrosive environments[3,17]. In these tests, the frequency of CF tests were determined based on the testing standards[17].

The reported fatigue lives are compared with the predicted fatigue curve for riveted plate girders, as shown in Fig. 2. Eurocode detail category 71 represents the fatigue strength of riveted members[5]. The proposed S-N curve for an urban environment was plotted using the formulae given in Eqs. (4) and (7), as shown in Fig. 2. The model parameters are selected from Table 1, corresponding to detail category 71. Fig. 1(b) shows that the fatigue test results of corroded plate girders have a good match with the proposed fatigue curve formula, and this deviates from the detail category 71 curve. The fatigue lives of 7 out of 131 test results are below the predicted fatigue curve, and some of the rivet heads of these plate girders were severely corroded. Those girders were extracted from Blumberg Bridge and Westkreuz Bridge, which are old. The chemical composition of the material might be quite different from the structural steel, and different temperature

conditions were reported during the test. Apart from detail category 71, the WI-rivet detail-based S-N curve, which is given in the UK railway assessment code[4,19,20], has also been used for fatigue life estimation of many ageing riveted bridges. The proposed S-N curve, based on the WI-rivet detail category, was plotted using the formula given in Eqs. (4) and (7), as shown in Fig. 3. The model parameters given in Table 1 have been used. The proposed S-N curve, which was predicted by the WI-rivet detail category, shows a good match with the test results, as shown in Fig. 3, in the case of those joints whose rivet heads have severely corroded.

Fig. 2. Comparison of proposed S-N curve, corresponds to detail category 71, with full-scale fatigue tests of riveted plate girders: (a) for all the girders, (b) for corroded and uncorroded girders separately

Fig. 3. Comparison of proposed S-N curve, corresponds to WI-rivet detail category, with full-scale fatigue tests of riveted plate girders: (a) for all the girders, (b) for corroded and uncorroded girders separately

Full-scale test results of riveted truss girders/lattice girders[5] are compared with proposed Eqs. (4) and (7), as shown in Fig. 4. The full-scale test includes a four-point bending test, cantilever test and tension test. Two sets of the proposed S-N curves were predicted, based on detail categories 71 and WI-rivets, respectively, and compared with test results: the same as previous verification of the riveted plate girder. As the corrosion state was not properly reordered in the dissertation[5], both corroded and uncorroded test results were used in the comparison. Fig. 4 shows that the fatigue test results of corroded truss girders have a reasonable match with the proposed fatigue curve formula.

Fig. 4. Comparison of proposed S-N curve with full-scale fatigue tests of riveted truss girders: (a) S-N curve for urban environment predicted by detail category 71, (b) S-N curve for urban environment predicted by WI-rivet detail category

A recently proposed strain-life model[8,9] predicted sample S-N curves of three different corrosion rates, which are compared with the S-N curves for marine and urban environments predicted by Eqs. (4) and (7), as shown in Fig. 5. The corrosion factor of zero was considered for obtaining the S-N curve in air. Both proposed models show good agreement, as shown in Fig. 5.

Fig. 5. Comparison of proposed S-N curve with Aghoury's strain-life model's[8,9]

predicted fatigue endurances for different corrosion factors

4. Case study bridge and stress evaluation

A riveted railway bridge in an urban corrosive environment is considered for fatigue life estimation in this paper.

4.1. Considered riveted bridge and current status

The considered riveted railway bridge (Fig. 6) was constructed in 1885. It is a Warren truss girder bridge and 160 m in length. The bridge material is wrought iron. The use of wrought iron was replaced by that of mild steel throughout the world by the end of the 19th century. The full-scale fatigue test results of riveted members illustrate no significant difference between steel and wrought iron[5]. The loading details and geometrical details were presented in the first author's previous article[4]. The members of the bridge are categorized into several sets, based on similar cross-sectional properties, as shown in Fig. 7.

Fig. 6. General view and some of the corroded locations of the bridge

Fig. 7. Member designations: (a) main truss girder, (b) horizontal bridge deck[4]

Uniform corrosion has been investigated during many periodical inspections, which are reported in Tables 2 and 3 of the first author's previously published paper[4]. Cross girders, stringers, the bottom chord of the Warren truss and truss diagonal members have been mainly subjected to corrosion, as shown in Fig. 6. Patch corrosion has been detected, and minor maintenance activities have been carried out. Surface treatments and over-coating have not been properly attended to, due to lack of funding and facilities. Therefore, a sign of corrosion was observed in the same locations before the end of the coating life[4]. Pitting and crevice corrosion have been reported in a few places of the bridge where water and soil deposits accumulate. A detailed assessment of the structural integrity was carried out in 2001, and the mechanical properties, geometric details and loading details were obtained from the published literature[4,31].

4.2. Determination of stress histories/stress evaluation

The time-dependent loss of material due to uniform corrosion (i.e. corrosion wastage) changes the cross-sectional properties; hence, the overall structural stiffness changes with the service life. The corrosion wastage has been presented by a nonlinear function for the considered bridge, as below[4,23],

$$C(t) = 0.0706(t - t_0)^{0.789}; t > t_0 \quad (8)$$

where $C(t)$ is the average corrosion penetration in millimetres, t is the age in years and t_0 is the time in years of the first appearance of general corrosion. The effective cross-sectional area, the second moment of area, the torsional constants and the warping constants were calculated, considering the reduction in plate thickness due to corrosion by the following proposed formulae in previously published paper[4]. These cross-sectional properties were utilized with a validated Finite Element (FE) model[31], to obtain the stress histories of the fatigue-critical members. A time history dynamic analysis was conducted for each train passage, based on past, present and future time schedules. The rain-flow cycle counting algorithm was used to calculate the equivalent nominal stress ranges.

5. Fatigue life assessment by deterministic approach

The fatigue assessment for the above-mentioned railway bridge was performed by deterministic stress-life approach. The proposed S-N curve in an urban corrosive environment was used, and obtained lives were then compared with the conventional approach-predicted fatigue lives.

5.1 Fatigue strength curves/S-N curves

The bridge was constructed by means of built-up members, connected by rivets. Fig. 2 shows that the obtained S-N curves of the corroded riveted joints (refer to air S-N curve of detail category 71) have good agreement with former fatigue test results, if the state of corrosion is not severe and the rivet heads are protecting the holes from corrosion[5]. The WI-rivet detail category, which is given in the UK railway assessment code[4,19,20], shows a good match with test results, as shown in Fig. 3, in the case of the joints whose rivet heads have severely corroded. Therefore, both of the curves were used for fatigue life calculation in this case study. The proposed S-N curves for corroded riveted joints are plotted by Eqs. (4) and (7), as shown in Fig. 8. The model parameters given in Table 1 were used to obtain the proposed fatigue curves.

Fig. 8. S-N curves for riveted details/joints in the bridge in urban corrosive environment: (a) developed based on WI-rivet detail category, (b) developed based on detail category 71 in Eurocode

5.2 Fatigue life estimation

The fatigue lives of the bridge were calculated based on a combination of the obtained

nominal stress ranges in Section 4.2, the S-N curve shown in Fig. 8 and Miner's rule[32]. The calculated fatigue lives of critical members of each member set (Fig. 7) are shown in Table 2. Three different methods were considered in this life estimation. In Method 1, lives were calculated based on a combination of nominal stress histories, without considering corrosion wastage, the uncorroded S-N curve and Miner's rule. A combination of the nominal stress ranges obtained by considering corrosion wastage (i.e. Section 4.2), the S-N curve without cut-off limit (i.e. without constant amplitude fatigue limit)[4,12,13,16] and Miner's rule[32] is used in Method 2. In Method 3, the calculation was performed based on a combination of the nominal stress ranges obtained by considering the corrosion wastage (i.e. Section 4.2), the proposed S-N curve obtained by Eqs. (4) and (7) and Miner's rule[32].

Table 2(a). Fatigue lives calculated by deterministic approach based on WI-rivet detail category S-N curve

Table 2(b). Fatigue lives calculated by deterministic approach based on DC71 detail category S-N curve

5.3 Comparison and discussion of results

The fatigue lives predicted by the proposed curve (i.e. Method 3) are compared with the previous conventional approaches (i.e. Methods 1 & 2). The time-dependent change of member stiffness, which was discussed in Section 4.2, was not taken into account in the previous fatigue assessment approach. Lives calculated by Method 3, which includes the proposed fatigue strength curve shown in Eqs. (4) and (7), show a significant reduction in fatigue lives from Method 1. This reduction is observed when the precise fatigue strength curve and the time-dependent change of stiffness of the members are considered. About 50% and 15% reductions in the fatigue lives which refer to Method 1 were observed for the truss girder members and deck members, respectively. The reductions which refer to Method 2 are about 40% and 10% for the truss girder members and deck members, respectively. This comparison reveals the significance of using the proposed fatigue curve to perform safe life assessment of corroded constructional details.

6. Fatigue life assessment by probabilistic approach

The fatigue assessment was performed for the considered riveted railway bridge by means of the probabilistic stress-life approach in this section. The proposed S-N curve for WI-rivet detail category in an urban corrosive environment is only used for the

probabilistic fatigue life assessment. The obtained lives were then compared with the conventional approach-predicted fatigue lives.

6.1 Fatigue reliability index

The fatigue reliability index is determined for the riveted bridge, based on a probabilistic bilinear *S-N* approach. The definition of the fatigue reliability index is given as,

$$\beta = \emptyset^{-1}(1 - P_f) \tag{9}$$

where $\emptyset^{-1}$ is the inverse of the standard normal distribution function. The P_f is the failure probability of the fatigue limit state, and the function of the limit state is defined as,

$$g(t) = \Delta - D_{cor} \tag{10}$$

where Δ is fatigue damage accumulation threshold. The Δ follows lognormal distribution with a mean value of 1.0 and coefficient of variation (COV) of 0.3. The D_{cor} is the cumulative damage of the riveted detail in a corrosive environment, which can be derived as,

$$D_{cor} = \frac{N(t)}{A_{cor}}(S_{re})^{m_{cor}} \tag{11}$$

where S_{re} is the equivalent constant amplitude stress range, calculated using a bilinear *S-N* approach, as shown in Eq. (12). The *N(t)* is the subjected number of cycles of the considered detail at age *t*. From Eqs. (4) and (7),

$$\text{If } S_{re} \geq \Delta\sigma_{D,cor};\ m_{cor} = m_1 = {}^{1}\!\Big/\!_{c + {}^{1}\!/\!_{m}} \text{ and } A_{cor} = A_1 = \left[\Delta\sigma_D N_{f,LCF}^{c} N_{f,CAFL}^{{}^{1}\!/\!_{m}}\right]^{m_1}$$

$$\text{If } S_{re} < \Delta\sigma_{D,cor};\ m_{cor} = m_2 = -{}^{1}\!\Big/\!_{c} \text{ and } A_{cor} = A_2 = N_{f,CAFL}\Delta\sigma_{D,cor}^{{}^{-1}\!/\!_{c}}$$

The m_1 and m_2 are slopes of the bilinear *S-N* curve of riveted details in corrosive urban environments. The considered deterministic parameters are m_1, m_2, $\Delta\sigma_{D,cor}$ and *N(t)*. The stress range, S_{re}, and fatigue detail coefficient, A_{cor}, are considered random variables. The corrosive parameters of mean *S-N* curves of the WI-rivet detail category are obtained from Fig. 8 (a) and Table 1. Hence, the values of m_1, m_2, A_1 and A_2 were calculated as 3.11, 4.2, 2.785×10^{11} and 1.023×10^{13}, respectively. The S_{re} can be determined for a bilinear *S-N* approach as[33],

$$S_{re} = \left[\frac{\Sigma(n_i^{\varrho} S_{ri}^{m_1}) + \left(CAFT^{m_1 - m_2}\right).\Sigma(n_j^{\varrho} S_{rj}^{m_2})}{\Sigma(n_i^{\varrho}) + \Sigma(n_j^{\varrho})}\right]^{{}^{1}\!/\!_{m_1}} \tag{12}$$

where n_i^Q is the number of cycles in the i^{th} stress range when S_{ri} is greater than the $\Delta\sigma_{D,cor,}$ and $n_j^Q$is the number of cycles in j^{th} stress range when S_{rj} is less than the $\Delta\sigma_{D,cor}$. If the probability density faction (PDF) is available for stress ranges of the riveted detail, S_{re} can be calculated by[31],

$$S_{re} = \left[\int_0^{CAFT}(CAFT^{m_1 - m_2}).S^{m_2}.f_s(s).ds + \int_{CAFT}^{\infty} S^{m_1}.f_s(s).ds\right]^{1/m_1} \qquad (13)$$

Monte Carlo simulation is utilized with Eqs. (10) and (11) to calculate the fatigue reliability index (β) versus lifetime of the riveted details of the bridge. The fatigue life of each detail can be predicted when β reaches the target reliability index (β_{target}).

6.2 Fatigue assessment

The equivalent nominal stress ranges of each member obtained in Section 4.2 were plotted in histograms, and PDFs were obtained. These PDFs follow lognormal distribution. Then Eq. (13) was used to determine S_{re} for each critical riveted detail of the bridge. The COVs of $S_{re,}$ A_{cor} and Δ are 0.1, 0.45 and 0.3, respectively[34,35]. The fatigue reliability index β can be derived, based on Eqs. (10) and (11), as all the random variables follow the lognormal distribution,

$$\beta(t) = \begin{cases} \dfrac{\lambda_\Delta + \lambda_{A_1} - m_1.\lambda_{S_{re}^L} - \ln N(t)}{\sqrt{\zeta_\Delta^2 + \zeta_{A_1}^2 + (m_1.\zeta_{S_{re}^L})^2}} & for\ N(t) \le \dfrac{A_1}{CAFT^{m_1}} \\ \dfrac{\lambda_\Delta + \lambda_{A_2} - m_2.\lambda_{S_{re}^B} - \ln N(t)}{\sqrt{\zeta_\Delta^2 + \zeta_{A_2}^2 + (m_2.\zeta_{S_{re}^B})^2}} & for\ N(t) > \dfrac{A_1}{CAFT^{m_1}} \end{cases} \qquad (14)$$

where λ and ζ are lognormal parameters of the various random variables. The equivalent constant amplitude stress ranges, S_{re}, can be calculated using either linear or bilinear *S-N* approaches, respectively. The S_{re}^L is the one calculated by a linear *S-N* approach, while S_{re}^B is calculated by a bilinear *S-N* approach. Hence, the fatigue reliability profiles were obtained by Eq. (14) for each critical member and plotted in Fig. 9. Based on a survival probability of 95%, the target reliability indices were considered as 1.65. The calculated fatigue lives are shown in Table 3.

Fig. 9. Fatigue reliability index versus life of the bridge components

Table 3. Fatigue lives calculated by probabilistic approach based on WI-rivet detail category S-N curve

6.3 Comparison and discussion of results

The probabilistic fatigue lives predicted by the proposed curve (i.e. Method 3) are

compared with those of the previous conventional Method 1. In the Method 1 (i.e. conventional probabilistic approach), lives were calculated based on the combination of nominal stress histories, without considering corrosion wastage, the uncorroded S-N curve and Miner's rule (as discussed in Section 5.2). The Eq. (11) is not used in Method 1. The cumulative damage of the riveted detail in air is obtained based on Eq. (1). The corresponding values of m_1, m_2 and $\Delta\sigma_D$ are taken from Table 1. Hence, the values of m_1, m_2, A_1 and A_2 were calculated as 4, 6, 3.117×10^{13} and 5.489×10^{16}, respectively. Lives calculated by Method 3, which includes the proposed fatigue strength curve shown in Eqs. (4) and (7), show a significant reduction in fatigue lives from Method 1. This reduction emphasises the importance of using the proposed S-N curve formula to perform safe life assessment of the riveted joints, members and components which are exposed to corrosive environments.

7. Conclusions

A fatigue strength formula is proposed for riveted structural details which are exposed to urban corrosive environments. The S-N curves predicted by the proposed formula are in very good agreement with experimentally obtained fatigue lives of riveted plate girders and truss girders tested in urban environments. Some of the test members are already weathered and deteriorated. The main reason for having a good match with the full-scale fatigue test results is that the CF mechanism and concept of the derivation have been studied at a micro-structural level, in specimen scale and finally incorporated into structural member and joint scale. The values of the curve parameters were determined for two commonly used detail categories, i.e. detail category 71 given in Eurocode and WI-rivet detail category given in the UK railway assessment code. The main advantage of the proposed formula is that it can directly apply to any steel or wrought iron riveted structural details, without requiring additional CF tests or any corrosive parameters. Fatigue lives calculated by a deterministic approach show a significant reduction when the effect of corrosion is considered. This reduction is not very significant when probabilistic fatigue life estimation is used, as this approach takes into account the uncertainties of the mean S-N curve and stress evaluation. These reductions in fatigue lives further highlight the importance of having accurate S-N curves for ageing riveted bridges for conservative maintenance practices. The effect of the frequency in variable amplitude CF tests should be studied, especially for full-scale structural details.

References

1. Imam BM, Righiniotis TD. Fatigue evaluation of riveted railway bridges through global and local analysis. *J. Constr. Steel. Res*. 2010; 66: 1411-1421.
2. Helmerich R, Kuhn B, Nussbaumer A. Assessment of existing steel structures: A guideline for estimation of the remaining fatigue life. *J. Struct. Infrastruct. Eng*. 2007; 3: 245-255.
3. Adasooriya ND, Hemmingsen T, Pavlou D. Fatigue strength degradation of metals in corrosive environments. *Proceedings of First Conference of Computational Methods in Offshore Technology-COTech 2017, IOP Conf Ser: Mater. Sci. Eng.*: IOP Publishing; Stavanger, Norway: 2017: Article number 276 012039.
4. Adasooriya ND, Siriwardane SC. Remaining fatigue life estimation of corroded bridge members. *Fat. Fract. Eng. Mater. Struct*. 2014; 37: 603-622.
5. Larsson T. *Fatigue assessment of riveted bridges, PhD dissertation*. Sweden: Luleå University of Technology; 2009.
6. Johannes MM. *Fatigue strength of weathered and deteriorated riveted members, MSc dissertation*. USA: Lehigh University; 1984.
7. Imam B, Righiniotis TD, Chryssanthopoulos MK. Fatigue assessment of riveted railway bridges. *Int. J. Steel Struct*. 2005; 5: 485-494.
8. Aghoury I El. *Numerical tool for fatigue life prediction of corroded steel riveted connections using various damage models*, *PhD thesis*. Canada, Montreal: Concordia University; 2012.
9. Aghoury I El, Galal K. Corrosion-fatigue strain-life model for steel bridge girders under various weathering conditions. *J. Struct. Eng*. 2014; 140 (6): Article number 04014026.
10. Kayser JR, *The effects of corrosion on the reliability of steel girder bridges. PhD thesis*. Ann Arbor. Mich., USA. University of Michigan; 1998.
11. Mohamed ELM, Thierry PL, Nicolas S, Olivier D. Effect of corrosion on the high cycle fatigue strength of martensitic stainless steel X12CrNiMoV12-3. *Int. J. Fatigue.* 2013; 47: 330-9.
12. Wahab MA, Sakano M. Corrosion and biaxial fatigue of welded structures. *J. Mat. Proc. Tech. 3*. 2003; 143-144: 410-415.

13. Nguyen KT, Garbatov Y, Soares CG. Spectral fatigue damage assessment of tanker deck structural detail subjected to time-dependent corrosion. *Int. J. Fatigue.* 2013; 48:147-155.
14. Roberge PR. *Handbook of Corrosion Engineering. 1st ed.* New York: McGraw Hill; 2000.
15. Mikkelsen O, Rege K, Hemmingsen T, Pavlou D. Numerical estimation of the stop holes-induced fatigue crack growth retardation in offshore structures taking into account the corrosion effect. *Proceeding of International Society of Offshore and Polar Engineers Conference Series*. San Francisco: American Society of Mechanical Engineers, 2007: ISOPE-I-17-552: 451-458.
16. Gerhard S, Christian K, Bertram K, Hensen W. *Condition assessment and inspection of steel railway bridges, including stress measurements in riveted, bolted and welded structures: Sustainable Bridges-Background document SB3.4*. Sweden: Digital Vetenskapliga Arkivet; 2007.
17. Adasooriya ND, Pavlou D, Hemmingsen T. Fatigue strength degradation of corroded structural details: A formula for *S-N* curve. *Fat. Fract. Eng. Mater. Struct*. Online from 26.11.2019. https://doi.org/10.1111/ffe.13156
18. NS EN 1993-1-9. *Eurocode 3: Design of steel structures - Part 1-9: Fatigue*. Belgium: European Committee for Standardization; 2005+NA 2010.
19. Imam B, Righiniotis TD, Chryssanthopoulos MK. Fatigue assessment of riveted railway bridges. *Int. J. Steel Struct*. 2005; 5: 485-494.
20. RT/CE/C/025, Railtrack Line Code of Practice: The structural assessment of underbridges, Railtrack, 2001.
21. Zhao T, Liu Z, Du C, Dai C, Li X, Bowei Z. Corrosion fatigue crack initiation and initial propagation mechanism of E690 steel in simulated sea water. *Mat. Sci. & Eng. A*. 2017; 708: 181-192.
22. Gangloff RP. Environmental cracking - corrosion fatigue, In: Baboian R, Dean Jr. SW, Hack HP, Hibner EL, Scully JR, eds. *Corrosion Tests and Standards Manual*. ASTM Internationals; 2005.
23. Yasser Y, Jeom KM. Ultimate strength reliability analysis of corroded steel-box girder bridges. *Thin-Walled Struct*. 2011; 49: 157-166.
24. Revie RW, Uhlig HH. *Corrosion and Corrosion Control, An Introduction to*

Corrosion Science and Engineering. 4th ed. US: Wiley and Sons; 2008.

25. Glaser W, Wright LG. *Mechanically Assisted Degradation. ASM Handbooks*. ASM Internationals; 1992: 137-144.
26. Vucko F, Bosch C, Delafosse D. Effects of cyclic plastic strain on hydrogen environment assisted cracking in high-strength steel. *International Hydrogen Conference (IHC 2012): Hydrogen-Materials Interactions*. WY, United States: American Society of Mechanical Engineering; 2012.
27. Vucko F, Bosch C, Aoufi A, Delafosse D. *Palladium coating on quenched-tempered martensitic steel for hydrogen electrochemical permeation tests. Technical Reports- ENSMSE-SMS-2014-01*. France: EMSE-00951142; 2014.
28. Wang R. *Corrosion fatigue of metal materials*. Xi'an: Press of Northwestern Polytechnical University; 2001.
29. Boyer HE. *Atlas of Fatigue Curves*. USA: ASM International; 1986.
30. Bandara CS. *Fatigue Damage Assessment of Steel Structures and Components, Improvements in Stress-Life Approach*. Germany: LAP Lambert Academic Publishing; 2015.
31. Siriwardane S, Ohga M, Dissanayake R, Taniwaki K. Structural appraisal-based different approach to estimate the remaining fatigue life of railway bridges. *Int. J. Health Monitoring.* 2010; 9: 323-339.
32. Miner MA. Cumulative damage in fatigue. *J. Appl. Mech*. 1945; 12: 159-64.
33. Soliman M, Frangopol DM, Kown K. Fatigue assessment and service life prediction of existing steel bridges by integrating SHM into a probabilistic bilinear S-N approach. *J. Struc. Eng*. 2013; 139:1728-1740.
34. Kwon K, Frangopol DM, Soliman M. Probabilistic fatigue life estimation of steel bridges by using a bilinear S-N approach. *J. Bridge Eng*. 2012; 17: 58-70.
35. Kwon K, Frangopol DM. Bridge fatigue reliability assessment using probability density functions of equivalent stress range based on field monitoring data. *Int. J. Fat.* 2010; 32: 1221-1232.

Table 1. Parameters used in the proposed fatigue strength curve of riveted details in corrosive environments

Parameter	Eurocode Detail category 71		WI-rivet detail category	
$N_{f,LCF}$	10^4		10^4	
$N_{f,CAFL}$	5×10^6		10^7	
$N_{f,VAFL}$	10^8		10^8	
m, $\acute{m}$	3, 5		4, 6	
$\Delta\sigma_D$ (MPa)	52.3		44.0	
$\Delta\sigma_L$ (MPa)	28.7		30.0	
Corrosion parameters	Urban environment		Urban environment	
	Mean value	Conservative value	Mean value	Conservative value
$\Delta\sigma_{D,cor}(MPa)$	33.5	28.0	26.8	22.0
$\Delta\sigma_{L,cor}$ (MPa)	14.9	11.5	15.5	12.0
c	0.072	0.100	0.072	0.100
$\acute{c}$	-0.271	-0.298	-0.238	-0.263

Table 2(a). Fatigue lives calculated by deterministic approach based on WI-rivet detail category S-N curve

Bridge component	Member set	Fatigue life (years)			
		Method 1	Method 2	Method 3	
				Mean	Design
Truss diagonal (Tension members)	DT3	247	228	144	134
Main girder bottom chord	MT2	272	248	147	136
Cross girders	CG	136	132	120	118
Stringers	ST	140	138	122	119

Table 2(b). Fatigue lives calculated by deterministic approach based on DC 71 detail category S-N curve

Bridge component	Member set	Fatigue life (years)			
		Method 1	Method 2	Method 3	
				Mean	Design
Truss diagonal (Tension members)	DT3	271	215	152	140
Main girder bottom chord	MT2	300	228	157	143
Cross girders	CG	141	129	122	120
Stringers	ST	146	133	123	121

Table 3. Fatigue lives calculated by probabilistic approach based on WI-rivet detail category S-N curve

Bridge component	Member set	Fatigue life (years)			
		Method 1		Method 3	
		β_{target}=1.65	β_{target}=0	β_{target} =1.65	β_{target} =0
Truss diagonal tension	DT3	108	157	95	123
Main girder bottom	MT2,3	102	150	99	132
Cross girders	CG1	119	170	105	151
Stringers	ST2,4	135	191	110	154

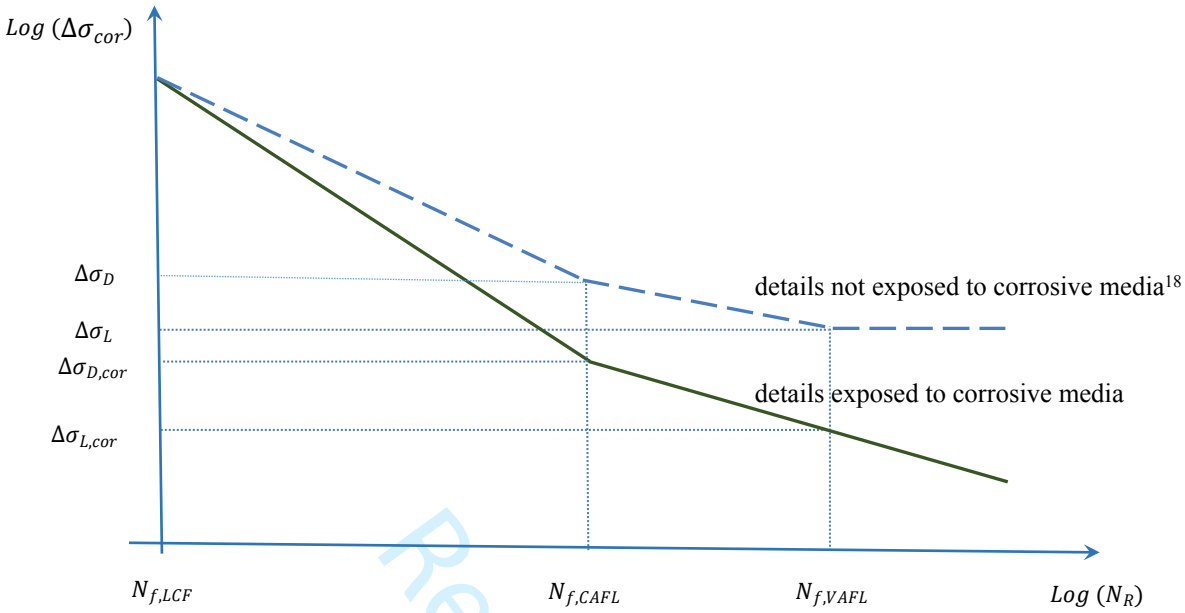

Fig. 1. Schematic representation of fatigue strength curve of riveted details exposed to corrosive environments

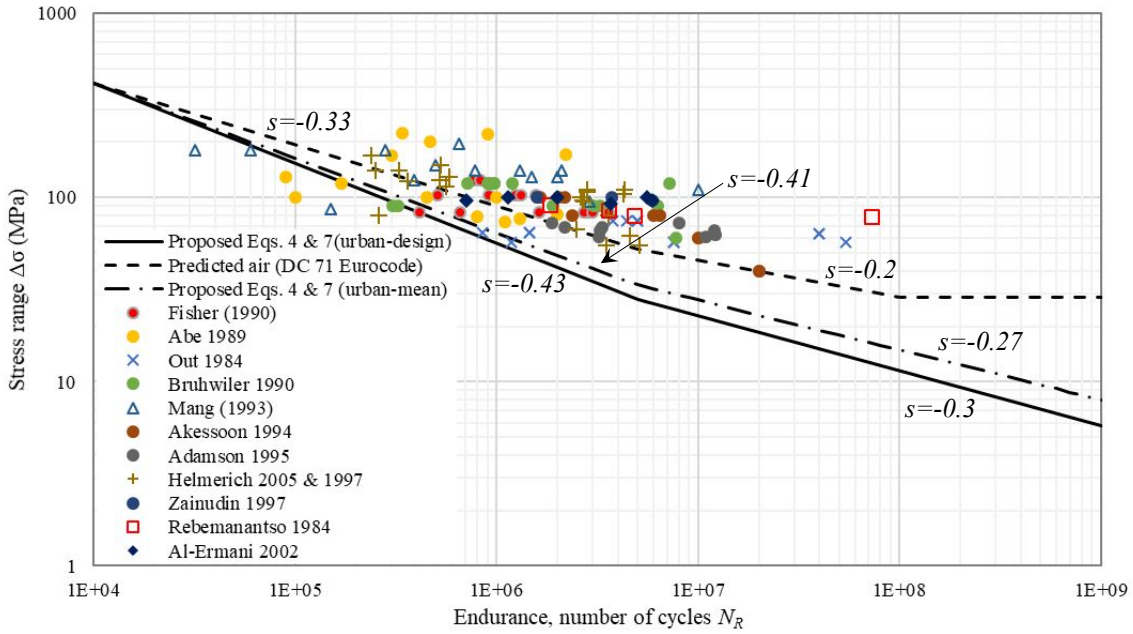

(a)

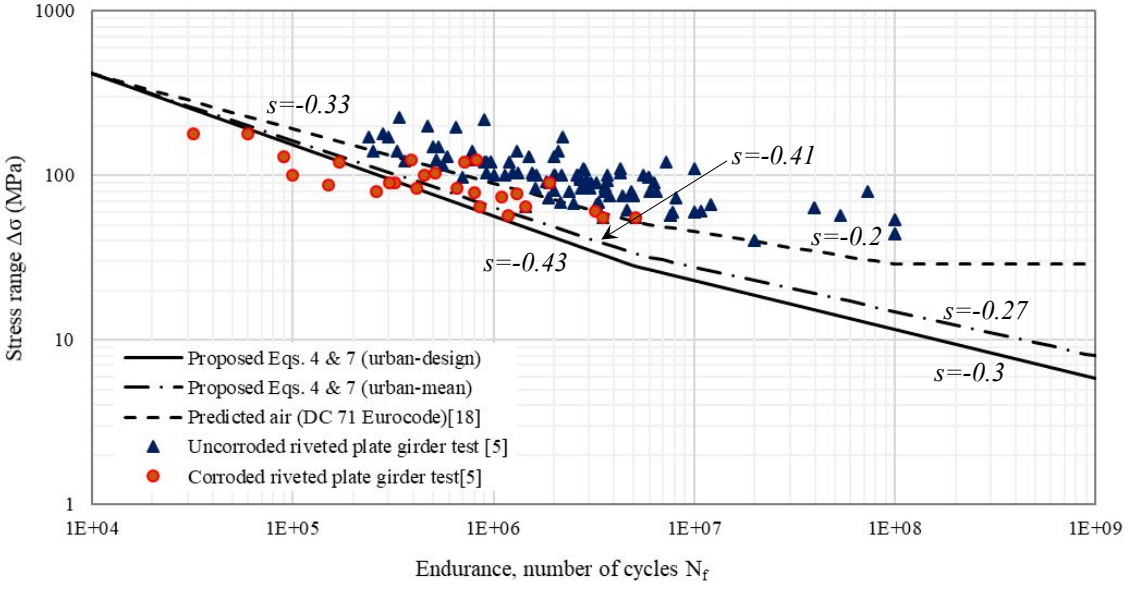

(b)

Fig. 2. Comparison of proposed S-N curve, corresponds to detail category 71, with full-scale fatigue tests of riveted plate girders: (a) for all the girders, (b) for corroded and uncorroded girders separately

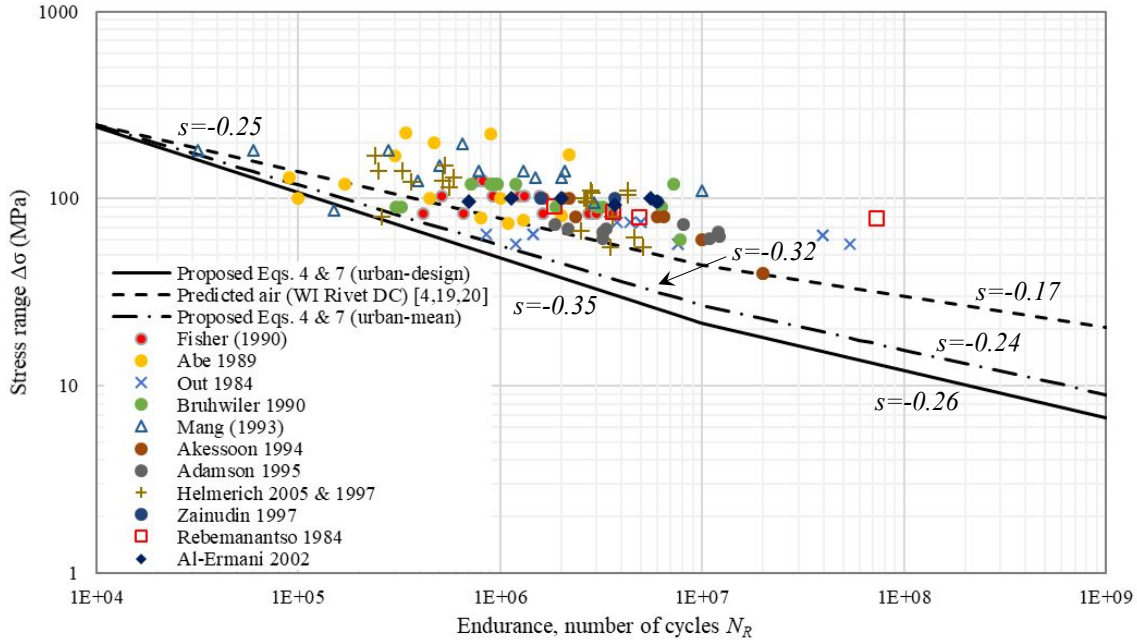

(a)

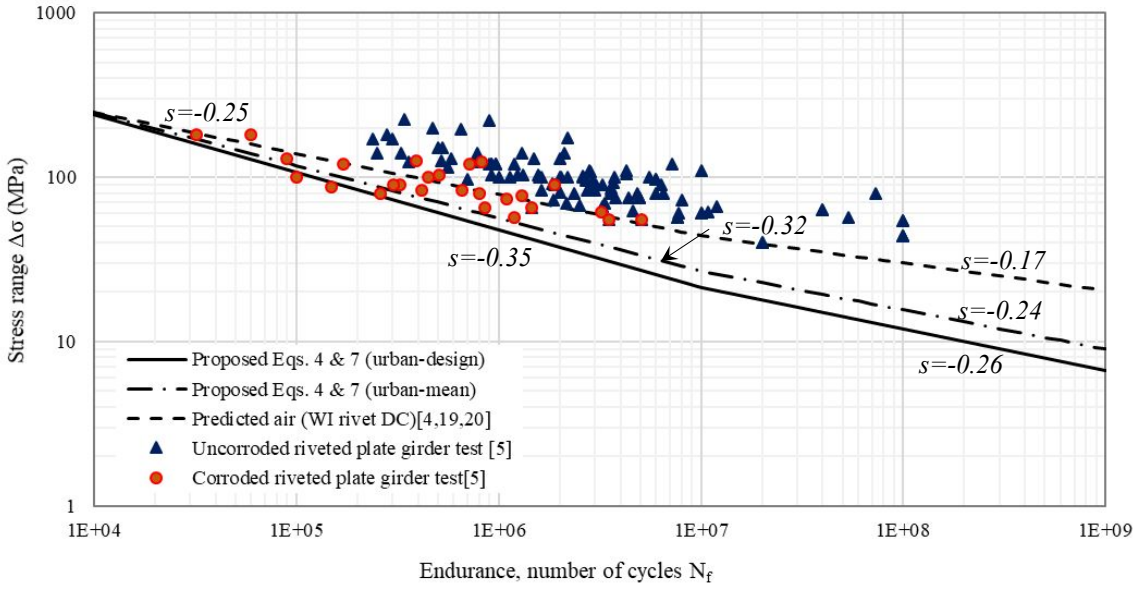

(b)

Fig. 3. Comparison of proposed S-N curve, corresponds to WI-rivet detail category, with full-scale fatigue tests of riveted plate girders: (a) for all the girders, (b) for corroded and uncorroded girders separately

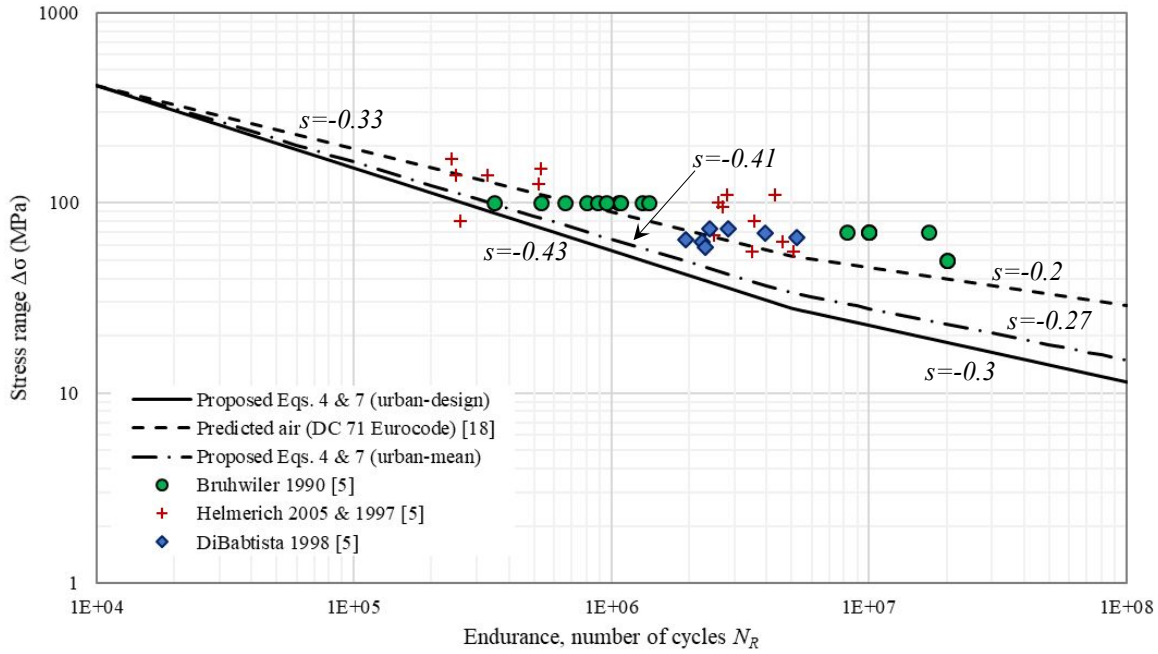

(a)

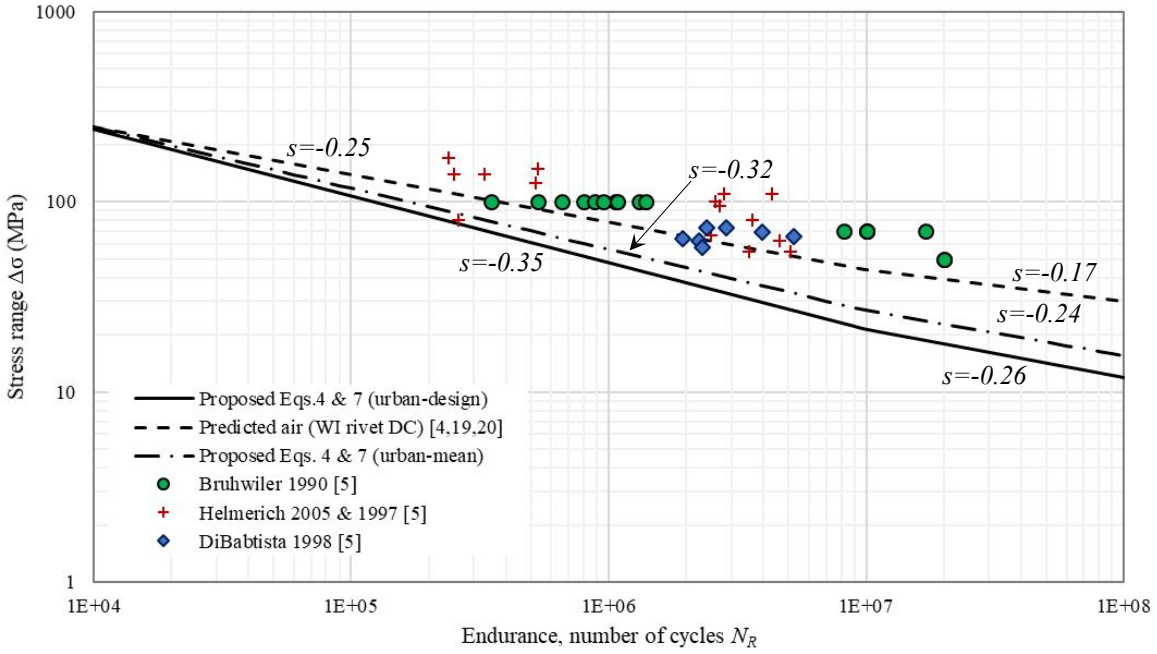

(b)

Fig. 4. Comparison of proposed S-N curve with full-scale fatigue tests of riveted truss girders: (a) S-N curve for urban environment predicted by detail category 71, (b) S-N curve for urban environment predicted by WI-rivet detail category

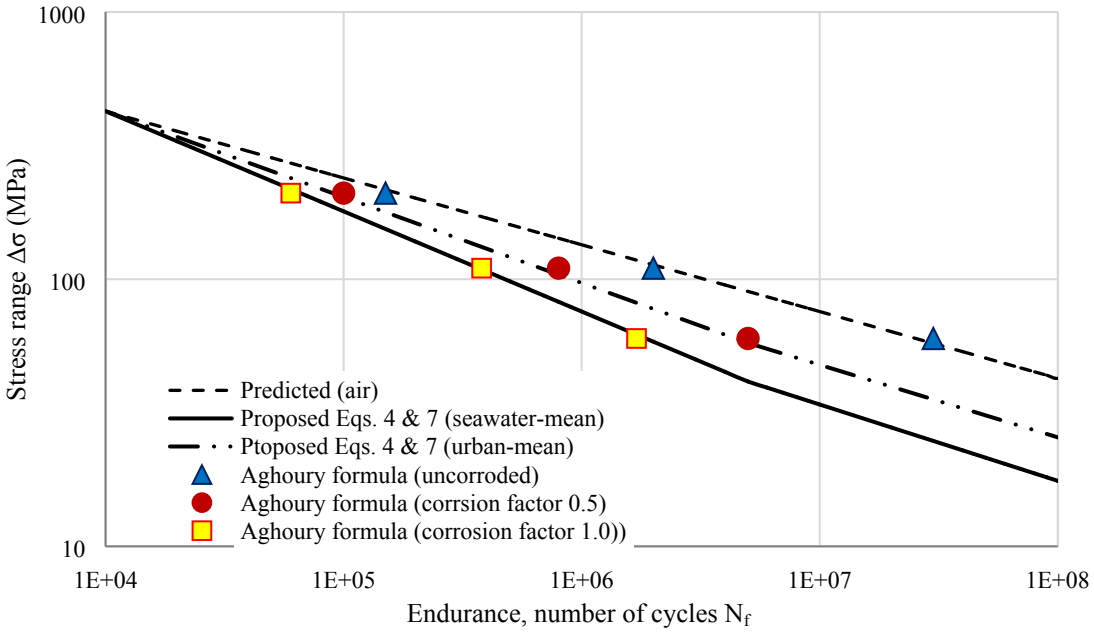

Fig. 5. Comparison of proposed S-N curve with Aghoury's strain-life model's[8,9] predicted fatigue endurances for different corrosion factors

Fig. 6. General view and some of the corroded locations of the bridge[4]

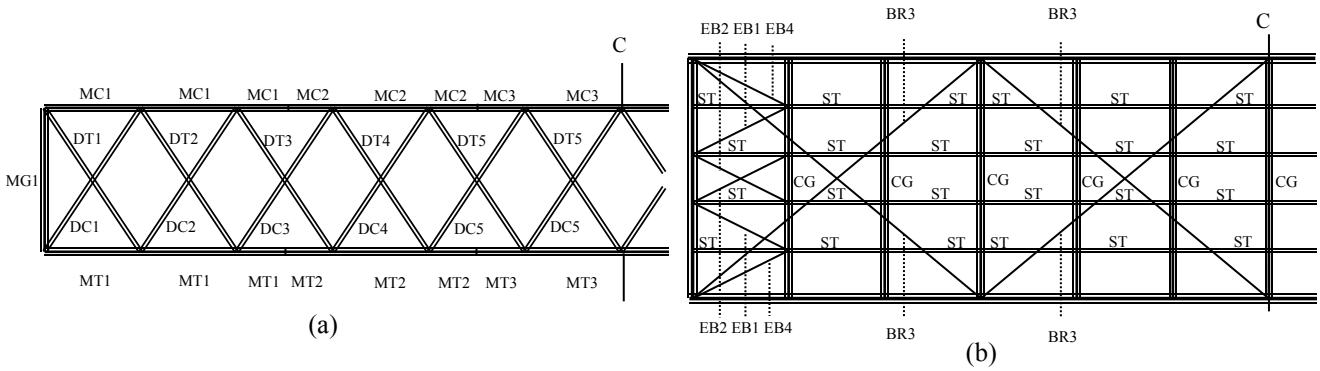

Fig. 7. Member designations: (a) main truss girder, (b) horizontal bridge deck[4]

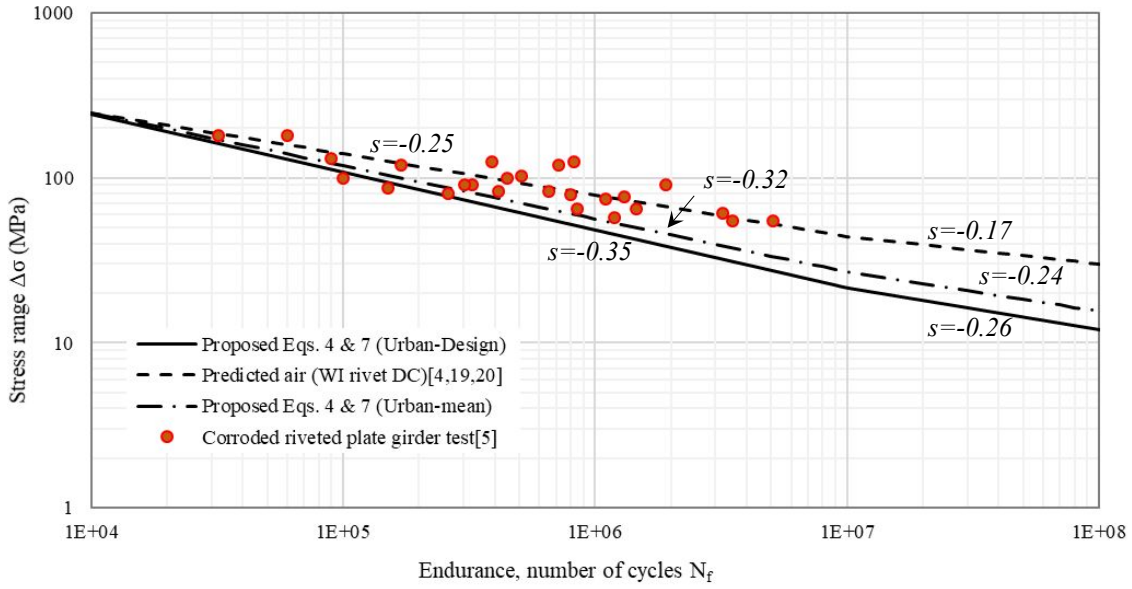

(a)

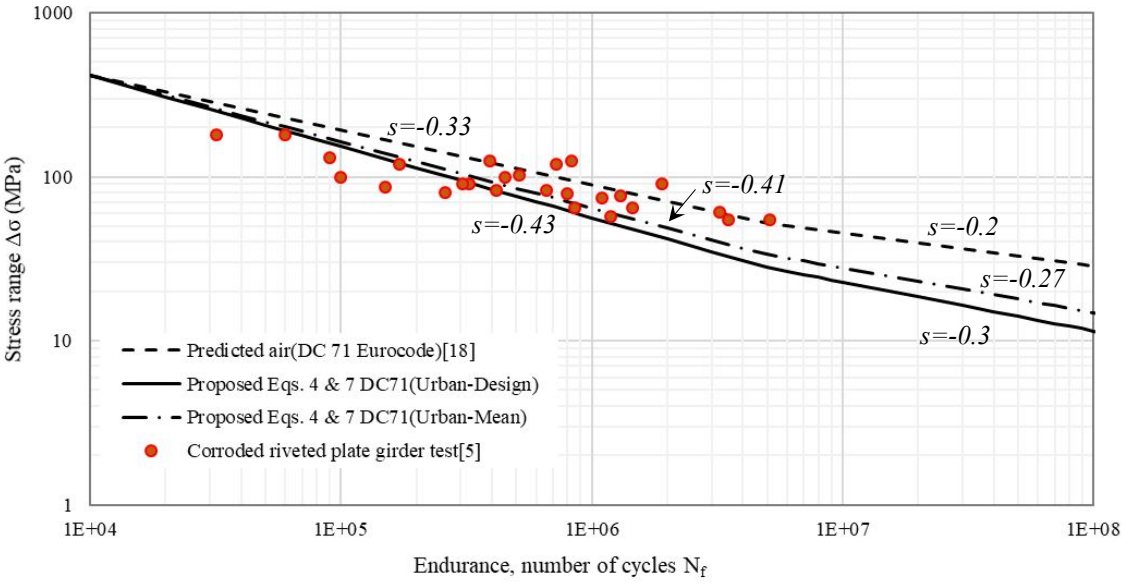

(b)

Fig. 8. S-N curves for riveted details/joints in the bridge in urban corrosive environment: (a) developed based on WI-rivet detail category, (b) developed based on detail category 71 in Eurocode

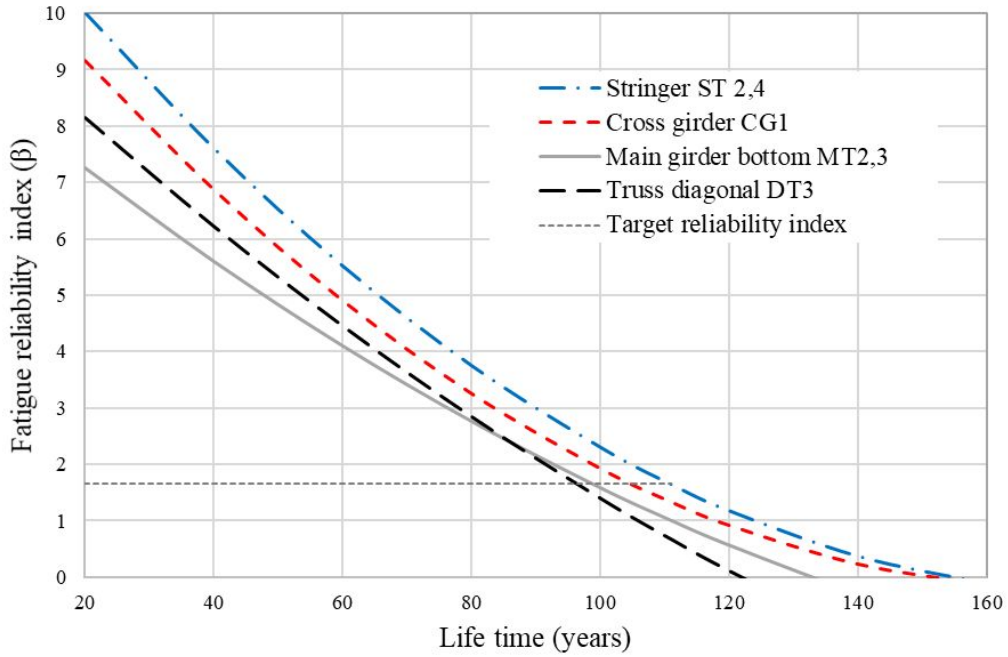

Fig. 9. Fatigue reliability index versus life of the bridge components

Paper 5

An Experimental Study on Environment-Assisted Cracking of Structural Steel in 3.5 wt% NaCl Solution

Conference Paper

International Ocean and Polar Engineering Conference,
The 2nd ISOPE Environment-Assisted Cracking (EAC) Symposium,
ISOPE 2019

Honolulu, Hawaii, USA

Paper 6

Effect of Hydrogen on Mechanical Properties and Fracture of Martensitic Carbon Steel under Quenched and Tempered Conditions

Journal Paper

Materials Science and Engineering: A

December 2019, Under Review

Elsevier Editorial System(tm) for Materials Science & Engineering A

Manuscript Draft

Manuscript Number: MSEA-D-19-06787

Title: Effect of hydrogen on mechanical properties and fracture of martensitic carbon steel under quenched and tempered conditions

Article Type: Research Paper

Keywords: Martensitic steel; Hardness; Hydrogen embrittlement; Slow-strain rate tensile test

Corresponding Author: Mrs. Nirosha D Adasooriya, M Eng

Corresponding Author's Institution: University of Stavanger

First Author: Nirosha D Adasooriya, M Eng

Order of Authors: Nirosha D Adasooriya, M Eng; Wakshum Mekonnen Tucho; Erlend Holm; Terje Årthun; Vidar Hansen; Karl Gunnar Solheim; Tor Hemmingsen

Abstract: The change in the mechanical properties of tempered high strength carbon steel (AISI 4130) due to hydrogen embrittlement (HE) has been investigated using slow strain rate tensile tests (SSRT). The heat treatment processes consisted of austenitization at 873 oC for about 45 minutes before quenching in salt bath and tempering at temperatures between 350 oC to 550 oC for about one hour. The SSRT tests were performed on both hydrogen pre-charged and uncharged samples. Vickers hardness test was carried out to study the variation in hardness with the tempering temperature. Microstructural characterizations and fracture surface analysis were done by using Scanning Electron Microscopy (SEM) and Transmission Electron Microscopy (TEM). The fracture surface analysis of such samples shows a transition of failure mechanism from brittle intergranular cracking at the lowest tempering temperature to ductile micro void coalescence at the highest temperature. TEM analysis reveals probably carbide precipitates at all tempering temperatures. The AISI 4130 was subjected to HE for hydrogen charging when the tempering temperatures were 460 oC and lower, corresponding to a hardness value of 450 HV and greater.

Research Data Related to this Submission

There are no linked research data sets for this submission. The following reason is given:
Data will be made available on request

Effect of hydrogen on mechanical properties and fracture of martensitic carbon steel under quenched and tempered conditions

Nirosha D. Adasooriya[a,*], Wakshum Mekonnen Tucho[a], Erlend Holm[a], Terje Årthun[a], Vidar Hansen[a], Karl Gunnar Solheim [b], Tor Hemmingsen[a]

[a]*University of Stavanger, Department of Mechanical and Structural Engineering and Materials Science, Stavanger N-4036, Norway.*

[b]*Subsea 7, Kanalsletta 9, NO-4033 Stavanger, P.O. Box 205, NO-4065 Stavanger, Norway*

[*] Corresponding author: E-mail address: mudiyan.n.adasooriya@uis.no

Abstract

The change in the mechanical properties of tempered high strength carbon steel (AISI 4130) due to hydrogen embrittlement (HE) has been investigated using slow strain rate tensile tests (SSRT). The heat treatment processes consisted of austenitization at 873 ºC for about 45 minutes before quenching in salt bath and tempering at temperatures between 350 ºC to 550 ºC for about one hour. The SSRT tests were performed on both hydrogen pre-charged and uncharged samples. Vickers hardness test was carried out to study the variation in hardness with the tempering temperature. Transmission Electron Microscopy (TEM) and Scanning Electron Microscopy (SEM) were performed for Microstructural characterizations and fracture surface analysis. The fracture surface analysis of such samples shows a transition of failure mechanism from brittle intergranular cracking at the lowest tempering temperature to ductile micro void coalescence at the highest temperature. TEM analysis reveals probably carbide precipitates at all tempering temperatures. The AISI 4130 was subjected to HE for hydrogen charging when the tempering temperatures were 430 ºC and lower, corresponding to a hardness value of 450 HV and greater.

Keywords: Martensitic steel; Hardness; Hydrogen embrittlement; Slow-strain rate tensile test

Abbreviations

CF	Corrosion fatigue	I_{HE}	Relative HE susceptibility index
CNC	Computer numerical control	SEM	Scanning Electron Microscopy
EAC	Environmental assisted cracking	TEM	Transmission Electron Microscopy
HD	Hydrogen damage	SCC	Stress corrosion cracking
HE	Hydrogen embrittlement	SSC	Sulfide stress cracking
HV	Vicker's hardness value	SSRT	Slow strain rate tensile tests

1. Introduction

High-strength steels such as AISI 4130 have been widely used in different structures, structural components and mechanical systems within many fields, such as construction, oil and gas, aviation, agriculture and defense. To improve ductility, post heat treatments are common processes for such high strength martensitic steel. Even though much improvement has been achieved through heat treatments, many failures of high strength steel structures are still observed. The suspension cable wire fractures of Lysefjord bridge [1], Lake Maracaibo bridge and Hamburg bridge [2, 3] are examples of these failures. About 40% of the failures of oil and gas pipelines are due to corrosion associated with environment-assisted cracking [4]. Corrosion is one of the principal deterioration processes that affects the integrity of steel structures. Thickness reduction, surface roughness and cyclic loading accelerate the crack initiation under different types of corrosion. There are three major types of environment-assisted cracking (EAC) [5]: stress corrosion cracking (SCC), hydrogen damage (HD) and corrosion fatigue (CF). The SCC is generally defined as failure caused by continuously applied stress in corrosive media. Fractures due to cyclic stress in corrosive media are designated as CF. The EAC is considered one of the main causes of the degradation of steel structures. Thus, most of the research in this area focuses on EAC due to the combined effect of the inherent nature of corrosion and loading [6-8].

Hydrogen embrittlement (HE) in metals leads to cracking and may cause catastrophic failures. HE is often classified as (i) internal hydrogen embrittlement, which occurs due to pre-existing hydrogen in the material, or (ii) hydrogen environment embrittlement, which occurs due to hydrogen picked up from the environment under cathodic protection or presence of hydrogen gases [9]. The HE of steel may reduce ductility, toughness, strength and accelerate crack growth [9]. The HE of steel is a function of concentration of the formed hydrogen, temperature, stress state and microstructure of the material [8-10]. The HE susceptibility is material dependent and there is no generalized guidelines to control the HE of high strength steels. In general, HE susceptibility is decreasing with increasing tempering temperature for martensitic steel (i.e. a decrease in hardness) [8].

In some structural materials manufactured as-quenched or under tempered conditions, precipitated carbide may reduce the hydrogen diffusivity in the materials and cause intergranular fracture [11]. The carbide precipitates are also dependent on the factors such as carbon content, cooling rate, quenching media and tempering temperature [11-14].

Several scholars have studied the effects of internal HE of mild steel and the loss of ductility with intergranular cracking and work hardening [8, 9, 15, 16]. These processes depend on the strain rate, the method of hydrogen charging and the microstructure of the material [8, 17-21]. The two most commonly used experimental hydrogen charging methods are electrochemical (i.e. cathodic protection) and exposure of to hydrogen gas [8]. Slow strain rate tensile tests (SSRT) are often used for HE susceptibility investigations of steel [22]. In order to avoid HE, the NORSOK standard recommends the use of a material with a hardness of 350 HV or lower value or a material with low carbon steel for structural/mechanical parts/components that are cathodically protected [23]. As the HE susceptibility depends on the material, environment and application, case specific investigations are required in order to determine HE susceptibility limits.

AISI 4130 steel with 620 MPa yield strength is considered one of the suitable materials for use in hydrogen sulfide environment according to a previous report [24]. The effects of anisotropy on the hydrogen diffusivity and stepwise cracking of AISI 4130 steel with a banded ferrite/pearlite structure have been studied by Gao et al. and Lee et al. [25, 26]. The hydrogen diffusivity was at similar levels in longitudinal and in transverse directions of the materials. On the other hand, the effect of hydrogen on the fatigue strength of quenched and tempered AISI 4130 steel showed a variation in crack propagation, and toughness values were deeply influenced by the presence of hydrogen [27, 28]. The HE effect during fracture toughness test of quenched and tempered AISI 4130 steel has been simulated by a three-step procedure using the simulation software by Gobbi and Vergani [29]. A cohesive model was proposed to simulate HE on fracture toughness and its reliability was proved by a sensitivity analysis. The electro metallization of an aluminum coating was proposed to ensure the reliable operation of oil and gas equipment made by AISI 4130 hull steel [30]. Even though several studies have been carried out for AISI 4130, according to literature, there is a lack of investigations into the relationship between the HE susceptibility and hardness and thus on tempering temperature for cathodically protected AISI 4130 steel. In addition, the limiting/conservative values for tensile strength and fracture strain (i.e. ultimate fracture strain) are not available for cathodically protected tempered AISI 4130 steel.

The objective of this study is therefore to investigate the HE susceptibility of tempered high strength carbon steel, AISI 4130 by SSRT of hydrogen pre-charged samples under hydrogen charging while straining. The samples were first austenitized and quenched to martensitic structure, then tempered to improve the ductility and reduce the hardness. Before SSRT done at strain rate of $1x10^{-6}s^{-1}$ with samples under hydrogen charging, the specimen from the different tempering state was pre-charged with hydrogen. Microstructure and fracture surface are also studied. The relationship between the HE susceptibility and hardness are also presented.

2. Materials and experimental procedure

2.1. Materials

The chemical composition of the high strength carbon AISI 4130 steel used for this work is given in Table 1. For tensile testing, 24 samples were prepared according to ASTM E8 standard [31]. The geometry of the samples is shown in Fig. 1. The samples were austenitized at 873 ºC for 40 to 50 minutes and rapidly transferred into a salt bath maintained at 180°C for quenching. An agitator in the salt bath provides an extra cooling effect by circulating the salt. To minimize the risk of bending during quenching, the samples were submerged in a vertical position.

The samples were divided into three groups, each with 8 samples, as shown in Table 2. The samples from one of the three groups were tested only in air. The as-quenched sample of this group is labelled as AQ, whereas A-xxx (i.e. xxx represents tempering temperature) represent the tempered samples. The other two groups were subjected to hydrogen charging and the samples are suffixed as H1and H2, respectively. H1Q and H2Q stand for as-quenched hydrogen charged samples of the two groups. H1-xxx and H2-xxx represent tempered samples of the hydrogen charged of the two groups and xxx represents tempering temperature. The description of the samples together with some of the measured data are shown in Table 2.

Table 1. The chemical compositions of AISI 4130 (in wt%)

C	Si	Mn	P	S	Cu	Cr	Ni	Mo	V	N	Al	Nb	As	Sn	Ti	Co	Ca	Fe
0.31	0	0.5	0.01	0	0.2	1.1	0.1	0.2	0.004	0.006	0.023	0	0.01	0.01	0.003	0.01	1	Bal.

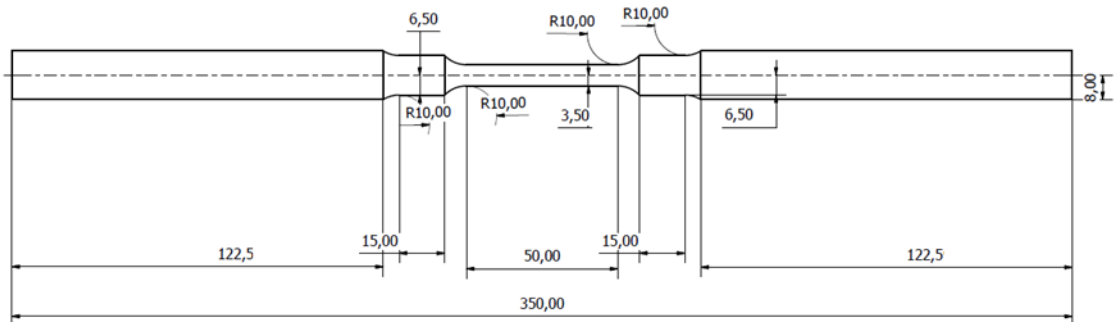

Fig. 1. Dimensions of the tensile test sample in mm.

2.2. Electrochemical hydrogen charging

Samples in H1 and H2 groups were charged with hydrogen for approximately two weeks' duration under similar conditions as shown in Table 2, prior to SSRT. The test samples would be saturated with hydrogen during this incubation period. A 20L square plastic container with the capacity of holding 16 samples was filled with 3.5 wt% NaCl in distilled water as electrolyte. The NaCl electrolyte was particularly chosen to simulate the marine environment. The set up for pre-charging included an AISI 4130 sample as working electrode (tensile samples), an Inconel 625 steel (58 wt% nickel) bar with approximately same surface area as the samples as a counter electrode, and a saturated calomel electrode (SCE) (radiometer analytical probes, REF201) as a reference electrode. A Labor-Netzgerat EA-3021S was used as a power supply and a Hioki 3803 digital multimeter was used for controlling the voltage with reference to the SCE. The voltage was set at -1050mV ($\pm$50mV) SCE for the entire hydrogen charging period of the samples. The electrolyte was changed four times during the incubation period in order to maintain the composition of the electrolyte.

Table 2. The samples studied, average hardness and SSRT test results

Sample Designation	Tempering temperature (°C)	Hydrogen charging duration (hrs)	Hardness (HV)	Tensile strength (MPa)	Fracture strain /Strain to failure	Reduction of area (%)
AQ	quenched	0	557±9	2049	0.0943	39
A-350	350	0	490±5	1705	0.0631	-
A-400	400	0	461±5	1562	0.0795	56
A-430	430	0	447±4	1282	0.0817	63
A-460	460	0	425±3	1308	0.0964	66
A-490	490	0	402±3	1125	0.0946	64
A-520	520	0	378±4	1119	0.0947	64
A-550	550	0	360±4	1100	0.1144	67
H1Q	quenched	428.5	541±12	1269	0.0198	3
H1-350	350	409.8	493±4	1057	0.0137	2
H1-400	400	412.6	472±3	1242	0.0165	3
H1-430	430	382.3	445±2	1240	0.0262	4
H1-460	460	343.9	421±3	1150	0.0194	3
H1-490	490	341.8	400±3	1227	0.039	8
H1-520	520	344.0	381±4	1207	0.0468	11
H1-550	550	340.2	352±4	980	0.0439	18
H2Q	quenched	309.7	545±13	1249	0.0208	0
H2-350	350	292.6	489±4	1157	0.0166	2
H2-400	400	316.6	465±3	1182	0.0161	1
H2-430	430	292.5	445±3	1192	0.0175	4
H2-460	460	295.0	422±4	1259	0.0254	5
H2-490	490	295.9	401±3	1225	0.0285	9
H2-520	520	388.6	380±5	1152	0.0454	12
H2-550	550	413.4	353±3	1068	0.0447	17

2.3. Slow strain rate tensile test

In order to determine the effect of hydrogen charging on mechanical and fracturing properties, an experimental set up as shown in Fig.2 (a) was used for the SSRT tests. The setup consisted of electrochemical cell, tensile testing machine and data acquisition system. A three-electrode cell was used in the tests as shown in Fig. 2 (b) for in-situ hydrogen charging. In a cylindrically polycarbonate plastic container filled with a 0.5 M NaCl electrolyte, each sample wa potentiostatically charged under dynamic tensile load. The three-electrode cell included a tensile test sample as working electrode, an equal sized Inconel 625 bar as a counter electrode, and a saturated calomel electrode as a reference electrode. The potential was set at -1050 mV SCE by use of a Gamry interface 1010E potentiostate. The samples were mounted to an INSTRON 5985 dual column floor frames testing machine and tested at various strain rates.

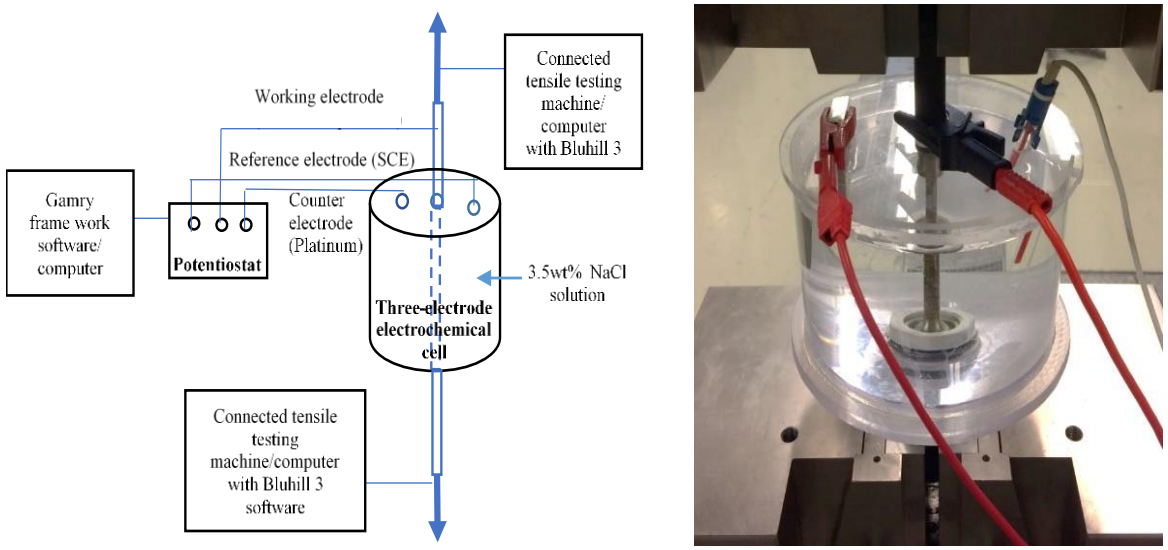

Fig. 2. (a) Schematic diagram of SSRT experimental set-up; (b) Combined electrochemical/ strain cell with a three-electrode set up.

For the SSRT tests, the hydrogen charged samples (-1050 mV SCE) were transferred from the incubation container to the tensile test cell within 2-3 minutes, in order to minimize hydrogen loss from the surface of the samples. Slow strain rate of 10^{-6} s^{-1} was applied for allowing hydrogen to migrate to crack tips during propagation [31]. The tensile test for the uncharged samples were done in air (Table 2). The first two samples (i.e. AQ and A-350) were tested at the same strain rate as that of the hydrogen charged samples. The rest of the samples were tested at the strain rate of $0.0025s^{-1}$ [31, 32].

The load versus displacement data were recorded during the test. The tensile strength, reduced cross-sectional area and total elongated length were measured after the samples were fractured. The relative HE susceptibility index (I_{HE}) was calculated for the hydrogen charged samples. The I_{HE} is defined by the ratios of stress-strain curve characteristic parameters of samples tested after hydrogen charging using the characteristic parameters of the samples tested in air as shown below [4,11,33,34].

$$I_{HE}\% = \left(\frac{\text{hydrogen uncharged mechanical property} - \text{hydrogen charged mechanical property}}{\text{hydrogen uncharged mechanical property}}\right) \times 100\% \quad (1)$$

$$I_{HE}\% = (1-\alpha) \times 100\% \qquad \text{where} \quad \alpha = \begin{cases} \frac{\varepsilon_{u,ch}}{\varepsilon_{u,uc}} \\ \frac{A_{ch}}{A_{uc}} \end{cases} \quad (2)$$

$\varepsilon_{u,uc}$ and A_{uc} are fracture strain and percentage reduction of cross-sectional area, respectively of the uncharged samples tested in the air. $\varepsilon_{u,ch}$ and A_{ch} are stress-strain curve characteristic parameters of the hydrogen charged samples. The $\varepsilon_{u,uc}$, $A_{uc,}$ $\varepsilon_{u,ch}$ and A_{ch} are the measured mechanical properties for $I_{HE.}$

2.4. Hardness test

Hardness is one of the material properties that could give an indication of how susceptible a material is to hydrogen embrittlement. The measurement with Vickers hardness was done on samples extracted from each of the quenched and tempered samples. The samples for the test were prepared by grounding and polishing with up to 2000 grit emery paper. The hardness was calculated from 24 indentations for each samples according to NS-EN ISO 6507 [35].

2.5. Microscopy

The microstructures of the samples and fracture surfaces were studied using Scanning Electron Microscopy (SEM), Gemini SUPRA 35VP (ZEISS). The sample extracted from fracture surfaces of tested samples were cleaned with acetone and their fracture morphologies were observed by SEM. For microstructure studies, selected samples were prepared from both charged and uncharged groups (Table 2). Sample preparation for the microstructure investigations with SEM consisted of mechanical grinding, fine polishing and etching based on Struers application notes [36]. The etching was performed with LectroPol-5 electro-polishing system using A2 electrolyte at 40 kV, for a duration of about 12 s.

Finer details of the microstructure, including phases and defects, were further investigated with Transmission Electron Microscopy (TEM), JEOL-2100 (LaB_6 filament), operating at 200 kV. The investigations with TEM were performed on selected samples: HQ1, H2/400, H1-490,

H1-550, AQ and A-490 (Table 2). For the TEM analysis, thin foils were prepared, first by thinning down mechanically to a thickness of about 100 µm, and then punched 3 mm disks from the foils. These disks were then electro-polished using a dual jet polishing system, Struers TENUPOL-5 operated at 13 V and at -30 °C in an electrolyte solution of 95% methanol and 5% perchloric acid.

3. Results

3.1 Hardness

The average hardness measured is tabulated in Table 2. In addition, the plot of hardness as a function of tempering temperature is given in Fig. 3. The plot indicates a linear dependency of hardness in the temperature range between 350 °C to 550 °C, corresponding to hardness between 557 HV to 353 HV respectively.

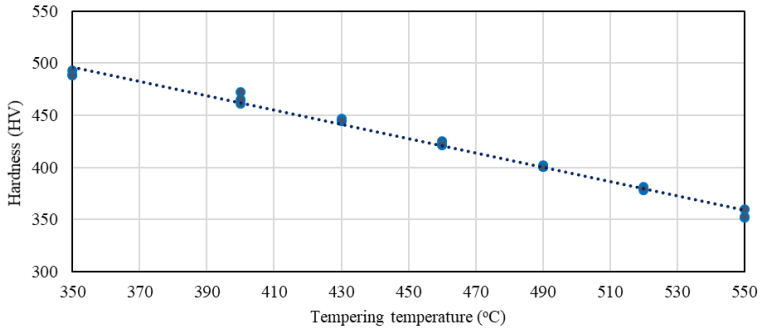

Fig. 3. Hardness as a function of tempering temperature of the AISI 4130 steel.

3.2 Stress-strain behaviour and mechanical properties

Numerical values of tensile strength, fracture strain, percentage reduction of cross-sectional area, average hardness and hydrogen charging durations are listed in Table 2. For studying the tensile properties, the nominal stress-strain behaviour of hydrogen pre-charged and uncharged samples is given as a function of tempering temperature in Fig. 4 (a) to 4(h). The loss of ductility after hydrogen charging is clearly demonstrated in these results. The austenization heat treatment followed by quenching forms pure martensitic steel that increases the hardness and tensile strength of the material. For tempering temperatures of 490 °C and lower, the tensile

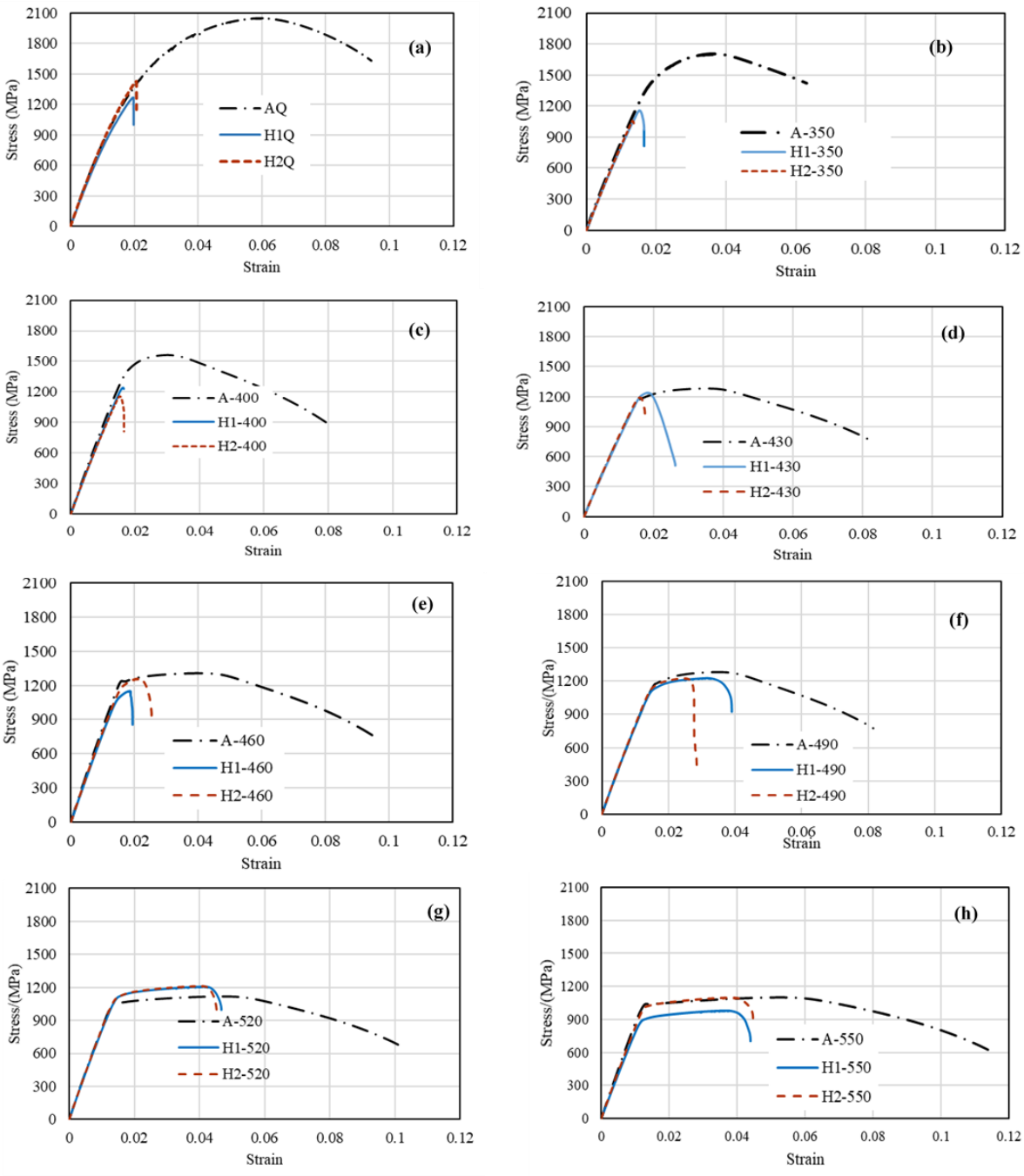

Fig. 4. Comparison of stress-strain curves of uncharged and hydrogen pre-charged samples: (a) as quenched sample, (b) using tempering temperature (TT) 350 ˚C, (c) TT 400 ˚C, (d) TT 430 ˚C, (e) TT 460 ˚C, (f) TT 490 ˚C, (g) TT 520 ˚C and (h) TT 550 ˚C

strength for charge specimen is almost constant at 1200 MPa. After tempering and hydrogen charging, the samples exhibited reduction in ductility and tensile strength. Ductility is however increasing with tempering temperature as shown in the Fig. 4. A similar trend is also observed for tempered with maximum ductility corresponding to highest temperature.

The reduction of the cross-sectional area (A%) of tensile tested samples was decreased with lower tempering temperature as shown in Fig. 5(b). The hydrogen charged samples were subjected to significant decrement of A%. Negligible A% reduction is observed for the material tempered below 430 ˚C. Fig. 5(c) shows the decrement of ductility (fracture strain) with increased hardness for the samples tested in air. The fracture strain reaches a constant value when hardness is larger than 465 HV (< 460 ˚C) for charged samples. There is a clear trend between tensile strength and tempering temperature for the samples tested in air as shown Fig. 5(f). In contrast, the tensile strength attains a constant value for the charged samples tempered below 460 ˚C (hardness > 450 HV). An increased tempering temperature successively reduces

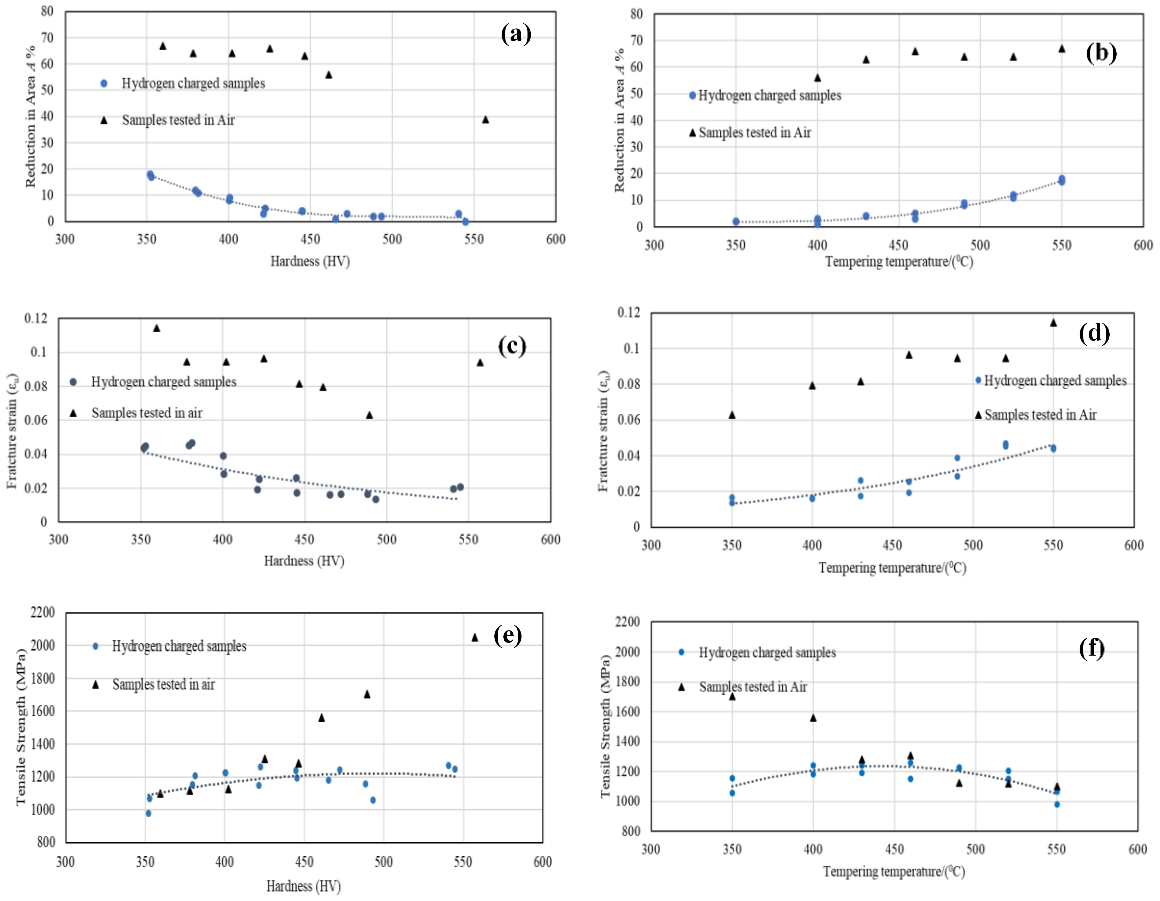

Fig. 5. (a) Reduction of cross-sectional area versus hardness, (b). Reduction of cross-sectional area versus tempering temperature, (c) Fracture strain versus hardness, (d) Fracture strain versus tempering temperature, (e) Tensile strength versus hardness, (f) Tensile strength versus tempering temperature

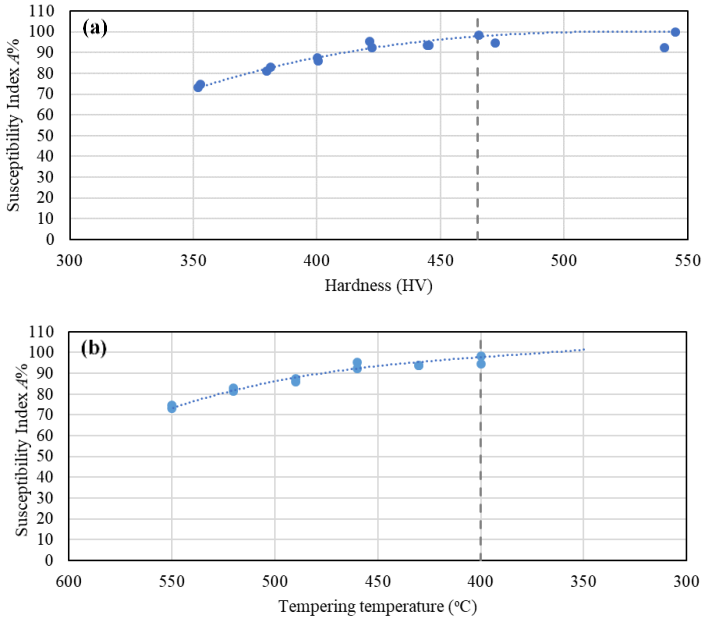

Fig. 6. HE susceptibility index of reduction of cross-sectional area of the AISI 4130 samples versus, (a) Hardness, (b) Tempering temperature.

the tensile strength and increases the ductility, both for charged and for uncharged samples. The area reduction is significantly reduced with hydrogen pre-charging. The ductility of uncharged samples decreased for the two lowest temperatures (350 and 400 ˚C), and slightly increased at higher temperatures. For charged samples, the trend is opposite, almost no changes at the lowest temperatures, and a small increase for the highest.

3.3 Susceptibility of hydrogen embrittlement

The relative HE susceptibility indices (I_{HE}) are calculated for each stress-strain curve of tempered states, with respect to the characteristic parameters of the tested samples as explained in Section 2.3. The percentage reduction of cross-sectional area, tensile strength and fracture strain versus the mean HV hardness values of the samples are plotted and shown in Figs. 5(a)-5(c). I_{HE} of the fracture strain and percentage reduction of cross-sectional area (A%) are plotted as a function of hardness in Figs. 6 and 7, respectively. Fig. 8 shows the HE susceptibility index versus hydrogen pre-charging durations. The charging period was sufficient to have saturated samples in the vicinity of crack initiation.

Fig. 6 (a) shows a significant increment of HE susceptibility index of *A%* with the hardness. More than 70% of HE susceptibility is observed for all the samples. 100% HE susceptibility is obtained for samples with hardness of 465 HV and larger. 100% HE susceptibility is also observed for samples heat-treated below 400 ˚C tempering temperature as shown in Fig. 6(b). Fig. 7(a) shows the increment of HE susceptibility index of fracture strain with the hardness. More than 50% of HE susceptibility is observed for all samples. About 80% of HE susceptibility is observed for material with hardness larger than 465 HV. This suggests that the AISI 4130

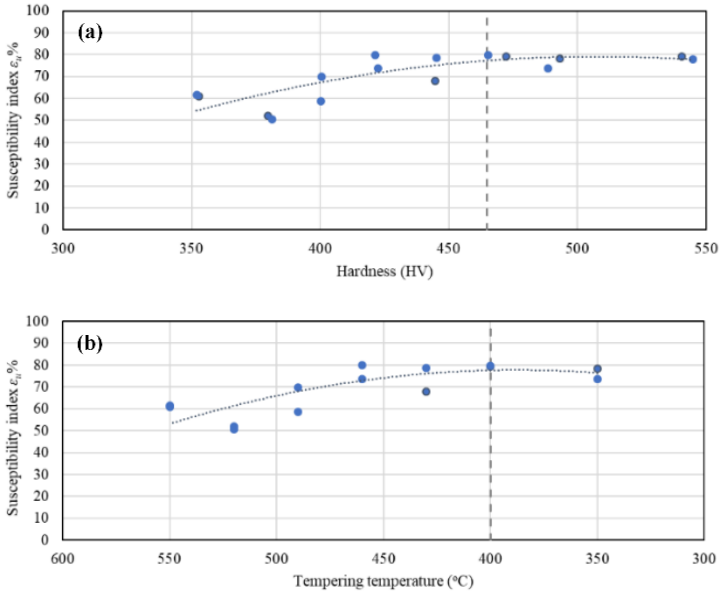

Fig. 7. HE susceptibility index of fracture strain of the AISI 4130 samples versus, (a) Hardness, (b) Tempering temperature.

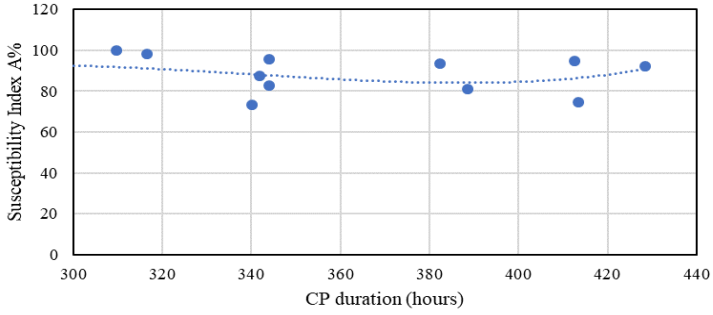

Fig. 8. Variation of HE susceptibility versus hydrogen charging duration of the AISI 4130 samples.

material is most likely subjected to HE due to hydrogen charging when the hardness is larger than 465 HV. It is also accompanied with loss of ductility. Similarly, Fig. 7(b) shows that about 80% of the samples which were tempered at temperatures lower than 400 ^{o}C are susceptible to the HE. In general, the study shows that AISI 4130 is susceptible to HE due to the hydrogen charging when the tempering temperature is below 400 ^{o}C. The samples, which were quenched and subjected to tempering temperature of 400 ^{o}C and less, are 100% susceptible to HE when considering the susceptibility of *A%*.

3.4 Fractrography

The fracture surfaces of the tempered and hydrogen charged samples in group 2 were examined by SEM. Morphology of the fracture surfaces for three of the samples are shown in Fig. 9. These samples were tempered at 350 °C (Fig. 9a and 9b), 430 °C (Fig. 9c and 9d) and 490 °C (Fig. 9e and 9f). At lower tempering temperatures (Fig. 9a-9b), “intergranular” surfaces with numerous secondary cracks perpendicular to the surface, following prior austenitic grain boundaries were observed as expected for brittle materials. Fig. 9 (b) shows (H-350) typical intergranular type fractures that clearly follow the prior austenite grain boundaries as compared to the fractures for the H2-430 (Fig. 9c and 9d). The latter exhibits mainly non-intergranular type fractures. Close inspection of the images reveals that the material became less brittle with increasing tempering temperature. Fig. 9 (e) and 9 (f) show fracture images for the samples tempered at 490 °C (H2-430), which exhibit mainly microcracks, which are of a more ductile nature. The samples tempered at 550 ^{o}C exhibit distinct dimples, which is a characteristic of plastic deformation before fracture as is seen in Fig. 9 (f).

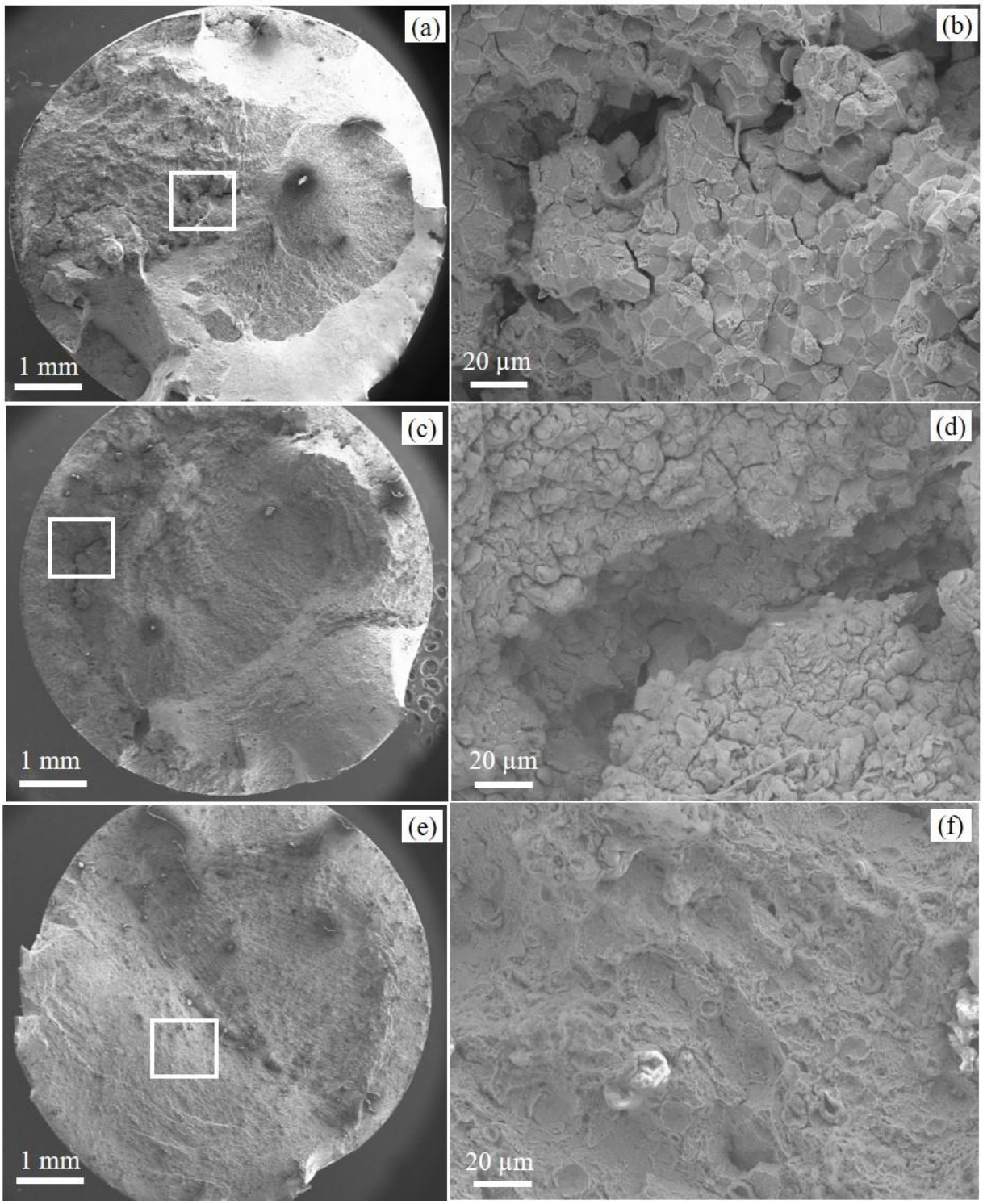

Fig. 9: Fracture surfaces of AISI 4130 in full and magnified view of (a,b) H2-350, (c,d) H2-430 and (e,f) H2-490. The magnified images are from the marked square regions of the images in full views.

3.5 Microstructure

SEM images shown in Fig. 10 represent the air-as quenched and H1-550 in (a) and in (b), respectively. The microstructure of both images are identified as martensitic laths with packets morphology revealing the prior austenitic grains. The analysis of Electron Back Scatter Diffraction (EBSD) patterns collected from as quenched and tempered (550 ºC) samples did not give indication of the presence of retained austenite. Examples of approximate prior austenite grain boundaries are marked in the images. These grains are about 6-8 μm in size whereas the average thickness of the martensitic laths of the air-as quenched lies in the range between a few tens of nanometers to hundreds of nm.

Typical TEM bright field (BF) images that show the morphology of the martensitic laths are given in Fig. 11. Bright field imaging have been done in order to do characterization of the microstructures of as quenched, 400ºC, 490ºC and 550ºC tempering. A typical TEM bright field (BF) image of the air-as quenched state shows a width of the martensitic laths, ~ 50 – 400 nm. Inside the laths it is numerous of contrast variations caused by residual stress, Fig 12. Tempering at 400ºC, have any influence on the martensitic lath size; on the other hand, a large quantities of 20 nm long and 15 nm thick carbides precipitate. These seems to be semi-coherent precipitates on a low index crystallographic type of plane. Tempering at 490ºC result in precipitates of the same type, precipitated on {100}-plan ascribed the matrix as a ferritic. In addition, this state has precipitates along the boundaries of the martensitic laths. Following Brice et al. [37], these precipitates will be referred hereafter as intralath and the ones inside the lath as interlath. Tempering at the highest temperature, 550ºC, have also both intralath and interlath carbides. The intralath precipitates have the same character as at 490ºC, but the morphology of the interlath precipitates is spheriodized with diameter of ~100 nm, Fig. 12.

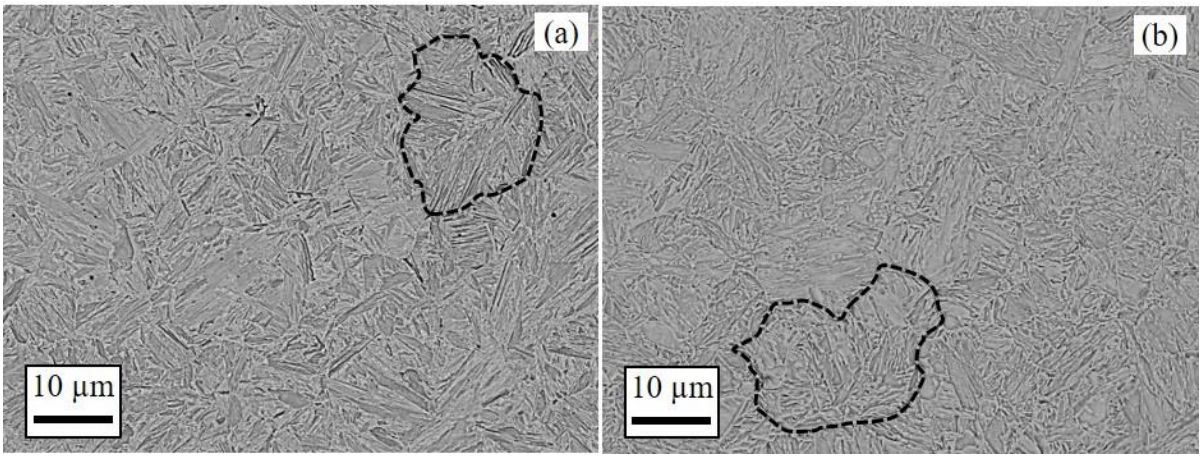

Fig. 10. SEM image of (a) air-as quenched and (b) H2-550

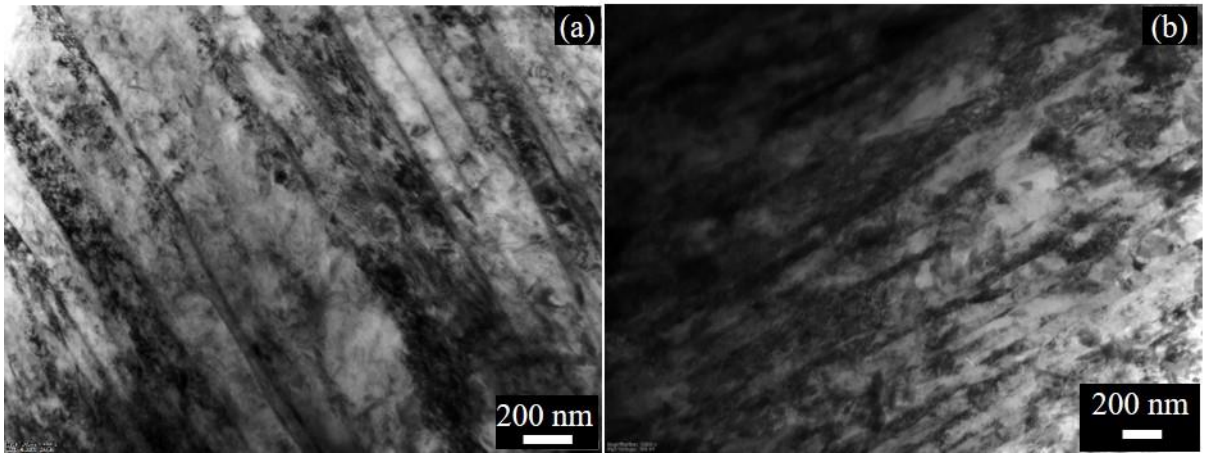

Fig. 11: TEM bright field images showing laths of martensitic structure (a) air-as quenched (b) H2-400.

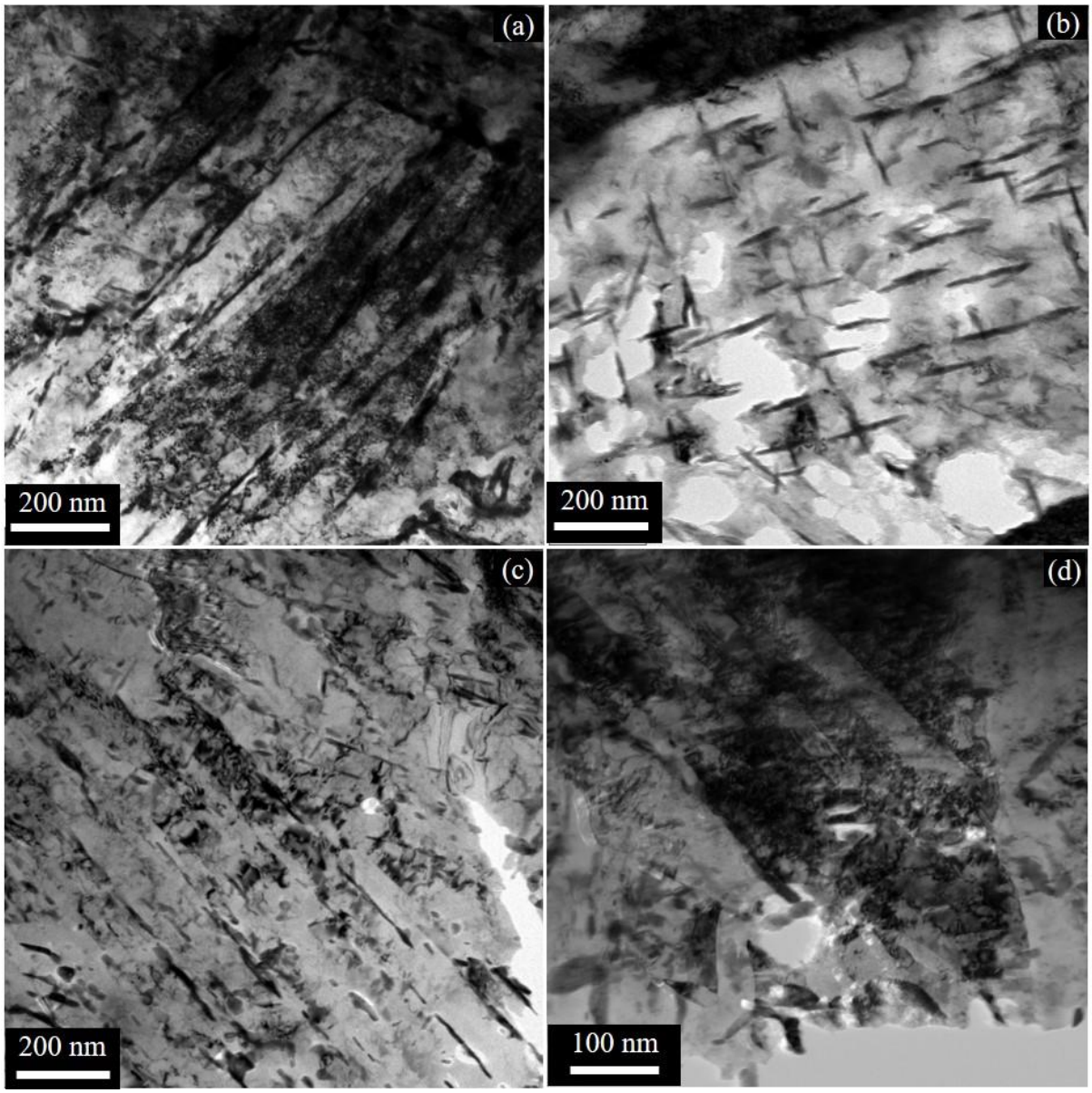

Fig. 12: Bright field TEM images of H2-490 (a, b), (c) H2-550 and (d) H2-400 showing dislocation. The carbides seen in (a) and (d) are precipitated along the lath boundaries (interlaths) whereas the carbides in (b) are precipitated within the laths (intralaths).

4. Discussions

4.1 Effect of tempering temperature on the mechanical properties

The results indicate that the hardness and tensile strength of the uncharged samples decrease with increased tempering temperatures, whereas ductility generally increases as expected. The highest hardness and tensile strengths are observed when the material is under as

quenched condition. Quenching results in a high density of dislocation that accumulates large amounts of stresses. Stresses are relieved by annihilation of dislocations and other lattice defects depending on tempering temperature. Under the solid solution condition, carbon was homogeneously distributed in the matrix. During tempering however, carbon was decomposed to form carbide precipitates. TEM images of the samples tempered at 400 ºC, 490 ºC and 550 ºC (Fig. 12) reveal a high density of metal carbides, confirming segregation of substantial amounts of the alloy elements during precipitation. Carbide can be precipitated at the lowest temperature, 350 ºC too. Similar phenomena have been reported previously [13, 38-41]. The structure of these precipitates have shown different morphologies. At 490 ºC, the carbide precipitates are mixed type- interlaths as well as intralaths. The interlaths form a certain orientation relationship with the matrix that effectively prevents dislocation movements. The highest temperature however results in more precipitates along the boundaries of the laths (interlaths), which are considered to be less efficient in preventing dislocation movements. In addition the interlath precipitates has spherodized, which also reduce the pin up effect by the dislocations. As for martensitic tempered steels, decreasing strength means increasing ductility.

The influence of hydrogen charging on mechanical properties can be revisited from the stress-strain curves shown in Fig 4. Generally, the ductility of martensitic steel is increasing while hardness is decreasing as reported by many scholars too [4, 38, 39]. There are considerable differences in ductility between hydrogen-charged samples and uncharged samples (see for example Fig. 4(a)). The ductility of the charged sample was increased for tempering temperatures above 460 °C. The poor ductility condition for the charged samples below the tempering temperature of 460 °C is believed to be due to the large quantity of trapped hydrogen in the material. Lattice defects, such as dislocations, are considered as the main trapping sites of hydrogen. As it is already discussed, the amount of dislocation density is decreasing with increasing tempering temperature and thus less trapped hydrogen. Therefore,

low ductility corresponds with higher density of lattice defects (dislocation) that could trap large amounts of hydrogen. This may be why the material is more susceptible to HE when the tempering temperature is below 460 ^{o}C.

The morphology of the fracture surface can also be explained in terms of the concentration of hydrogen absorbed in the sample. As shown in Fig. 9 (section 3.4), the tendency of crack formation is higher with samples that trapped larger amounts of hydrogen, e.g. at lower tempering temperature. The microstructure of the samples tempered at lower temperature contains a high concentration of stress that can trap hydrogen to a high extend. There are formed default regions with high residual stress in areas with previous austenitic ground boundaries. This leads to decreasing of cohesive strength and high concentration of hydrogen in the prior austenitic grain boundaries. The grain boundaries then act as crack initiation sites that tend to propagate at the lowest applied stress to fracture with intergranular character. This mechanism is generally referred as hydrogen enhanced localized plasticity and decohesion [4].

During the SSRT testing, hydrogen enters the dislocations generated during straining and diffuses further into the material [4, 11].The tested charged samples which are fully hydrogen saturated can be a cause for the reduction of strain after onset of yielding by promoting “intergranular” cracking along the prior austenite grain boundaries [4]. The intergranular cracking along the prior austenite grain boundaries greatly reduces the strain hardening of hydrogen charged samples. This is demonstrated in this study where the first crack tends to increase to a critical size and is formed in the region of the prior austenite grain boundaries. At lower temperatures, hardness, yield and tensile strengths are quite high and consequently a small crack will lead to a high stress concentration factor. The bonds between the prior austenite grain boundaries are weaker than the boundaries between martensitic laths. In addition, the concentration of hydrogen in the vicinity is high. The width of martensitic lath, dislocation density and carbide precipitates can affect mechanical properties of the material [42]. The

coarsening of carbides at higher tempering temperature and carbon content reduce the tensile strength and the rate of strain hardening [43]. This may be the cause for the very low work hardening rate for hydrogen uncharged samples, tempered at 460 ^{o}C and higher, and uncharged samples tempered at 520 ^{o}C and higher (Fig. 5).

Probably, the critical stress around 1200 MPa for crack initiation and propagation is less than the yield stress for all the charged and tempered states at temperatures below 460 ^{o}C. Interestingly, when the tensile strength for the non-charged and charged samples reaches the same level, around 1200 MPa at 460 ^{o}C, the susceptibility index for hydrogen embrittlement drops. At higher temperatures, the yield strength of the charged samples decreases and elongation increases with increasing temperature. The fracture surface tends to have more ductile character behaviour with spherical dimples for the samples tempered at highest temperature (Fig. 9 (f)).

The elongation for non-charged samples becomes substantially longer. In addition to tempering, the mechanisms leading to hydrogen embrittlement need to be considered to understand the irregularity of yield strength and elongation. Solubility and diffusion rate and ductility near crack at different temperatures should be addressed to understand the phenomenon.

The AISI 4130 material is susceptible to HE, when hardness is larger than 465 HV or when the tempering temperature is below 400 ^{o}C as shown in Figs. 6 and 7. Hydrogen intake, diffusibility and trapping capacity are reduced when the tempering temperature increases due to coarsening of carbide precipitates [4, 38]. It is more complicated than coarsening of carbide precipitates in this study. Hydrogen traps are characterized by the trapping energy. Dislocations are typically low energy traps, which will allow hydrogen to diffuse at room temperature. Coherent precipitates may also result in low energy traps and increased solubility due to the distortion of the surrounding atomic lattice. The amount and nature of precipitates can thus

influence the hydrogen solubility and diffusion, and hence may affect HE susceptibility. The mobile hydrogen is mainly trapped by dislocations and governed the HE susceptibility [11]. In general, the results from this study is in agreement with previous reports [13, 41] that showed susceptibility of AISI 4130 to HE when the hardness of the material is high (at lower tempering temperature). In contrast, when tempering temperature increases, the resistance to HE increases. The mobile and diffusible hydrogen may not have an effect on the elastic behaviour of hydrogen charged samples as the slope of stress-strain curves were not changed due to tempering temperature [44].

4.2 Effect of tempering temperature on the fracture behaviour and microstructure

Dislocation density is considerably high when the steel is as quenched, but reduced after the steel is tempered. Thus, the concentration of trapped hydrogen is lowered with increasing tempering temperature [4, 38]. An increase in trapped hydrogen may therefore be the reason for a higher amount of developed intergranular cracks in the martensitic steel that was tempered at lower temperature as described in Section 3.4. In contrast, a ductile fracture behaviour with dimples may be observed for the hydrogen charged samples with higher tempering temperature [4, 38]. These observations support the conclusion made above, i.e. AISI 4130 material is subjected to HE due to hydrogen charging, when the hardness is above 465 HV.

As shown in Figs.10 to 12, the as quenched and tempered martensitic steel microstructure consists of prior austenite grain boundaries, martensitic lath boundaries and carbide-matrix interfaces. The diffused hydrogen is trapped near the crack tips and helps to propagate the cracks. The hydrogen trapping in the material and diffusion near the crack tip are of interest. The high amount of hydrogen near the crack tips can be considered as one of the factors responsible for the propagation of the cracks. Even though hydrogen causes the embrittlement, strain rate, local stress concentrations and microstructure have substantial influences on the embrittlement.

Mobile hydrogen can be trapped by carbide precipitates, which may reduce the diffusivity inside the material. The carbide precipitates change with the tempering time [11, 16]. If tempering temperature and the time are higher, the amount of carbide precipitate changes and hence trapped hydrogen concentration may change [14, 38, 39]. Furthermore, diffusivity may vary with the factors such as their interfaces and stress field according to coherence, which trap the hydrogen. In addition, when carbide forms, it may deplete the martensitic matrix, which results in ductile behaviour, which subsequently reduces the embrittlement.

5. Conclusions

Susceptibility to Hydrogen embrittlement (HE) of the tempered and hydrogen charged high strength carbon steel, AISI 4130, was investigated by slow strain rate tensile test (SSRT). Microstructural characterization and fracture surface examination were done in order to study the effects of hydrogen in relation to embrittlement. The following conclusions are made from the study.

- When hardness is larger than 465 HV (corresponding to tempering temperature less than 430 °C):
    - The HE susceptibility index of reduction of cross-sectional area and fracture strain (i.e. strain to failure) are about 100% and 80%, respectively.
    - The as quenched samples experienced the highest hydrogen embrittlement susceptibility and are subjected to intergranular cracking due to hydrogen charging.
    - The percentage reduction of cross-sectional area is negligible.
    - The fracture surface examination showed transition of ductile microvoid coalescence to brittle intergranular cracking.

- The limiting tensile strength (ultimate tensile strength) and fracture strain (ultimate fracture strain) can be conservatively considered as 1200 MPa and 0.02, respectively for hydrogen pre-charged high strength carbon steel, AISI 4130.
- The fracture behaviour is ductile and hydrogen embrittlement susceptibility decreases when tempering temperature is higher than 490 ºC.
- Generally, the hydrogen charged high strength carbon steel, AISI 4130 is subjected to HE when the hardness is larger than 465 HV.

Acknowledgement

The authors would like to thank Johan Andreas Thorkaas, Adugna Deressa Akessa, Mona Minde, Tor Gulliksen, Jan Magne Nygård and John Grønli for their support in the labs. Erlend Sølvberg from Kverneland Group is highly appreciated for conducting the heat treatments.

References

[1] K. Gjerding-Smith, R. Johnsen, H. I. Lange, B. H. Leinum, G. Gundersen, B. Isaksen, G. Nærum, Wire fractures in locked coil cables, Bridge Structures Assessment, Design and Construction 2 (2007) 63-77.

[2] J. M. Kulicki, Z. Prucz., D.F. Sorgenfrei, W. T. Young, Guidelines for evaluating corrosion effects in existing steel bridges, Transportation Research Bboard National Research Council, Washington, D.C. 1990.

[3] Y. Cung, L.K Fulton, Environmental hydrogen embrittlement of G41400 and G43400 steel bolting in atmospheric versus immersion services, Journal of Failure Analysis and Prevention 17 (2017) 330-339.

[4] B. S. Kumar, V. Kain, M. Singh, B.Vishwanadh, Influence of hydrogen on mechanical properties and fracture of tempered 13 wt% Cr martensitic stainless steel, Materials Science and Engineering A700 (2017) 140-151.

[5] R.W. Revie, H. H. Uhlig, Corrosion and Corrosion Control, An Introduction to Corrosion Science and Engineering, Wiley and Sons 2008.

[6] I.M.E. Aghoury, K. Galal, Corrosion-Fatigue Strain-Life Model for Steel Bridge Girders under Various Weathering Conditions, Journal of Structural Engineering, 140 (2014), Article no: 04014026

[7] I. E. Aghoury, Numerical tool for fatigue life prediction of corroded steel riveted connections using various damage models, PhD Thesis, Canada, Montreal, Concordia University 2012.

[8] P. Roberge, Handbook of Corrosion Engineering, McGraw Hill 2000.

[9] G. P. Tiwari, A. Bose, J. K. Chakravartty, S. L. Wadekar, M. K. Totlani, R. N. Arya, R. K. Fotedar, A study of internal hydrogen embrittlement of steels, Materials Science and Engineering A 286 (2000) 269-281.

[10] C. L. Lai, L. W. Tsay, C. Chen, Effect of microstructure on hydrogen embrittlement of various stainless steels, Materials Science and Engineering A 584 (2013) 14-20.

[11] T. Depover, K. Verbeke, Hydrogen trapping and hydrogen induced mechanical degradation in lab cast Fe-C-Cr alloys, Materials Science and Engineering A 669 (2016) 134-149.

[12] Y. Zheng, F.Wang, C. Li, Y. Lin, R.Cao, effect of martensite structure and carbide precipitates on mechanical properties of Cr-Mo alloy steel with different cooling rate, High Temperature Materials and Processes, 28 (2019) 113–124.

[13] N. Nanninga, J. Grochowsi, L. Heldt, K. Rundman, Role of microstructure, composition and hardness in resisting hydrogen embrittlement of fastener grade steels, Corrosion Science 52 (2010) 1237–1246.

[14] V. H. B. Hernandez, S. S. Nayak, Y. Zhou, Tempering of martensite in dual-phase and its effect on softening behavior, Metallurgical and Materials Transactions A 42 (2011) Article number: 3115.

[15] L. Marchetti, E. Herma, P. Laghoutaris, J. Chêne, Hydrogen embrittlement susceptibility of tempered 9%Cr–1%Mo steel, International Journal of Hydrogen Energy 36 (2011) 15880-15887.

[16] T. Das, S. K. Rajagopalan, S. V. Brahimi, X. Wang, S. Yue, A study on the susceptibility of high strength tempered martensite steels to hydrogen embrittlement (HE) based on incremental step load (ISL) testing methodology, Materials Science and Engineering A 716 (2018) 189-207.

[17] M. B. Djukic, G. M. Bakic, V. S. Zeravcic, B. Rajicic, A. Sedmak, R. Mitrovic, Z. Miskovic, Towards a unified and practical industrial model for prediction of hydrogen embrittlement and damage in steels, Procedia Structural Integrity 2 (2016) 604-611.

[18] M. B. Djukic, V. S. Zeravcic, G. M. Bakic, A. Sedmak, B. Rajicic, Hydrogen damage of steels: A case study and hydrogen embrittlement model, Engineering Failure Analysis 58 (2015) 485-498.

[19] D.P. Escobar, C. M., L. Duprez, K. Verbeken, M. Verhaege, Internal and surface damage of multiphase steels and pure iron after electrochemical hydrogen charging, Corrosion Science 53 (2011) 3166-3176.

[20] G. Biggiero, A. Borruto, I. Taraschi, Effects of hydrogen charging methods on ductility and fracture characteristics of AISI 9840 steel, International Journal of Hydrogen Energy 20 (1995) 465-470.

[21] Q. Liu, A. D. Atrens, Z. Shi, K. Verbeken, A. Atrens, Determination of the hydrogen fugacity during electrolytic charging of steel, Corrosion Science 87 (2014) 239-258.

[22] T. Michler, J. Naumann, Microstructural aspects upon hydrogen environment embrittlement of various BCC steels, International Journal of Hydrogen Energy 35 (2010) 821-832.

[23] NORSOK M-001 Materials Selection, NTS, 2003

[24] J. L. Battle, T.V. Miller, M.E. True, Resistance of commercially available high strength tubular goods to sulfide stress cracking, American Society of Mechanical Engineers 14 (1975) 11-22.

[25] M. Gao, P. Wei, A, Hydrogen partitioning model for hydrogen assisted crack growth, Metallurgical Transactions A 16 (1985) 2039–2050.

[26] H. Lee, S.L. Chan, Hydrogen embrittlement of AISI 4130 steel with an alternate ferrite/pearlite banded structure, Materials Science and Engineering A 142 (1991) 193-201.

[27] L. Vergani , C. Colombo, G. Gobbi, , F.M. Bolzoni, G. Fumagalli, Hydrogen effect on fatigue behavior of a quenched & tempered steel, 17th International Colloquium on Mechanical Fatigue of Metals, ICMFM 2014. Verbania, Italy, Procedia Engineering 74 (2014) 468-471.

[28] G. Gobbi, C. Colombo, L. Vergani, A cohesive zone model to simulate the hydrogen embrittlement effect on a high-strength steel, Fracture and structural Integrity 10 (2016) 260-270.

[29] I. C. C. Gobbi, L. Vergani, Sensitivity analysis of a 2D cohesive model for hydrogen embrittlement of AISI 4130, Engineering Fracture Mechanics 167 (2016) 101-111.

[30] H. Chumalo, M. Student, B. Datsko, Y. Kharchenko, Some ways to ensure reliable operation of oil and gas equipment in hydrogen sulfide environment, Journal of Corrosion Science and Engineering 21 (2018).

[31] NS-EN ISO 6507-1:2018- Metallic materials – Vickers hardness test - Part 1: Test method, Norsk Standard, Standard online AS.

[32] A. Jemal, M. Birihane, Hydrogen Embrittlement in High Strength Carbon Steel AISI 4130, Mater Thesis, University of Stavanger, 2017.

[33] Y. Zhang, W. Hui, X Zhao, C Wang, H Dong, Effects of hot Stamping and tempering on hydrogen embrittlement of a Low- carbon Boron-Alloyed steel, Materials 11 (2018)-Article number: 2507.

[34] S. Shen, X. Song, Q li, X. LI, R. Zhu, G. Yang, A study on stress corrosion cracking and hydrogen embrittlement of Jethete M152 martensitic stainless steel , Materials Science and Engineering A 740-741 (2019) 243-251.

[35] NS-EN ISO 6892-1:2009 - Metallic materials - Tensile testing - Part 1: Method of test at room temperature,

Norsk Standard, Standard online AS.

[36] Preparation of ferrous metals Struers application notes, https://www.struers.com/en/Material.

[37] Bruce D. Crajg, George Krauss, The structure of tempered martensite and its susceptibility to hydrogen stress cracking, Metallurgical Trans. A 11A (1980) 1799-1808.

[38] S. Lee. A Joseph, Ronevich, G. Krauss , D. K. Matlock, Hydrogen embrittlement of hardened low carbon sheet steel, ISIJ international 50 (2010) 294-301.

[39] W. Lee, T Su, Mechanical properties and microstructural features of AISI 4340 high-strength alloy steel under quenched and tempered conditions, Journal of Materials Processing Technology 87(1999) 198–206.

[40] L.D. Barlow, M. D. Toit, Effect of austenitizing heat treatment on the microstructure and hardness of martensitic stainless steel AISI 420, Journal of Materials Engineering and Performance 21 (2012) 1327–1336.

[41] A. R. Troiano, The role of hydrogen and other interstitials in the mechanical behavior of metals, Metallography, Microstructure, and Analysis 5 (2016) 557–569.

[42] D. Zhao, S. Zhang, H. Zhang, S. Li, H. Xiao, Y. Wang, X. Wang, Effects of tempering temperature on the microstructure and mechanical properties of T92 heat-resistant steel, Metals 9, 194 (2019): doi:10.3390/met9020194.

[43] G. Krauss, D. Matlock, Effects of strain hardening and fine structure on strength and toughness of tempered martensite in carbon steels, Journal de Physique IV Colloque 05 (C8) (1995) 51-60.

[44] M.Wang, E. Akiyama, K Tsuzaki, Effect of hydrogen on the fracture behavior of high strength steel during slow strain rate test, Corrosion Science 49 (2007) 4081-4097.